Quasi-one-dimensional magnetism in TiOCl and a theory of a lightly doped dimerized insulator

by

Alexander Seidel

Submitted to the Department of Physics
in partial fulfillment of the requirements for the degree of

Doctor of Philosophy

at the

MASSACHUSETTS INSTITUTE OF TECHNOLOGY

August 2003

Author .....
Department of Physics
August 18, 2003

Certified by .....
Patrick A. Lee
William and Emma Rogers Professor of Physics
Thesis Supervisor

Accepted by .....
Thomas J. Greytak
Associate Department Head for Education

Quasi-one-dimensional magnetism in TiOCl and a theory of a lightly doped dimerized insulator

by

Alexander Seidel

Submitted to the Department of Physics
on August 18, 2003, in partial fulfillment of the
requirements for the degree of
Doctor of Philosophy

Abstract

Transition metal oxides with low dimensional geometry have displayed fascinating new phenomena such as high temperature superconductivity and unconventional magnetism. The first part of this thesis is related to this rich and diverse subject, where TiOCl is studied as an example of an $S = 1/2$ layered Mott insulator. Earlier experiments on this material indicating two-dimensional spin-liquid behavior are reviewed critically and are compared to new susceptibility data. The latter suggest a new picture, where band structure effects produce quasi-one-dimensional spin chains formed by t_{2g} orbitals. Based on these findings, TiOCl is proposed to be a new example of Heisenberg-chains which undergo a spin-Peierls transition. Within this picture, the effect of doping with non-magnetic Sc impurities can be explained in good agreement with the experiment. The magnetic energy scale of $J \approx 660K$ and the frustration of the interchain geometry render TiOCl unique among materials with a spin-Peierls transition. This unusual geometry is interpreted as the main reason for the failure of conventional mean-field theory to describe the details of the transition such as its first order character. It will be shown that a simple Ginzburg-Landau theory which takes proper account of interchain-frustration is capable of explaining this unconventional behavior.

In the second part of the thesis, the problem of a doped dimerized spin chain is studied in the context of the tJJ'-model one dimension. The focus is on the regime $J'/J \approx .5$ where a spin gap is present at small doping and the undoped spin chain is strongly dimerized, and on the limit of small hole doping x as well as small J/t, J'/t. In this regime, earlier numerical calculations have not been able to yield conclusive results. Using a perturbative approach and Luttinger liquid arguments, it will be demonstrated for this non-integrable class of models that the charge degrees of freedom behave as non-interacting spinless solitons in the dilute hole limit. These results are verified up to third order in perturbation theory. The same approach is also used to evaluate the energy and mass renormalization of a single hole, where non-analytic corrections in powers of $\sqrt{J/t}$ are obtained. At $J'/J = .5$ a variational spin-polaron wave function for the hole is constructed and good agreement with the perturbative results is found.

Thesis Supervisor: Patrick A. Lee
Title: William and Emma Rogers Professor of Physics

Acknowledgments

Intuition and concepts constitute . . . the elements of all our knowledge, so that neither concepts without an intuition in some way corresponding to them, nor intuition without concepts, can yield knowledge.

Immanuel Kant

My past five years at MIT have been a supremely enriching period of time, both for my professional as well as my private life. On the professional side, this has foremostly been due to the mentorship and kind tutelage of my advisor, Patrick Lee, which I have had the great privilege to enjoy for almost four years. Even if I had never been given the chance to work with Patrick, I would nonetheless be deeply indebted to him for opening my eyes to the beauty of the problems that arise in strongly correlated many-body systems during his genuinely original lectures. This had put an immediate end to my at that point quite aimless meandering between the various subfields of physics. All the more am I grateful to Patrick for his bold decision to make me a student of his, although I had been an outsider to CMT at that time. Working for Patrick meant to enjoy an atmosphere of great trust and complete freedom to explore even some of my crazier ideas when I wished to. At the same time, his judgment has never failed to put me back on the right track. Over the years I benefited enormously from his uniquely intuitive way to grasp and communicate physics, his ever invitingly open door, and his friendly advise and support on many levels.

I was also fortunate to receive the teachings of a number of other excellent lectures at MIT, who tremendously helped me to adopt the thinking of a condensed matter physicist in no time: John Joannopoulos, whose solid introduction to solid state physics was always a pleasure to listen to, Xiao-Gang Wen, whose deep insights into both high energy physics and condensed matter theory make him a profound lecturer on the applications of quantum field theory to condensed matter systems and more, and Senthil Todadri, whose highly communicative teaching style was always something to look forward to and very efficiently conveyed his deep physical insights into critical phenomena. I also wish to thank Senthil for his counseling on various occasions. Furthermore, I am grateful to Xiao-Gang Wen and Young Lee for accepting to be on my thesis committee.

Naturally, my smooth transition to a condensed matter physicist was made possible by the great environment of people that I found at the CMT corridor. It has been really easy to feel at home working alongside my Austrian cubicle mate Walter Rantner, with whom I felt I had more than language in common. It was Walters mentoring by which I quickly became familiar with the basics facts and people of the condensed matter community. I have not forgotten either that he was the very person from whom I learned about the existence of a cond-mat server... The community of room 12-127 received a further valuable addition when, after a while, Tiago Ribeiro moved in, along with him a most useful and impressive library. I joyfully remember countless stimulating conversations with my two office mates, that tended

to go beyond a strictly scientific level, notably our lunch discussions at the Whitehead institute. Fluctuations are inevitable in a strongly correlated office, and in the past year I shared my cubicle with a new nearest neighbor, Ying Ran, after Walter had left. Not only did I benefit from our regular discussions, but also from Ying's talent at finding inexpensive hardware deals online, and his gift to discover all sorts of interesting books, that I try to keep track of as they appear and disappear on his desk. At this point I would also like to express some special gratitude to Don Kim, who I do not know personally, but who left a small literary treasure behind in our office.

Leaving the spheres of my office behind, there are many more people to name who I had the chance to interact with during my studies. These include my present and former fellow disciples in Patrick's group, Adam Durst, Kevin Beach, Patrick Sit, Cody Nave, and the gentleman whose desk I am proud to have inherited, Dima Ivanov. In addition, there were many other inmates of the corridor that I enjoyed an occasional chat with: Dan Greenbaum, Casey Huang, Dima Novikov, Michelle Povinelli, Maksim Skorobogatiy, Kimani Stancil, Joshua Weitz and Dicle Yesilleten. A special league is formed by our postdocs, who have greatly contributed to make the CMT corridor an active and intellectually stimulating environment: Bernd Braunecker, Misha Fogler, Ilya Gruzberg, Carsten Honerkamp, Lesik Motrunich, and Ashvin Vishwanath. Leisik and Ashvin have done a terrific job in organizing the "Informal Condensed Matter Seminars", one of the most useful institutions for young researchers at CMT. I feel particularly thankful to Misha Fogler for sharing some of his many insights with me, hoping that we will eventually be able to resume this frequent interaction.

A substantial part of the results reproduced in chapter 2 of this thesis are due the work of excellent collaborators: Chris Marianetti and his advisor Gerbrand Ceder, who performed the LDA and LDA+U band structure calculations, and Fangcheng Chou, without whose very nice crystals and measurements we would not have gotten far. Furthermore, a number of people outside of MIT have contributed significantly to my research. I remember lots of enlightening correspondence with Philippe Monthoux and Peter Lemmens. I, too, remember with great pleasure the classes of Ian Affleck on one-dimensional magnetism, that he happened to teach at Boston University right before the subject became essential to my own research. Finally, I am highly grateful to Duncan Haldane, whose vivid and continued objections to a premature result of mine made it possible for me to set things right just on time. His two and a half hour private lecture on Luttinger liquids and one-dimensional lattice models remains as comprehensive in my memory as an entire one-term course on the subject.

I also wish to say very special thanks to Bruno Coppi, who made me a member of his group upon my arrival at MIT and thus made my studies at MIT possible in the first place. From him I learned a great deal, too, and I hope he has forgiven me my inability to resist the desire to work on quantum phenomena. I also feel very grateful for the companionship of my fellow student Ronak Bhatt during this time.

I do not want to forget a number of people that played an important role in my studies before I attended MIT. I could not have successfully applied to MIT without the kind support of Christian Simader, Dierk Rainer and Lorenz Kramer. Prof. Rainer's first term "Introduction to Theoretical Physics" at the University of

Bayreuth has had a long lasting impact on me, where equations were of a secondary importance compared to the lecturers asides on the cultural aspects of theoretical physics. The latter had a subtle tendency to work in favor of the impression that there hardly is a more desirable thing in the world than to become a theoretical physicist. During my time at Bayreuth, and long after, I have been most fortunate to receive the mentoring of Prof. Simader. He has given me a tremendous amount of support and advice throughout years, deepening my mathematical knowledge and much more. I highly enjoyed working as a teaching assistant in three of his courses on complex and functional analysis, and I very much appreciate that I was able to keep in touch with him as I gradually moved away from pure mathematics. I have never experienced a mathematician who was more enthusiastic about communicating mathematics to theoretical physicists, and I am sure if this were a more common phenomenon, there would be greater unity between the two fields. Also at Bayreuth, I was given the opportunity to write a term paper under the most inspiring supervision of Friedrich Busse. Finally, out of the many good friends and fellow students that shaped my student life before MIT I wish to give special thanks to Philipp Hoffmann, Horst Neuss, Tobias Sebald, Michel Grüneberg, Thomas Liebethal and Alexander Fink. During my stay in Boston I was most delighted to receive multiple visits from many of my faithful old world friends, that made sure I would stay in touch with my roots: Matthias Waal, Thomas Hasiba, Katharina Schickert, Rolf Imig. Most of all, however, my dear old friend Klaus Hakes, who made it over the Atlantic a total of four (!) times just to see to it that I would not forget the taste of his favorite traditional beverage.

My time at MIT has influenced my life way beyond the mere professional level. Before my first term had started, I had met my wonderful wife, Haiyan. She and our two children Max and Sophie have made the happiness of my life complete. I am forever grateful to my wife that she has been able to bear my strongly alternating moods during the past five years, a phenomenon that may probably seize even the most even-tempered young scientist. Moreover, I thank her and my children for their love and great emotional support at all times. At the same time, I thank my parents, whose love, encouragement, and total support I have always felt in many ways. The same is true for my grand parents, my brother and my grandaunt, who would never cease to call and inquire about the progress of my work. Finally, I wish to express my sincere gratitude to my mother-in-law, Fu Zhen Luo, who sacrificed the last months of her life by looking after our children and giving us homely comfort, together with her husband. The same gratitude goes to my father-in-law, Jiang Shao Kui, who nonetheless returned to stay with us the following year, being a tremendous help.

I gratefully acknowledge the support of the Studienstiftung des Deutschen Volkes during 1995-2001

To my family

Contents

List of Figures

List of Tables

Chapter 1

Introduction

I'll have my bond,
speak not against my bond,
I have sworn an oath that I will have my bond.

William Shakespeare

The theory of strongly correlated systems encompasses all phenomena in interacting many-body systems that cannot be understood by regarding the interactions of their constituent particles as weak. This is typically the case in systems with such great anisotropy that they can be thought of as effectively having a reduced dimensionality, as exemplified by the high temperature superconductors. The discovery of these fascinating cuprate superconductors by Bednorz and Müller in 1986 [1] has dramatically shaped the field. Since then the task of formulating a new theoretical phenomenology with predictive power for these materials and providing its microscopic foundation has been a major challenge. Many of the key question asked in the theory of high temperature superconductors apply at least in part to other strongly correlated materials, and they provide a framework within which many other systems can be discussed. This is particularly true and also tempting for a different, much less studied class of materials, the titanium oxyhalides TiOX. These materials have been investigated a few years after the discovery of the cuprates by Wilson et al. [2, 3], and a large part of this thesis is directly related to or motivated by the study of TiOCl. The obvious - though to a certain degree superficial - parallels between the TiOX materials and the cuprates continue to drive current research efforts on the TiOX family, but have also led to early misunderstandings of their basic nature. For this reason I will first give a short review of the phenomenology of the cuprate superconductors. Extensive reviews are available in the literature [4, 5, 6].

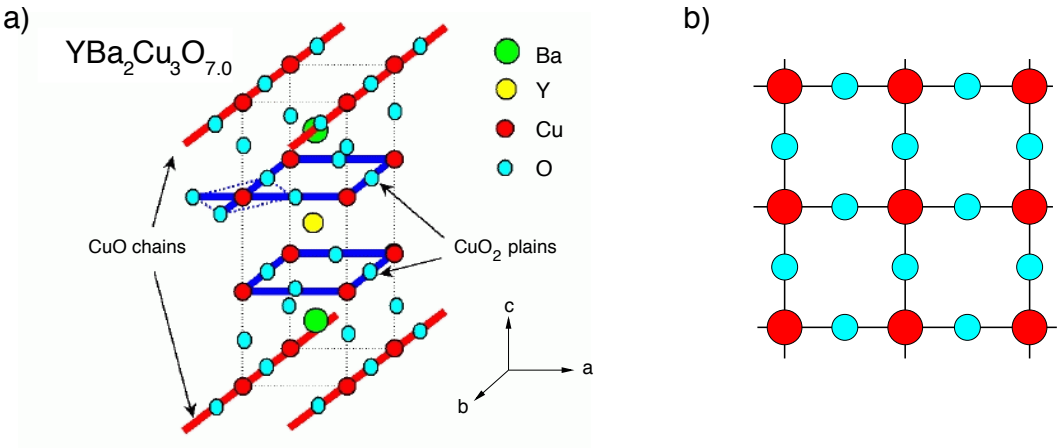

Figure 1-1: a) Structure of YBCO high temperature superconductors b) Cu-O plane

1.1 High temperature superconductors and RVB - spin liquids

The parent compounds of the high temperature superconductors are layered insulating materials featuring Cu-O planes (Fig 1-1 b), where Cu is in a d^9 configuration and has a spin 1/2. While band theory predicts these materials to have a half-filled conduction band formed by d-orbitals with $x^2 - y^2$ symmetry, the Coulomb repulsion in the plane is so strong that the electrons in this band "Mott-Hubbardize", giving rise to localized magnetic moments. This defines the high-T_c parent compounds as magnetic Mott-insulators. The admixture of oxygen p-levels into the magnetic d-orbitals gives rise to a superexchange between the local moments which has antiferromagnetic sign. Hence the parent compounds may be understood as two-dimensional antiferromagnets which Neel-order below a finite transition temperature T_N. When mobile holes are introduced by means of chemical doping, the general phase diagram sketched in Fig. 1-2 is obtained: Upon carrier doping, the materials become conductors and the antiferromagnetic phase (AF) is quickly destroyed. At zero temperature, the AF phase is either followed by a disordered spin glass state (LSCO) or directly by a superconducting phase (YBCO). The superconducting transition temperature first raises with doping and then reaches a maximum at an optimal doping of about 16%, upon which T_c decreases to zero by roughly 25 % doping. The bell shaped phase boundary is often referred to as the superconducting "dome" which resides between 5% and 25 % of doping. The maximum T_c at optimal doping is very high when compared to that of conventional superconductors, especially those known at the time of the discovery of the high-T_c superconductors. In the initially discovered LaBaCuO the optimum T_c was $35K$, whereas the highest T_c known to arise from a conventional BCS-mechanism at that time was $23K$ (Nb_3Ge). In the meantime, other classes of materials have been found to superconduct at temperatures comparable to those of the initially discovered La-based cuprates, such as the metallic compound MgB_2 with a T_c of $39K$ [7]. The mechanism giving rise to superconductivity in these materials is arguably the conven-

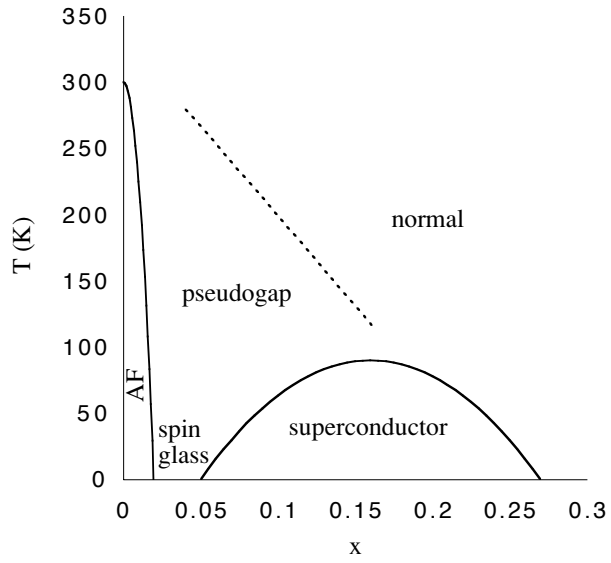

Figure 1-2: Phase diagram of high-T_c superconductors

tional Bardeen-Cooper-Schrieffer mechanism based on an effective electron-electron attraction mediated by phonon exchange. In the cuprates, however, the transition temperature had been further raised dramatically within a few months of the original discovery by varying the chemical composition. The discovery of $T_c = 93K$ in YBCO (Fig. 1-1a) first broke the liquid nitrogen barrier [8]. The current record holder at normal pressure is $HgBa_2Ca_2Cu_3O_8$ with a T_c of $133K$, and under pressure transition temperatures of $160K$ can be obtained.

While certainly, the instant popularity of the high-T_c cuprates among theorists and experimentalists alike was due to their extremely high value of T_c, this is by far not the only aspect of their complex phase diagram which is remarkable and puzzling. In fact, on a phenomenological level it is the superconducting phase which can be regarded as the most conventional phase of the cuprates. It features charge $2e$ superconducting carriers with an extremely short coherence length or order $20\mathring{A}$ in the plane and even much less perpendicular. Hence the superconducting phase can be understood as an extreme type-II superconductor with an experimentally well established d-wave pairing phenomenology. However, a superconductor is in a highly non-trivial collective state, and one can argue that such a state cannot be fully understood without a good picture of the normal state from which it is derived.

It is the non-superconducting phases of the cuprates which provide the most immediate challenges to theory. Away from the overdoped regime to the right of the superconducting dome, the normal state does not seem to conform to a Fermi-liquid picture. The temperature dependence of the resistivity is to a very good approximation linear. Although this behavior terminates abruptly when the superconducting transition temperature is reached, the proportionality between resistivity and temperature is so striking down to this point (see, for example, [9]) that it is in severe disagreement with Fermi-liquid theory, where a T^2 dependence is expected. Direct evidence for the breakdown of Fermi-liquid theory comes from angular resolved photo

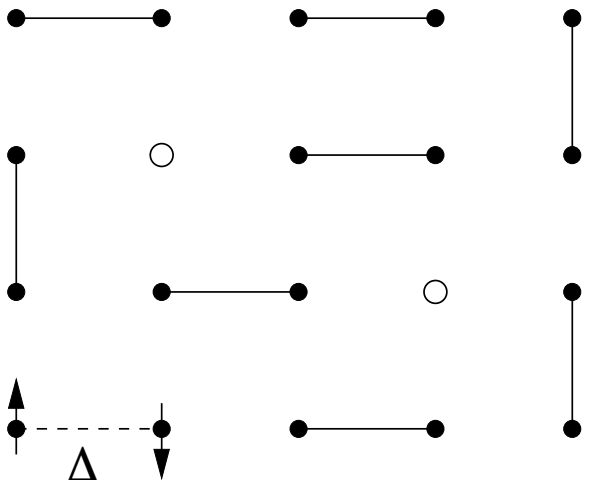

Figure 1-3: Snapshot of an RVB liquid. Lines represent singlet pairs of electrons, and open circles represent holes. The breaking of a dimer will cost a finite energy Δ

emission data (ARPES). There it is seen that a quasi-particle peak develops sharply at the transition temperature and is ill defined in the normal state [10], except in the highly overdoped regime. This is a severe difference from a conventional BCS-superconductor where the entities that form the superconducting Cooper-pairs are just given by the quasi-particles of the normal Fermi-liquid state above the transition. Therefore, in a conventional superconductor the quasi-particle is well-defined both above and below the transition, and its spectral weight is not much affected by the transition.

Another remarkable feature is the formation of a so called pseudo-gap in the underdoped regime. This means that all observations which probe the spin degrees of freedom such as NMR [11] and the Knight-shift [12] are consistent with the formation of a spin gap, while the charge excitations remain gapless. In addition, ARPES experiments measure the size of the gap as function of momentum k [13, 14] and show that it resembles the d-wave superconducting gap.

It is the description of the pseudo-gap phase where the various theoretical approaches to high-T_c problem differ most in a qualitative sense. Common to to many theories is a viewpoint formulated early on by Anderson [15], namely that the essential physics leading to the observed phenomena takes place in the Cu-O planes. Indeed, although more than 50 superconducting cuprates are known, they all share as a common feature that they have one or more Cu-O planes per unit cell, such as depicted in Fig. 1-1 b). No other class of materials has been found to exhibit the same phenomenology. This point of view suggests that the key question to be addressed by theory is the question of what happens when holes are doped into a two-dimensional Mott-insulating state. Anderson himself has formulated an answer which is known as the "resonating valence bond" (RVB) scenario. He observed that Néel order is not favorable for hole hopping, since one hop would lead to a pair of ferromagnetically

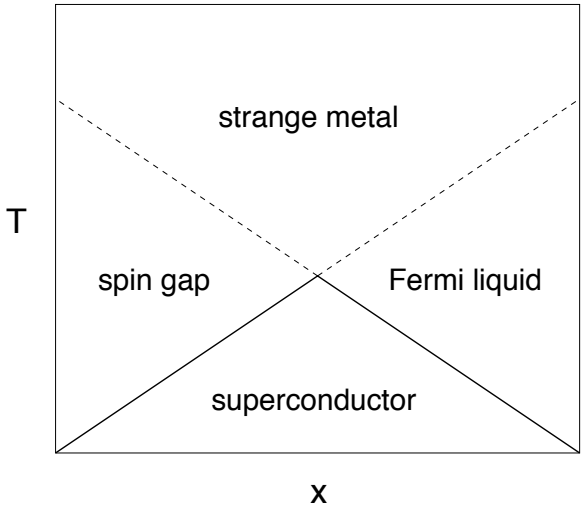

Figure 1-4: Generic phase diagram based on RVB mean-field theory.

ordered spins. He proposed that at a small finite concentration of holes it would be favorable for the spins to form fluctuating short-ranged singlet pairs which he termed "resonating valence bonds".

According to the RVB-picture the ground state is a complicated superposition of states such as shown in Fig. 1-3, and hence would be a singlet of unbroken rotational symmetry. Breaking a singlet pair will cost an energy Δ of order J, where J is the antiferromagnetic exchange between neighboring sites. This is independent of the fact whether the holes move coherently or not, hence the pseudogap phenomenology of a spin gap existing above T_c may be explained by this picture. These ideas may be formalized using sophisticated mean-field theories [16, 17, 18], which give rise to the generic phase diagram of an RVB-liquid displayed in Fig. 1-4 [19]. One notes the resemblance to the phase diagram of the cuprates Fig. 1-2. The pseudo-gap will make itself felt in the underdoped regime whenever the temperature is below the singlet pair breaking gap Δ, which is argued to be largest for the undoped insulator at $x = 0$[16]. Phase coherence, on the other hand, is determined by a different energy scale which is argued to be proportional to the doping x. The two scales associated with carrier coherence and singlet pairing give rise to the two lines drawn in Fig 1-4 and the four regions shown. The only phase exhibiting long range order in this scenario is the superconducting phase, given by the triangular "dome" below the coherence scale and the singlet pairing scale. Note that the narrow antiferromagnetic phase is not captured in the RVB-picture. Also, the boundary between the strange metal and the spin gap phase is regarded as a cross-over. In other approaches to the high-T_c problem, the pseudo-gap phase is sometimes viewed as a separate phase with a hidden order.

The idea of the separation of the spin and charge degrees of freedom is central to the approach reviewed here and is most evident in the spin-gap regime, where charge degrees of freedom are gapless while spin excitations are gapped. It is a great

theoretical challenge to support this concept from a microscopic point of view. An important technical tool which incorporates this is the introduction of slave particles. This has been applied to derive the phase diagram Fig. 1-4 both at the mean field level (e.g. [18]) and beyond in combination with non-abelian gauge fields [20]. The microscopic models that are widely believed to serve as a good starting point for a qualitative description of the cuprate physics are formally quite simple. Central to the RVB-approach is the one-band Hubbard model on a two-dimensional square lattice, according to the original proposal of Anderson [15]:

$$H = -t \sum_{<ij>} \left(c^{\dagger}_{i,\sigma} c_{j,\sigma} + h.c. \right) + \frac{U}{2} \sum_{i} (n_i - 1)^2 \tag{1.1}$$

Here, $c_{i,\sigma}$ destroys a fermion of spin projection σ on lattice site i, which is to be identified with one of the copper sites of the Cu-O plane shown in Fig. 1-1 b). The hopping sum goes over all nearest neighbor links $< ij >$ of the lattice. Each site may accommodate at most two electrons of opposite spin, which repel each other via the on-site repulsion U. Despite its simplicity, the Hubbard model is difficult to treat in two dimensions, which may be interpreted as a sign of its potential to capture the physics of a strongly correlated Fermi system. Often, another model is preferred which is related to the $U \to \infty$ limit of (1.1), the $t - J$ model:

$$H = -t \, \mathcal{P} \sum_{<ij>} \left(c^{\dagger}_{i,\sigma} c_{j,\sigma} + h.c. \right) \mathcal{P} + J \sum_{<ij>} \left(S_i \cdot S_j - \frac{n_i n_j}{4} \right) \tag{1.2}$$

The $t - J$ model is defined on a reduced Hilbert space where double occupancies of a site by two electrons is forbidden due a an infinite on-site repulsion. $\mathcal{P}$ is a projection operator that projects onto the singly occupied subspace which is otherwise not respected by the hopping term. The S_i are spin-$\frac{1}{2}$ operators. Naturally, the true large U limit of the Hubbard model can have only one free parameter, hence the $t-J$ model rigorously corresponds to this limit of the Hubbard model only at infinitesimal $J = 4t^2/U$ [21][1].

The $t - J$ model is the usual starting point for the aforementioned slave-particle approaches. Then main technical difficulty in treating this model is to deal with the constraint of no double occupancy in an appropriate manner. It has to be enforced "by hand" in some sense, since it is not embodied in the usual fermion commutation relations which do allow particles of opposite spin to have identical spatial coordinates. In the $t - J$ model, each lattice site has exactly three possible states: Spin up, spin down, or empty (= 1 hole present). It is not possible to incorporate such a three level site space into a simple enough algebra which also reproduces the usual fermion negative sign. This is why some approaches to the $t - J$ model do in fact live in larger Hilbert spaces with "artificial" degrees of freedom that introduce a gauge symmetry. This artificial symmetry ensures that the physics is precisely reduced to that of the $t - J$ model with its fewer degrees of freedom. In some sense, the larger gauged space simply consists of many redundant copies of the physical space without

[1] Also, when the large U-limit of (1.1) is taken, next-nearest neighbor terms appear which are higher order in the carrier concentration and may be dropped at small doping.

altering the physics. For much the same reason it is convenient to introduce gauge fields in electrodynamics, especially on the quantum level, in order to represent physical fields that are constrained by Gauss's law in terms of unconstrained fields. [2] For the $t-J$ model such a mapping onto a gauge theory may formally be achieved by the introduction of slave particles. However, this kind of mapping does by no means lead to an almost free theory, but rather to a very strongly interacting theory, making crude approximations necessary. The primary success of this approach has therefore been the qualitative derivation of the phase diagram Fig. 1-4. However, the interaction is so strong that in the simplest $U(1)$ slave particle gauge theory, the mean field solution is unstable towards fluctuations [22]. Only a more complicated non-abelian gauge theory, which preserve a hidden $SU(2)$ symmetry that exists only at half filling in the $U(1)$ formulation, gives rise to stable mean field results [20].

The slave particle methods discussed above can be tested successfully in one-dimensional systems (see, e.g., [23]), where much more powerful alternative mappings are available. The latter will be discussed in detail in a later chapter of this thesis. However, in one dimension the success of the slave particle techniques is made possible because the gauge fields may be integrated out exactly, which is not possible in higher dimensions. Indeed, one can argue that in one spatial dimension it is absolutely necessary to enforce the constraint exactly, otherwise results may be qualitatively wrong [24].

These difficulties are manifestations of the inherently strongly correlated nature of the high-T_c problem. Another problem is that, both theoretically and experimentally, no simple physical limit can be taken in describing the non-trivial normal state. For example, one would like to study the strange metal phase at very low temperatures, in order to understand it "ground state". However, the true ground state of the cuprates is superconducting. Hence, at least experimentally, a phase transition always intervenes when going to low temperatures. The only thing left to study then is the core state of magnetic vortices, which arguably will share some signatures of the normal state at low temperatures. Theoretically, one might also be interested in studying the limit of very small doping, or no doping at all. However, at small doping and sufficiently small temperatures the system is in a Néel ordered state, which is again quite unrelated to the strange metal phase. This is in fact very well captured by the Hamiltonian 1.2, which is reduced to a two-dimensional antiferromagnetic Heisenberg model at zero doping. Although this problem is lacking an exact solution, it is well known from numerics that this model indeed has a Néel ordered ground state [25].

It was again pointed out by Anderson that the latter problem may not be fundamental, and that a two-dimensional spin-$\frac{1}{2}$ system might be able to support a symmetry unbroken ground state, due to strong quantum fluctuations for a spin-$\frac{1}{2}$ system. Such a system is called a "spin liquid". The idea is that since the Néel order is so quickly destroyed by doping in the cuprates, its presence in the phase diagram is irrelevant and the physics of the normal state is that of a doped spin liquid. In the idealized RVB phase diagram there is no trivial Néel ordered state – the undoped system is a spin liquid, which is already a complicated correlated state

[2] I thank T. Senthil for this insight.

and is in principle not separated from the normal state by a phase transition, except for the absence of charge degrees of freedom. If indeed such a spin liquid exists in two dimensions, certainly much could be learned from it. It might not only cast light on the high-T_c problem, but being a complicated quantum phenomenon it would be interesting in its own right.

However, it has turned out that such quantum spin liquids are scarce and are very hard to stabilize in both theory and experiment. Since the Heisenberg model on a square lattice is known not to fulfill the requirement, the search is focused on systems with a frustrated exchange geometry. The term "frustrated" refers to a situation where competing antiferromagnetic exchange couplings are present that would favor different kinds of ordered states. Such systems tend to have hugely degenerate ground states in the classical limit. It is then intuitive that quantum fluctuations will destroy order even at zero temperature. Some systems such as a triangular lattice are automatically frustrated by lattice geometry, but frustration may also be present on a square lattice when diagonal exchange terms are added. Also discussed in the literature are *chiral* spin liquids [26], which do have the full lattice translational and rotational symmetry but have a broken time-reversal symmetry.

Although a number of models have been proposed to have a spin liquid ground state, a rigorous analytic proof for the existence of a two-dimensional quantum spin liquid is still an open problem (although recently some progress has been made numerically [27, 28]). This is not surprising, since even the negative result for the Heisenberg model on a square lattice – arguably the best understood spin-$\frac{1}{2}$ model in two dimensions – is ultimately based on numerical evidence. Clearly, even the undoped precursor of the high-T_c problem, the quantum spin liquid, is an enormously challenging problem.

1.2 Outline of the Thesis

Chapter 2 will discuss the properties of the layered Mott-insulating spin-$\frac{1}{2}$ system TiOCl. This material had been proposed in the early 90's to show spin liquid behavior down to very low temperatures [3]. These interpretations were based on measurements of the uniform magnetic susceptibility, that showed some extraordinary features such as comparatively strong paramagnetism with very weak dependence on temperature, and strong sensitivity to doping with non-magnetic impurities. These experiments were repeated recently at MIT and have lead to a quite different picture of TiOCl. The new data can be explained in terms of quasi one-dimensional spin chains, where the spins reside in certain t_{2g} orbitals with direct overlap. This picture is found to agree well with LDA band structure calculations. A first-order like transition into a spin-gapped low temperature phase is clearly revealed by the new data and is interpreted as a spin-Peierls transition. However, the detailed features of this transition deviate from the standard mean-field theory of a spin-Peierls transition. This may be explained in terms of the quite unique and frustrated interchain geometry of TiOCl. It will be shown that a simple Ginzburg-Landau approach, which properly

takes into account these frustration effects, can explain the unusual first order like nature of the transition. With the exception of this last aspect, the results of this chapter have been published in [29].

Although carrier doping has so far been unsuccessful in TiOCl, these new experimental findings have motivated a study of a carrier doped dimerized magnetic chain presented in chapter 3. It is argued that such a doped dimerized insulator may be an ideal environment for a one-dimensional realization of the the resonating valence bond scenario. This will be examined in the context of the tJJ'-model in one dimension. To this end, the phenomenology of gapless one-dimensional systems and their low-energy effective theory, the Luttinger liquid, will be reviewed in some detail. This way, some basic notation and elementary facts are established that the results of this chapter heavily rely upon. The numerical phase diagram of the tJJ'-model will be briefly discussed, which does exhibit pronounced regions of strong superconducting correlations. At small doping x, this is especially the case in the regime $J'/J > \alpha_c \approx .24$, in which the undoped spin chain is dimerized. However, the fate of these strong superconducting correlations at very small doping is not unambiguously revealed by the numerics. In particular, it is not clear whether the occurrence of these strong superconducting correlations requires a certain minimal ratio of the exchange scale and the band width scale J/t, or if they occur at any value of J/t for small doping x. A perturbative approach that manifestly incorporates spin-charge separation will be developed to clarify this. The convergence of this approach will be demonstrated at second order perturbation theory, and at higher order by general arguments given in appendix A. If present at small J/t, this perturbative approach should be able to access the regime of strong pairing correlations, as well as an instability towards phase separation, by which the pairing regime is bounded. However, the result for the existence of this kind of instability and its accompanying pairing correlations at small J/t will be negative. Instead, the liquid phase is found to be a stable gas of non-interacting charge solitons in the limit $x \to 0$ at small J/t, which move in a background formed by the gapped magnetic insulator. This behavior is a manifestation of spin-charge separation, and is generally expected for one-dimensional lattice models whose homogeneous phase is stable in the dilute carrier limit. However, a firm demonstration of this fact can usually be given only for integrable models. Here, it will emerge for a non-integrable model, based on a perturbative approach in combination with Luttinger liquid arguments. Naturally, this demonstration is limited to a finite order in perturbation theory. Since non-trivial cancellations are responsible for the results in second order perturbation theory, the same analysis is also carried out at third order perturbation theory (appendix C), where a more complicated but ultimately similar pattern emerges, confirming the result. Non-trivial quantities such as the single hole energy and mass renormalization are evaluated in second order perturbation theory. They are compared to a variational approach, which gives further insight into the polaronic effects of the holes on their spin environment and is in good agreement with the perturbative results. An important technical detail is discussed in appendix B.

Chapter 2

TiOCl – spin chain compound or two-dimensional RVB liquid ?

It is often safer to be in chains than to be free.

Franz Kafka

Transition metal oxides frequently exhibit a complicated low dimensional structure. As discussed in the previous chapter, this may give rise to interesting magnetic and other strongly correlated phenomena. Since the discovery of the high temperature superconducting cuprates, the primary focus has been on the study of compounds of transition metals at the upper end of the transition metal series, in particular involving Cu^{2+} with a d^9 configuration and a spin-$\frac{1}{2}$. More recently, increased emphasis is put on $S = \frac{1}{2}$ materials involving lower end transition metal ions, such as V^{4+} and Ti^3+, which have a single d-electron. These ions are predominantly encountered in a quasi-octahedral configuration. This lowers the energy of the t_{2g}-orbitals, whose lobes point away from the coordinating ligands (Fig. 2-1). The single d-electron is then placed in a t_{2g}-orbital. Such a configuration is energetically favorable and not very susceptible to Jahn-Teller effects, since the t_{2g}-orbitals usually do not have significant overlap with the ligand orbitals. As a result, the t_{2g}-orbitals may sometimes remain nearly degenerate. This can give rise to physics quite different from that in the cuprates, where the spin is attributed to a hole residing in an e_g orbital. The near degeneracy of t_{2g}-orbitals in Ti based compounds may lead to the importance of orbital fluctuations [30], as is probably the case in $LaTiO_3$[31].

Nonetheless, the Mott-insulating Ti oxyhalides TiOX had been under scrutiny back in the late 80's and early 90's by the group of Wilson et al. [2, 3], motivated by the idea of finding cuprate-like physics in a Ti^3+ system at the opposite end of the transition metal series. They studied the magnetic susceptibility of TiOCl and TiOBr and reported indications for an RVB spin liquid type of behavior in these materials. In the following chapter, their basic ideas and findings are reviewed and the structure of the materials is presented. Hereafter, more recent experiments and their theoretical interpretations will be reported.

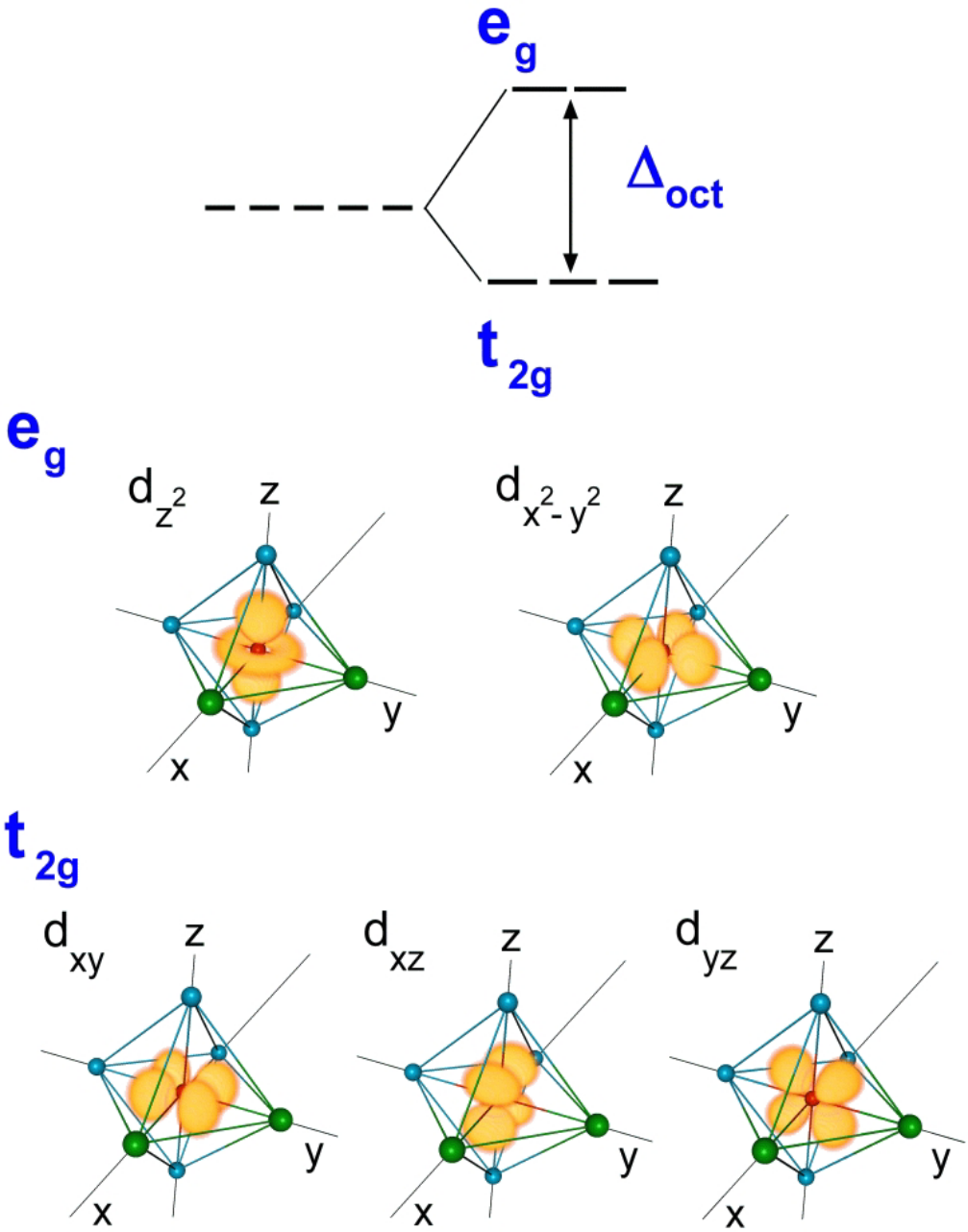

Figure 2-1: Octahedral splitting of *d*-states. In TiOCl the octahedra are formed by two Cl (front, slightly bigger) and four O atoms.

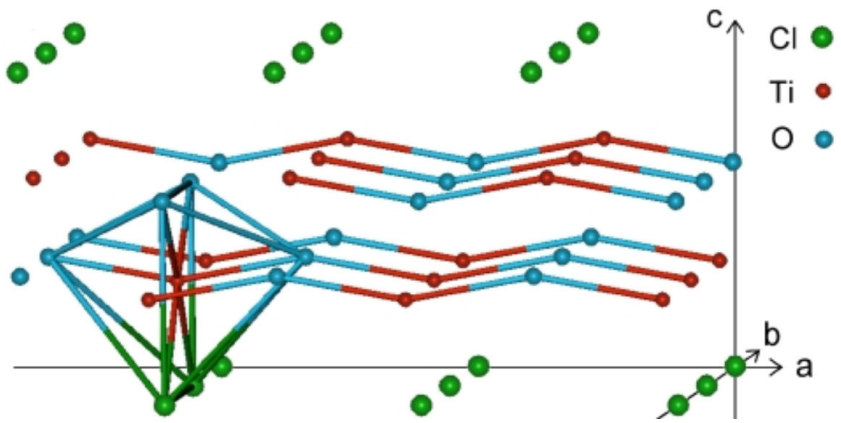

Figure 2-2: Structure of TiOCl. A single bilayer is shown. Note that each Ti is surrounded by 4 O and 2 Cl, forming a distorted octahedron. These octahedra are corner-sharing along a and edge-sharing along b.

2.1 TiOCl, TiOBr – Structure and Motivation

The structure of TiOCl is of the quite unfamiliar FeOCl-type. It consists of bilayers as displayed in Fig. 2-2. The symmetry is orthorhombic with $Z = 2$ atoms of each sort per unit cell. The layers repeat themselves in the c-direction of the crystal with a lattice constant of $c = 8.03$Å. Cl layers mediate a weak van der Waals interaction between successive bilayers. Within each bilayer, Ti and O form two layers of buckled chains along the a-direction, where Ti is always on the outer side with respect to the bilayer. Note that these buckled chains are introduced for the purpose of describing the crystal structure only, and are not supposed to imply anything about chemical bonding at this point. The O-Ti-O bond angle is 153°. Each Ti ion is surrounded by a distorted octahedron of O and Cl ions, as indicated in Fig. 2-2. These octahedra are formed by two O ions belonging to the same Ti-O chain, two O ions belonging to neighboring chains, and two Cl which lie on the outside of the bilayer. The point group of the Ti site is C_{2v}, which contains a two fold rotation axis (parallel to the c-direction) and two mirror plains containing this axis. The octahedral cages are corner-sharing in the a-direction along the Ti-O chains and edge-sharing in the b-direction.

Fig. 2-3 is a top view of the lattice showing only the Ti ions for clarity. The Ti sublattice consists of two rectangular layers with lattice parameters $a = 3.79$Å and $b = 3.38$Å in each layer. The top layer is shifted laterally and is displaced vertically from the bottom layer by 1.96Å. The shortest Ti-Ti bond length turns out to be that of the links shown in Fig. 2-3 connecting Ti in different layers. This bond length of 3.21Å is just slightly shorter than the Ti-Ti distance along b.

It is seen that apart from the staggering of the Ti lattice the Ti sites do roughly form a square lattice when projected into a single plain. From this point of view the Ti layers bear some resemblance to the Cu-plains of the cuprates shown in Fig. 1-1

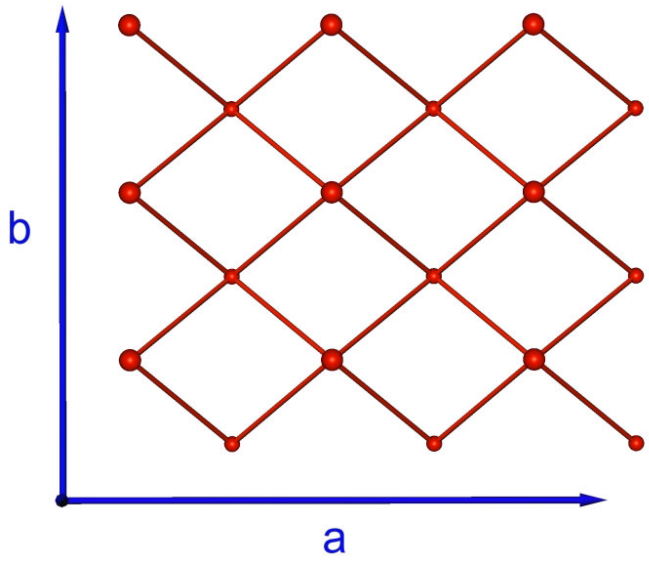

Figure 2-3: Ti sub-lattice. View from the top along the c-axis. Atoms that appear bigger are closer due to staggering.

b). Both materials feature two-dimensional planes of spin-$\frac{1}{2}$'s on a square lattice, or a somewhat distorted version thereof. This motivated Wilson and his collaborators to investigate whether the spins in this material show signatures of a resonating valence bond spin liquid at low temperatures even in the absence of doped carriers. This was certainly an exciting prospect, since the cuprates do not show quantum spin liquid behavior in their undoped insulating phase, but rather show quite classical Néel order. In order to investigate whether the spin state undergoes a phase transition at low temperatures or not, Wilson et al. measured the uniform magnetic susceptibility of the TiOCl (Fig. 2-4) and TiOBr (Fig. 2-5).

The susceptibility data of pure TiOCl as measured by Wilson, the curve labeled a) in Fig. 2-4, has some striking properties. One notes that the susceptibility is paramagnetic, and in a large temperature regime almost independent of temperature. Indeed, no sign of a phase transition can be noted even at temperatures of a few K. Such temperature independent paramagnetism is usually associated with metallic behavior. The TiOX materials, however, are insulating. Also, the magnitude of the measured susceptibility is very large compared to the Pauli susceptibility of a typical metal. To appreciate this, one may recall that on dimensional grounds the molar magnetic susceptibility of a spin-$\frac{1}{2}$ system is of the simple form

$$\chi^{mol} \sim \frac{N_A \mu_B^2}{\text{energy scale}} = .375 \, \frac{K}{\text{energy scale}} \, \frac{\text{cm}^3}{\text{mol}} \tag{2.1}$$

where N_A and μ_B are Avogadro's constant and Bohr's magneton, respectively [1].

[1] CGS units are assumed here. In SI-units, an overall factor of 4π appears

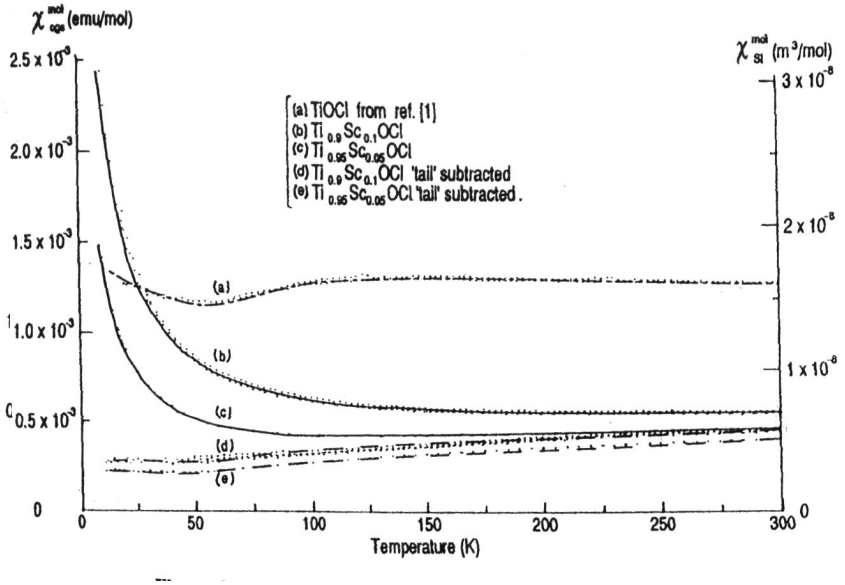

Figure 2-4: Susceptibility of TiOCl by Wilson et al. a) pure TiOCl b) $Ti_{.9}Sc_{.1}OCl$ c) $Ti_{.95}Sc_{.05}OCl$ d) $Ti_{.9}Sc_{.1}OCl$ with Curie-tail subtracted e) $Ti_{.95}Sc_{.05}OCl$ with Curie-tail subtracted

The energy scale which enters here greatly varies for different classes of materials. For free spins, it is to be set equal to the temperature T of the system, whereas in an antiferromagnet, T is to be replaced by the exchange energy scale J for $T \lesssim J$. In a metal, however, the energy scale is to be identified with the Fermi energy ϵ_f, which is typically a multiple of $10^4\,K$. This large energy scale is the reason why the susceptibility of metals is to a good approximation temperature independent, even at T much larger than room temperature. At the same time, it is the reason why metals have a relatively *small* paramagnetic susceptibility. From Fig. 2-4 however, the susceptibility of TiOCl at room temperature inferred by Wilson is comparable to that of free spins and stays at this value down to very low temperatures[2]. This observation makes it obvious that a conventional mechanism can hardly explain the curve measured by Wilson et al. Its flatness demands an energy scale considerably larger than room temperature, its magnitude implies an energy scale no larger than room temperature. However, it must be taken into account that the susceptibility measured in an experiment consists of several contributions:

$$\chi_{\text{experiment}} = \chi_{\text{spin}-\frac{1}{2}} + \chi_{\text{orbital}} + \chi_{\text{core}} + \chi_{\text{impurities}} \tag{2.2}$$

Only the first contribution one is usually interested in. It is due to the correlated spins. The second term arises from the polarization of the d-orbitals and is paramagnetic. When the d-orbitals are energetically well separated, this terms is small

[2]For free spin-$\frac{1}{2}$'s, relation (2.1) becomes an identity when the temperature is plugged in as energy scale.

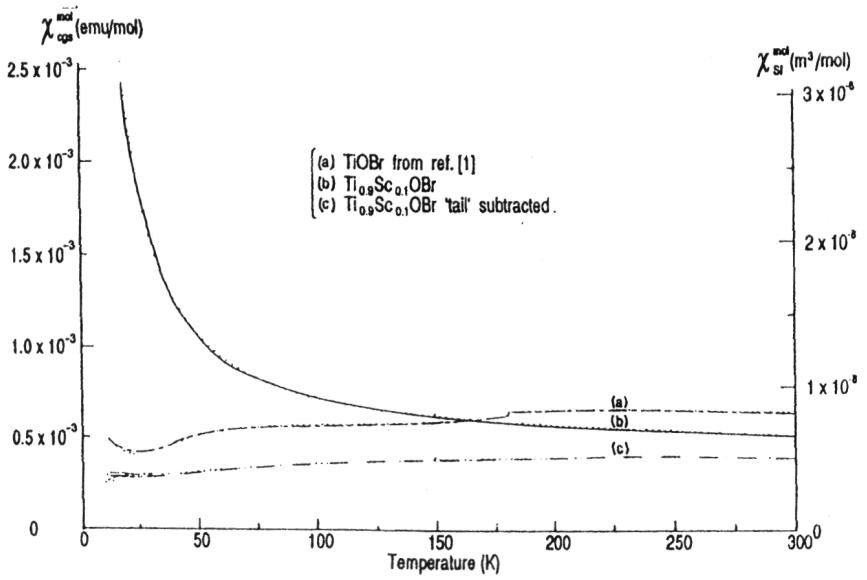

Figure 2-5: Susceptibility of TiOBr by Wilson et al.

and temperature independent, and is referred to as van Vleck paramagnetism which occurs already at the atomic level for atoms with partially filled shells. However, when the d-orbitals are almost degenerate, then one expects spin and orbital degrees of freedom to be correlated in a complicated manner. In this case one cannot separate the first two contributions in (2.2), neither theoretically nor experimentally, and one is naturally interested in measuring this combined contribution of the correlated spin-orbital degrees of freedom. However, it will later be argued that this is not the case in TiOCl, and the second term is to be thought as small paramagnetic background contribution. Similarly, the third term in (2.2) is a small diamagnetic contribution from the filled shells of the atomic cores, which is also temperature independent to good approximation. The last term is due to paramagnetic impurities. In a pure sample these are very dilute and act as free spins. This gives rise to a small Curie tail at very low temperatures which is easily subtracted, as has been done in curve a) of Fig. (2-4). On the other hand, the van Vleck and core-diamagnetic contributions may give rise to an uncertain temperature independent background. The magnitude of this background is hard to infer when the net susceptibility is almost featureless, such as curve a). Wilson et al. tried to clarify this point by doping the Ti lattice with non-magnetic Sc impurities. This may be thought of as the analogue of Zn doping in the cuprates, for Sc has one less valence electron than Ti. Sc will replace Ti on various sites, and will be in a d^0 configuration with no spin-$\frac{1}{2}$ left. Quite naturally, one expects this to affect only the first and presumably largest term in (2.2). Curves b) and c) in Fig. 2-4 show the results of 10% and 5% Sc doping, respectively, as measured by Wilson et al. First of all, one notes that a significant Curie tail is formed at low temperatures. Wilson et al. reported that the strength of this tail corresponds to the introduction of one free spin-$\frac{1}{2}$ per substituted Sc impurity.

It is even more remarkable that the flat high temperature part of the susceptibility is reduced by a large amount. Curves d) and e) show the Sc-doped curves after subtraction of the curie tail, upon which one again obtains flat curves. The interpretation which Wilson et al. gave for the observed drop in susceptibility was that the spin contribution to the susceptibility is due to a highly non-trivial mechanism which is very sensitive to doping of non-magnetic impurities and which is completely destroyed in the 5% and 10% doped samples. Hence, the almost identical flat curves d) and e) in Fig. 2-4 were assumed to correspond to the zero level of the spin susceptibility, where only the van Vleck and diamagnetic core contributions are present. This would seem to answer the question of background contributions, and suggests the presence of an unconventional mechanism which produces a spin susceptibility that is temperature independent and yet comparatively large. Wilson et al. took this as evidence that the physics of the spins in TiOCl may be that of and RVB spin liquid. Indeed, the original RVB scenario allows for the existence of a "spinon Fermi-surface" in the normal state, which renders the spectral properties of the spin degrees of freedom similar to those of a spinless metal [15].

However, the outcome of the TiOBr experiment casts some doubt on these interpretations. Fig. 2-5 shows the susceptibility of pure TiOBr (a) and 10% Sc doped TiOBr before and after Curie subtraction, (b) and (c) respectively. One notes that while most features look qualitatively similar to TiOCl experiment, the large drop of the high temperature part of the susceptibility is completely absent. This would then suggest – following the same reasoning – that the mechanism which is responsibly for the large difference in susceptibility between impurity doped and undoped TiOCl is either not at work in TiOBr at all, or gives rise to magnetism of a very different order of magnitude. Chemically, however, TiOBr is much the same as TiOCl; it has the same crystal structure where Br replaces Cl far away from the Ti-O layers. Such different behavior in two such similar chemical compounds does not seem likely.

These interesting and astounding findings by Wilson et al. have motivated further investigation at MIT. Those will be described in the following sections, and will lead to quite different interpretations.

2.2 Crystal field and band structure aspects

As far as the Ti d-orbitals are concerned, the most important structural feature of TiOCl is the octahedral coordination of the Ti site, as pointed out in the beginning of this chapter. The octahedral cages will dictate a local coordinate system at each Ti site, and – if other influences are neglected – impose certain geometries on the d- orbitals by symmetry, where the t_{2g}- orbitals are lowered in energy (Fig. 2-1). If these orbitals are just as given in Fig. 2-1 and are not significantly hybridized, then it turns out that the t_{2g}-orbitals have the tendency to form one-dimensional chains. This is illustrated in Fig. 2-6. The z-axis of the local coordinate system (not shown) is chosen along the a-direction. The x- and y- axes are rotated by 45° with respect to the a- and b- axes, such that they roughly (because of the distortion of the octahedra) coincide with the diagonals of the square formed by the upper two oxygen atoms and

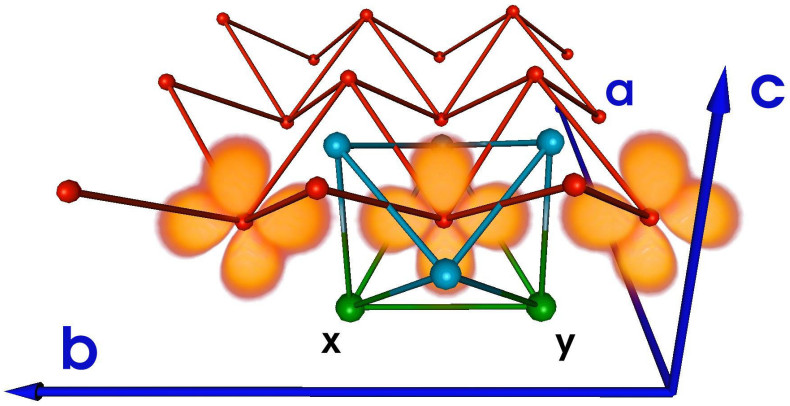

Figure 2-6: Front view on liner chains in b-direction formed by d_{xy}-orbitals. The Cl atoms labeled x and y correspond to those shown in Fig. 2-1 and roughly define the x- and y- directions of the local octahedral Ti- coordinate system (see text). The z-direction is given by the a-axis.

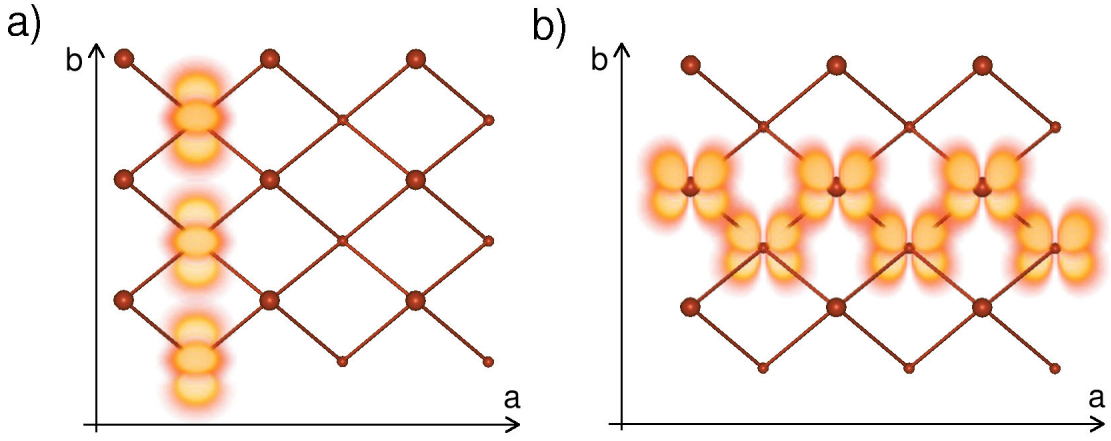

Figure 2-7: Top view on linear and zig-zag chains. a) Linear chains running along the b-direction formed by d_{xy}-orbitals. b) Zig-zag chains running along the a-direction formed by d_{yz}-orbitals.

the lower two Cl atoms of the octahedron shown in Fig. 2-6. With this choice of axes, the two Cl atoms labeled x and y correspond precisely to the two front most atoms on the x- and y-axis in Fig. 2-1. The $d_{x^2-y^2}$ and d_{z^2}-orbitals point towards the oxygen and chlorine neighbors as required for e_g-orbitals. The important orbitals are the t_{2g}'s (d_{xy}, d_{xz} and d_{yz}). It turns out that these orbitals link nearest- and next-nearest-neighbor Ti-sites. This is assured by the edge sharing property of the octahedral cages in the b-direction and by their corner sharing property in the a-direction (Fig. 2-2). This way, the links between two nearby Ti-atoms always cross one of the octahedral edges and are thus parallel to the lobes of the t_{2g}-orbitals.

The d_{xy}-orbitals form linear chains running along the b-axis, linking Ti ions in the same layer. This is shown in Fig. 2-6. Apparently, the overlap of these orbitals is essentially one-dimensional, for the two lobes perpendicular to the b-axis do not point at any neighboring atoms (see also Fig. 2-7a). The remaining t_{2g}-orbitals, the d_{xz} and d_{yz}-orbitals, have lobes pointing along the direction of the nearest neighbor Ti-Ti links. Thus two of their lobes will point at a nearest neighbor Ti atom on the opposite layer, while the other two lobes are not bonding. This way, they form one-dimensional zig-zag chains along the a-direction. Fig. 2-7b) shows this for the d_{yz} orbital – similar chains are formed by the d_{xz}-orbitals. The d_{xz} and d_{yz}-orbitals are degenerate by symmetry; note, however, that the point group C_{2v} of the Ti site does not have any two-dimensional irreducible representation. As a consequence, any single particle theory would always mix the d_{xz} and d_{yz}-orbitals. One may nonetheless ask the question whether correlation effects can lead to orbital ordering in the sense that only one of the two orbitals is occupied and zig-zag chains are formed.

All these considerations point at a possible one-dimensional character of the d-electrons. However, the arguments given thus far assume that the states at the Fermi level are t_{2g}-like electrons. In order to confirm this, and to investigate orbital ordering, the band structure has been calculated in linear density approximation (LDA), as well as LDA+U. The latter allows the inclusion of a non-local orbital-dependent potential that mimics the effects of an on-site repulsion in a self-consistent way [32]. Both these methods are preferred for the study of magnetic insulators, because of their ability to yield a magnetic solution.

Fig. 2-8 shows the results of these calculations carried out by C. A. Marianetti. All calculations made use of the full-potential LMTO [33] method and were performed using the LmtART code [34], and the experimentally determined unit cell [35]. Both LDA and LDA+U calculations yielded a magnetic moment of $1\mu_b$ per formula unit. This means that the solution is ferromagnetic. However, a qualitatively similar antiferromagnetic solution was close in energy but could not be stabilized [3]. Hence, in the following discussion, the band structures and DOS correspond to the majority spin bands, as the minority spin bands for the d-states are completely unoccupied.

Fig. 2-9 shows the site-decomposed density of states. As shown, the oxygen and chlorine p-levels form well separated bands from the Ti d-levels with only small hybridization between the two.

[3] C. A. Marianetti, private communication

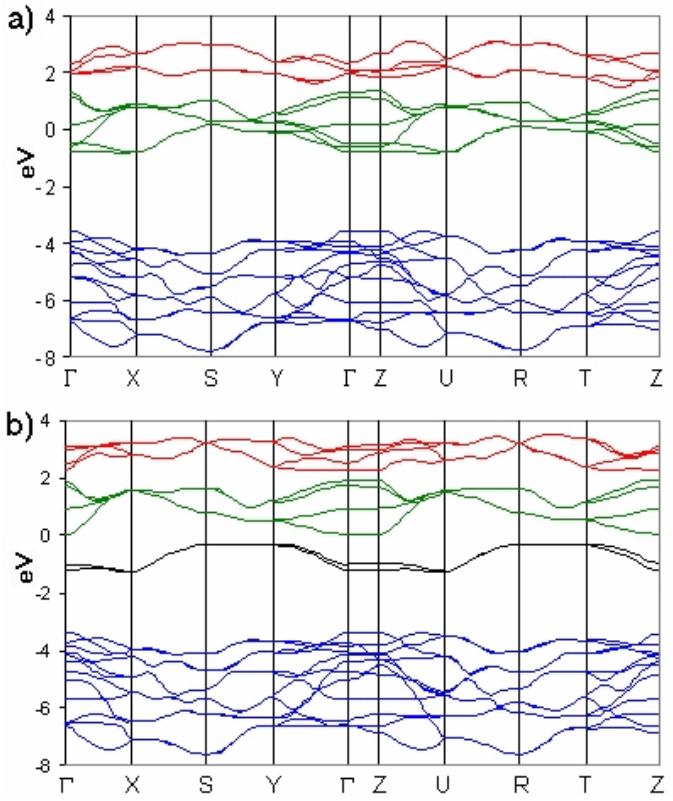

Figure 2-8: a) LDA band structure calculation for TiOCl. The Brillouin zone is orthorhombic with $X = 2\pi\hat{x}/a$, $Y = 2\pi\hat{y}/b$, $Z = 2\pi\hat{z}/c$ and S is the zone corner. The unit cell contains 2 Ti atoms. 6 bands around the Fermi level are identified as t_{2g} bands well separated from the e_g bands. b) LDA+U band structure calculation with split off d_{xy} bands.

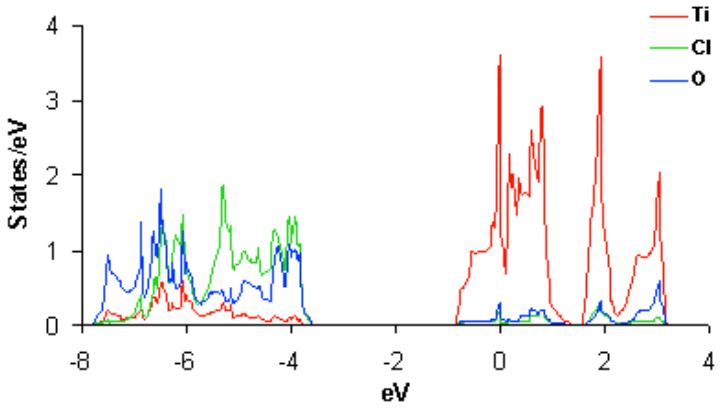

Figure 2-9: LDA-DOS projected onto Ti, O and Cl orbitals

Also, the octahedral crystal field has clearly split the d-states into t_{2g} and e_g contributions, with the Fermi level lying within the t_{2g} peak as expected for a d^1 configuration. These features can also be seen in the band structure (Fig. 2-8a)). Therefore, the assumption of t_{2g}-like electrons at the Fermi level is valid. However, LDA predicts this material to be metallic, and projecting the DOS onto the t_{2g}-orbitals indicates that all three orbitals are partially occupied (not shown). It was hence necessary to go beyond the LDA and explicitly include the effect of strong on-site interactions. This is achieved by the LDA+U calculation (Fig. 2-8b). Calculations were performed with $U = 3.3eV$ and an on-site Hund's coupling of $1eV$. As shown, two nearly degenerate, one-dimensional bands split off from the rest of the t_{2g} bands creating an insulator (note that there are 2 atoms per unit cell). These two bands are derived from the d_{xy}-orbitals corresponding to the linear chains in Figs. 2-6, 2-7a). Varying U only had a significant effect on the splitting between the occupied and unoccupied bands, not on the shape or width of the occupied bands. The LDA+U calculations thus seems to favor the picture of linear spin chains along the b-direction of the crystal discussed above.

We may use the band structure results to roughly estimate the order of magnitude of an antiferromagnetic exchange constant J in an effective Heisenberg model. We identify the band width of $0.9eV$ with $4t$, where t is the nearest neighbor hopping in a one-dimensional tight binding model. Using $U = 3.3eV$ as in the LDA+U calculation, we have reasonable values for the two parameters in eq. (1.1). The mapping that leads to eq. (1.2) then yields $J = 4t^2/U = 714K$.

2.3 New experimental data and theoretical fit

Although the LDA calculations cannot capture all aspects of a correlated magnet, they further strengthen the hypothesis that the physics of the Ti d-electrons is one-dimensional, rather than two-dimensional. Motivated by this discrepancy between theoretical considerations and the data described in 2.1, new susceptibility measurements were carried out at MIT [29].

Figs. 2-10 and 2-11 show the data for pure and 10% Sc doped TiOCl taken by F. C. Chou. The data for pure TiOCl shown in Fig. 2-10 were obtained from crushed crystals. When comparing Figs. 2-10 and 2-4, note that the data in Figs. 2-10 and 2-11 were taken over a wider temperature range than those in Figs. 2-4 and 2-5.
Fig. 2-10 shows the data for pure TiOCl, after subtraction of a small curie tail due to paramagnetic impurities. They are about a factor 3 smaller than those shown in Fig. 2-4 and show a sharp drop in the susceptibility at low temperatures. This can be seen even more clearly in the inset which shows single crystal data. There appears to be a first order like phase transition at a critical temperature $T_{c1} = 67K$. In addition, a noticeable inflection point appears at $T_{c2} \approx 95K$. The low temperature part is too flat for a meaningful fit to an exponential law. Nonetheless, such a very flat regime must be interpreted as the opening of a large spin gap. The flat line below $65K$ can therefore be taken to be the zero level of the spin part of the susceptibility (2.2). The high temperature part of the data (above $130K$) can then be fitted to the

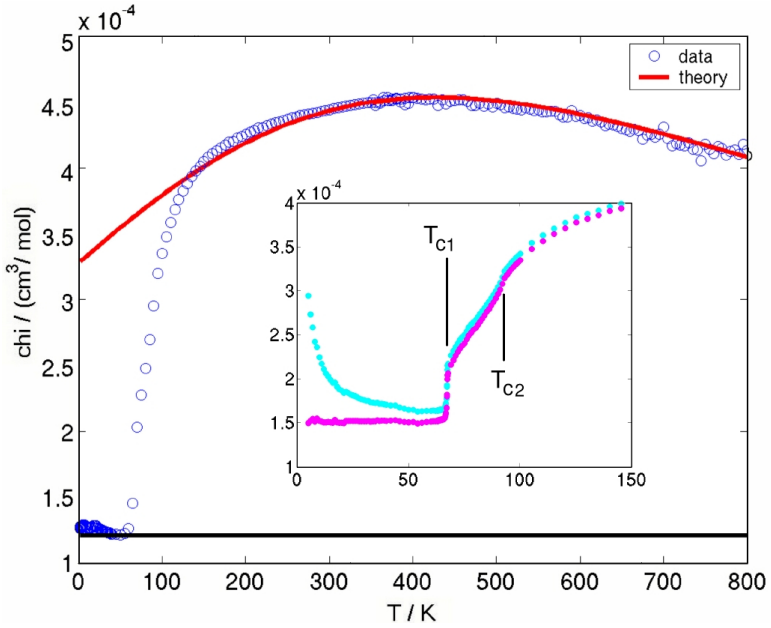

Figure 2-10: Susceptibility of crushed crystals of pure TiOCl. The inset shows single crystal data with and without Curie subtraction.

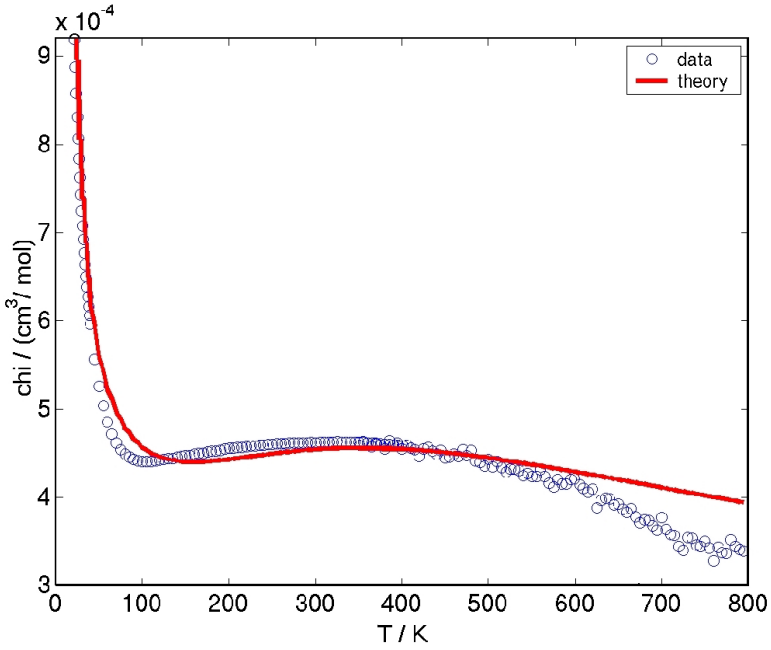

Figure 2-11: Susceptibility of 10% Sc doped TiOCl

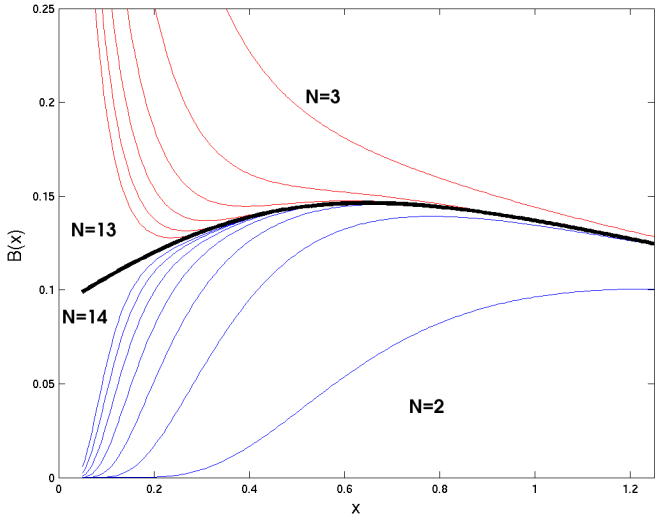

Figure 2-12: Bonner-Fisher curve, obtained by exact diagonalization of spin chains of size $N = 2 \ldots 14$. The even chains flow to zero at small t, showing spin-gapped behavior, whereas the odd chains diverge as $t \to 0$, showing free spin behavior.

susceptibility of a nearest neighbor Heisenberg spin-chain:

$$H = J \sum_i S_i \cdot S_{i+1} \tag{2.3}$$

where the S_i are spin-1/2 operators. The molar susceptibility of this model with $J > 0$ is of the form

$$\chi^{mol} = \frac{N_a g^2 \mu_B^2}{J} B(T/J) \tag{2.4}$$

where $B(T/J)$ is known as the Bonner-Fisher-curve [36] in the literature. One may obtain $B(T/J)$ at not too small $x \equiv T/J$ by means of exact diagonalization of a finite spin chains with periodic boundary conditions (Fig. 2-12). The relevant temperature regime for the fit of the data shown in Fig. 2-10 turns out to be $T/J < 1.25$. In this regime, the extrapolated numerical Bonner-Fisher curve can be well described by the following functional form:

$$B(x) = \frac{A + Bx}{C + Dx + x^2} \tag{2.5}$$

where $A = .1009$, $B = .1615$, $C = 1.1092$, $D = -.1919$ were chosen. This functional from apparently serves its purpose very well in the temperature regime shown in Fig. 2-12. It may not be used at much larger temperatures, where the Heisenberg chain will show free spin-$\frac{1}{2}$ behavior and therefore $xB(x) \to 1$ as $x \to \infty$. As it turns out, there is a functional form given in the literature which is very similar to (2.5) but

features two more parameters and is valid over a larger temperature regime including the asymptotic $x \to \infty$ limit [37]. Another subtle limit is that of $x \to 0$. This is difficult to calculate from finite chains, whose behavior is dominated by finite size effects at low temperatures (Fig. 2-12): The spectrum of a finite system is necessarily discrete and the ground state is therefore always gapped. This gap may vanish in the limit of infinite system size, as is the case for the Heisenberg model (2.3). The susceptibility of a finite chain will then resemble that of the infinite system only for temperatures above the gap. Below the gap temperature, the susceptibility decays exponentially for chains of even length where the ground state is a singlet. For chains of odd length, the ground state has a spin-$\frac{1}{2}$. In this case, the susceptibility will exhibit the behavior of a free single spin. Both these behaviors are clearly seen in Fig. 2-12. On the other hand, the susceptibility of the infinite chain remains finite as $T \to 0$, as required for a gapless antiferromagnet. However, it is not described by an analytic equation of the form (2.5) in this limit, but features a logarithmic cusp predicted by field theory methods. This crossover takes place at very small T/J and has been studied in [38]. It is not relevant to most real systems, which are described the Hamiltonian (2.3) only above a certain transition temperature T_c, below which the system is in a state of higher dimensional order.

Such a transition is indeed apparent at T_{c1} from the data in Fig. 2-10. The functional form (2.5) was used to fit the high temperature part of the data above $130K$ to the Bonner-Fisher curve. Using the flat plateau below $65K$ as zero-level, the only free parameter of this fit is the exchange constant J of the Heisenberg model. This way, J is determined to be $J = 660K$, which agrees well with the crude estimate from the previous section. Fig. 2-10 shows that the high temperature part of the data is indeed very well described by a Heisenberg spin chain with only nearest neighbor exchange. Note that both the absolute magnitude and the peak position are well accounted for by a single parameter J, justifying the choice of zero made above.

The new experimental data are thus consistent with a picture of one-dimensional spin chains in TiOCl. This allows an explanation for the Sc doping experiment (Fig. 2-11): One may assume that Sc replaces Ti on a fraction x of all Ti-sites. The Sc sites are non-magnetic, hence the Heisenberg-chains of our model are broken into finite open-ended chains of an average length of $1/x$. In such an environment, the probability that a given site belongs to a chain of length n reads:

$$P_x(n) = nx^2(1-x)^n \tag{2.6}$$

The above probability distribution is normalized to $\sum_n P_x(n) = 1-x$, since a fraction x of all sites is non-magnetic and does not belong to any chain. This reflects the fact that the molar susceptibility in Fig. 2-11 is the susceptibility per one mole of metallic ions, where both Ti and Sc are counted. Denoting the molar susceptibility of a finite open-ended Heisenberg chain of length n by $\chi^{mol}(n,T)$, we expect the measured susceptibility in the presence of Sc to be of the form:

$$\chi^{mol}_{Sc}(x,T) = \sum_{n=1}^{\infty} P_x(n)\chi^{mol}(n,T) \tag{2.7}$$

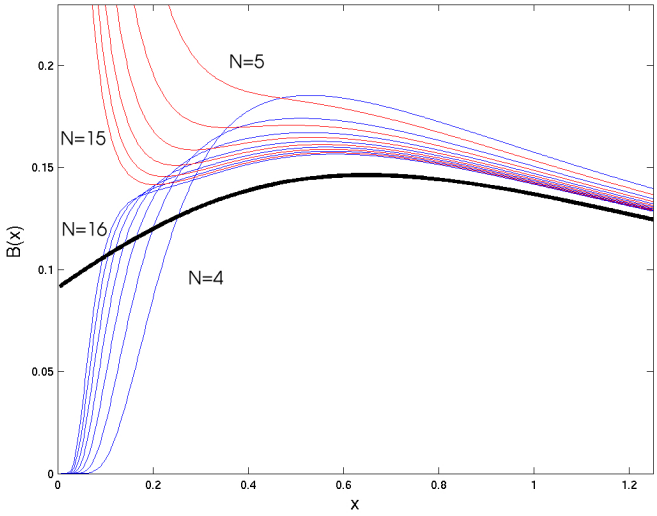

Figure 2-13: Susceptibility of open Heisenberg chains of length $N = 4 \ldots 16$. The fat curve is the large N limit (2.5) determined from closed rings.

$\chi(n, T)$ has been determined by exact diagonalization for $n = 1..16$ and extrapolation (Fig. 2-13).

As shown in Fig. 2-11, this model with $x = .1$ agrees well with the experiment at all temperatures below $600K$, above which the Sc doped sample begins to decompose. The computation was done using the exchange J and the background susceptibility level obtained from the pure sample. Thus in principle, no additional fit parameter needs to be introduced in the theoretical description of the impurity doped case. However, the exact Ti/Sc ratio in the final product does not precisely follow the initial Ti/Sc ratio of the chemical precursor mixture (which is a mixture of $Ti_2O_3/Sc_2O_3/TiCl_3$), due to the uncontrolled transport mechanism with excess $TiCl_3$ [35]. The low temperature Curie tail in Fig. 2-11 is then the only means of determining the actual doping level x. It was noted in the experiment that the thoroughly mixed and reacted powder samples have Curie constants which correspond to an amount of free spin-$\frac{1}{2}$'s that is roughly equal to half the initial Sc percentage. Assuming that indeed precisely half of the doped Sc atoms will give rise to a free spin-$\frac{1}{2}$ at low temperatures, the Sc doping level x can be determined from the Curie tail.

The model (2.7) indeed explains why every second Sc atom introduces a free spin-$\frac{1}{2}$. It is clear that in the limit of small x half of the broken chains in the system will have an odd length. It was already noted above in the case of closed Heisenberg rings that a chain of odd length has a spin-$\frac{1}{2}$ ground state doublet. The same applies for open boundary conditions. Below the gap temperature of the finite chain, odd chains behave as free spins (Fig. 2-13) with $S = \frac{1}{2}$. Since every second Sc atom will give rise to an odd chain, this explains the observed behavior. Note that the gap decreases as

$1/n$ as the chain length n increases. Hence, chains of different lengths will contribute to the Curie-like tail at different temperatures. The fitting to a Curie-tail is therefore imperfect, except at very low temperatures, where all odd chains contribute. This was also observed in Ref. [3]. However, the 1:1 correspondence of free spins and Sc atoms reported there was not confirmed by the MIT experiments.

More importantly, the drop of the high temperature part of the susceptibility upon Sc doping in TiOCl (Fig. 2-4) was not observed at MIT. Rather, the high temperature parts of the susceptibilities in the undoped and Sc doped cases (Fig. 2-10) and (Fig. 2-11) are remarkably similar in magnitude. A priori, this does not seem intuitive, since 10% of all magnetic sites are absent in the Sc doped sample, and one would thus expect some reduction of the net susceptibility. This, however, is nearly compensated at 10% doping by the fact that the open chains converge slowly and from above to the infinite chain limit (Fig. 2-13). More precisely, the convergence is an $1/n$, as opposed to $1/n^2$ for periodic boundary conditions (Fig. 2-12). The following argument may explain why in fact the susceptibility is very insensitive to Sc doping at high temperatures:

Imagine a very long Heisenberg chain of one mole of spins whose susceptibility is described by eq. (2.4). Now replace a fraction x of all spins by non-magnetic sites. This will introduce an overall factor of $(1-x)$. Each impurity destroys two magnetic bonds. Hence, we now have $(1-x)N_A$ spins connected via $(1-2x)N_A$ magnetic bonds of strength J. One may then argue that the "average" exchange constant of the system is given by

$$\bar{J} = \frac{\text{number of bonds}}{\text{number of spins}} J = \frac{1-2x}{1-x} J \approx (1-x)J \tag{2.8}$$

If this average $\bar{J}$ is to replace J in (2.4), then the factors of $1-x$ cancel and the susceptibility should be constant to linear order in x.

It is apparent from the nature of the above argument that it applies only to temperatures larger than the average finite chain gap of the system. In this temperature regime, however, it seems to be justified. Fig. 2-14 shows a superposition of the data taken from the impurity doped and the undoped sample. Recall that the Sc doped sample starts to decompose above $600K$.

From this reasoning, it is clear that the model (2.7) is not very sensitive to the assumed probability distribution $P_x(n)$. In fact, the only region where it will be somewhat sensitive to the choice of $P_x(n)$ is the onset of the Curie-tail. Here, the crossover predicted by (2.7) is less abrupt than the one seen in the actual experiment. This may suggest that the Sc impurities are more evenly spaced than assumed in the random distribution (2.6). Indeed, when the $P_x(n)$ in (2.7) is replaced by a distribution which is more peaked around its average, such that the occurrence of very short chains is suppressed, the resulting curve will fit the experimental data even better at the onset of the Curie-tail, while the rest remains essentially unchanged. However, other effects may also explain the deviation of the data from the prediction of (2.7) at the onset of the Curie-tail. The temperature at which the Curie-tail occurs is just slightly below the temperature at which the susceptibility of the undoped material starts to deviate

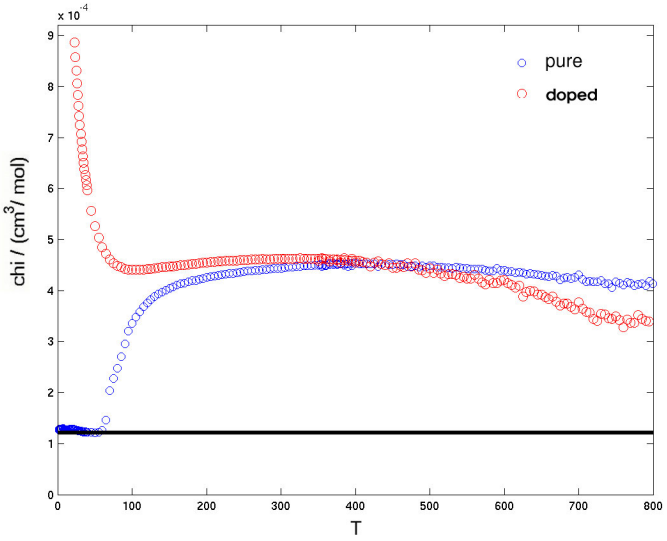

Figure 2-14: Superposition of the measured susceptibilities of TiOCl and $Ti_{.9}Sc_{.1}OCl$.

from the Bonner-fisher curve (Fig. 2-14), as a precursor to the phase transition at T_{c1}. It is hard to infer from this data whether a similar effect is present in the Sc doped material. In the following section, it will be argued that the gapped low temperature phase is a dimerized spin-Peierls phase. In fact, a dimerized phase may also lead to a Curie-tail of the same strength in the presence of non-magnetic impurities, since any odd chain segment will trap a spin-$\frac{1}{2}$ at low temperatures. Hence it is not obvious from the susceptibility data whether a phase transition similar to that of the undoped sample occurs in the Sc doped case at low temperatures. However, there is no clear sign for such a transition in the doped samples.

Finally, note that the order of magnitude of the high temperature susceptibility both for the Sc doped and the undoped sample in Fig. 2-14 is quite compatible to that of the Sc doped samples measured by Wilson et al. (Fig. 2-4). Also, the overall behavior found here for TiOCl resembles that found by Wilson for TiOBr (Fig. 2-5), as one would expect for two such similar chemical compounds. It therefore seems that Wilson's curve a) for pure TiOCl (Fig. 2-4) got shifted up by a large amount due to some mistake and was therefore plotted on the wrong scale, such that the drop in susceptibility around T_{c1} was barely noticeable.

2.4 The spin-Peierls picture of the low temperature phase

The evidence given so far suggests that in the high temperature phase, the spins of the *d*-electrons in TiOCl may be regarded as quasi one-dimensional. A quasi one-dimensional system is an idealized concept, and any system that shows one-

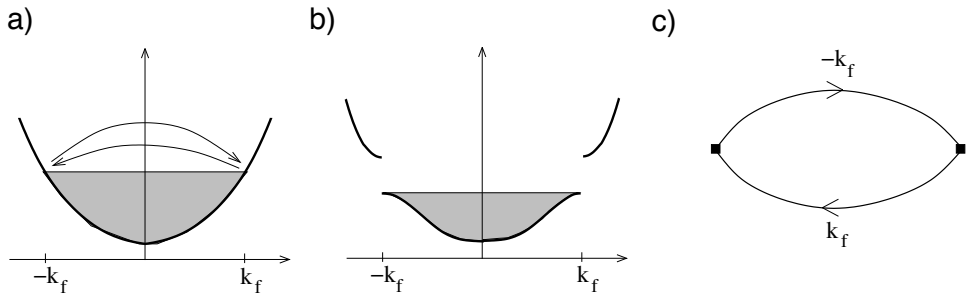

Figure 2-15: The Peierls instability. a) Fermi sea of a non-interacting electron gas. b) Gap opening due to a periodic modulation at wavevector $2k_f$. c) Divergent particle-hole bubble.

dimensional character at some finite temperature is expected to be in a different phase at very low temperatures, when higher dimensional couplings are important. Typically, the low temperature phase exhibits higher dimensional order. In the case of materials that can be described as quasi one-dimensional spin chains, interchain exchange couplings will usually give rise to two-dimensional Néel order at low temperatures. Prominent examples showing this behavior are the spin-$\frac{1}{2}$ compounds $KCuF_3$ [39] with and exchange constant of $J = 392K$ and a Néel ordering temperature of $T_N = 39K$, and Sr_2CuO_3 [40] with $J = 2300K$ and $T_N = 5.4K$. With the very small ratio $T_N/J \approx .002$, Sr_2CuO_3 is probably the most ideal antiferromagnetic Heisenberg chain found in nature.

However, a Néel transition leads to a state of broken rotational symmetry which possesses gapless Goldstone modes, i. e. a spin-wave mode. A Néel state therefore could not explain the gapped behavior observed in the low temperature part of the susceptibility. Rather, the opening of a gap may be explained in terms of another instability which is inherent to all gapless one-dimensional systems with dominantly repulsive interactions:

2.4.1 The Peierls instability

Peierls has pointed out that a one-dimensional metal would be unstable towards the formation of a periodic charge density wave at low temperatures [41]. This had been in the 1950's and was then considered a pure academic observation. The nature of this theorem may be understood most easily in terms of a one-dimensional gas of non-interacting particles. Fig. 2-15a) shows a non-interacting Fermi sea in one dimension. Imagine that the electrons spontaneously form a periodic density modulation:

$$\rho = \rho_0 + \delta \cos(2k_f x) \tag{2.9}$$

where $\rho_0 = k_f/\pi$ is the density of the uniform Fermi gas (assuming spinless particles here for simplicity). This periodic modulation destroys translational symmetry and introduces a reciprocal lattice, where the Fermi points become Bragg points. It is well known that the particle dispersion must be flat at such Bragg points, and hence a gap

is opened at the Fermi surface (Fig. 2-15b). It is clear that this will lower the energy of the system at low temperatures, where only states at $|k| < k_f$ are populated.

For free electrons, this effect can be calculated by assuming that the density modulation (2.9) gives rise to a mean-field potential of the same form, which will scatter electrons between the two Fermi points (Fig. 2-15a). It is then readily shown that this will lower the electronic energy of the system by an amount

$$\Delta E^{free}_{electronic} \sim -\delta^2 \log(\delta) \tag{2.10}$$

Furthermore, the density modulation (2.9) will cause a structural distortion of the underlying lattice and thus cost some elastic energy

$$\Delta E_{elastic} \sim \delta^2 \tag{2.11}$$

(If there is no lattice, but only a free electron gas, the electron kinetic energy cost will still be of this form. However, this is in principle already included in (2.10)). It is apparent from these equations that the electronic energy gain will always outweigh the elastic term, and thus the Fermi surface will be unstable.

Note that eq. (2.10) only applies to the non-interacting case. It turns out that this case is marginal where the Peierls instability just occurs. In [42], Kolomeisky et al. give a nice phenomenological derivation for the general form of the electronic energy gain in the presence of interactions:

$$\Delta E^{int}_{electronic} \sim -\frac{\delta^{\frac{2}{2-K}}}{1-K} \tag{2.12}$$

The parameter K is a measure of the interaction. $K = 1$ corresponds to the non-interacting case. For repulsive interaction one has $K < 1$, whereas for attractive interactions $K > 1$. It follows that the Peierls instability will always take over for repulsive interactions.

The arguments given here show quite firmly that a one-dimensional Fermi liquid is unstable at low temperatures. However, the above picture of a charge density wave ground state is based on a mean field treatment that does not allow for fluctuations of the parameter δ. In particular, when full translational symmetry is present, quantum fluctuations will always restore the symmetry of a purely one-dimensional system, where a continuous symmetry cannot be broken even at zero temperature. In this case, the system will be in a liquid state, but one where density fluctuations govern the low energy excitation spectrum and replace the quasi-particle excitations of the Fermi-liquid. The diagrammatic process responsible for this type of instability of the Fermi surface in one dimension is the divergent particle hole bubble of Fig. 2-15c), where two particles near the two Fermi points are exchanged. This instability competes with yet another instability that favors superconducting correlations and will dominate when the interactions are attractive [43, 44]. Hence, the Fermi surface of a one-dimensional Fermi system is always unstable, but the above picture of symmetry breaking and the opening of a gap will in general not be correct, especially in the presence of translational invariance. A gapless one-dimensional system can be

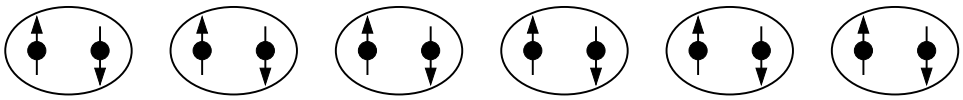

Figure 2-16: Spin-Peierls state. The lattice modulation at π leads to an alternation of the magnetic site distance. The ovals denote singlet pairs formed by two electrons on short magnetic bonds.

described as a "Luttinger liquid" [45]. The phenomenology of Luttinger liquids will be discussed more thoroughly in later chapters of this thesis. Here, we are concerned with real systems whose one-dimensional character is only approximate, where the Peierls transition may indeed occur. In a real system, the bubble shown in Fig. 2-15c) couples to three-dimensional phonons. In this case the mean field picture described above is qualitatively justified, and a symmetry breaking Peierls transition will open up a gap at low temperatures. However, it may happen that another phase transition occurs first and destroys the one-dimensional character of the system already before Peierls physics can take over.

2.4.2 The Spin-Peierls state as the low temperature phase of TiOCl

The above arguments were given in the context of a system that is metallic above the Peierls transition temperature. However, they carry over to any gapless one-dimensional system, such as a magnetic insulator formed by an array of antiferromagnetically coupled $S = \frac{1}{2}$ spins [46, 47]. It is well known that the Heisenberg Hamiltonian (2.3) can be transformed into a system of interacting spinless fermions by means of a Jordan-Wigner transformation [48]. The interaction of the spinless fermions is of the order of the bandwidth in the isotropic case and has repulsive sign. Then it follows as discussed above that the system may lower its energy by distorting the underlying lattice geometry. In the absence of a magnetic field, the corresponding spinless fermion band is half filled, where each particle (or hole, depending on choice) represents an up-spin. The resulting periodic modulation of the lattice will therefore have the commensurate wave vector $2k_f = \pi$ (Fig. 2-16). To some approximation one may regard the lattice as frozen in the spin-Peierls state. The spins then see an effective Hamiltonian of the form

$$H = J \sum_i (1 + \delta(-1)^i) S_i \cdot S_{i+1} \tag{2.13}$$

Here, the effect of the lattice distortion has been taken into account by a symmetry breaking modulation of the exchange coupling. There are now stronger and weaker magnetic bonds. This results in an enhanced tendency of the spins to form singlets that are centered on the stronger bonds, represented by ovals in Fig. 2-16. These singlets are also referred to as dimers, and the lattice is commonly said to be dimerized. Note that although the dimerization is achieved by explicitly symmetry breaking

terms in (2.13), the true Hamiltonian has the full translational invariance of the lattice and symmetry braking occurs spontaneously. This symmetry breaking can be characterized by the following "dimer" order parameter:

$$D = \frac{1}{N} \sum_i (-1)^i \langle S_i \cdot S_{i+1} \rangle \tag{2.14}$$

where N is the size of the lattice.

In Hamiltonian (2.13) the lattice dynamics are entirely ignored. In real systems, this may not be a good approximation, since the energy scales associated with the magnetic exchange can be comparable to phonon energies at the zone boundary. This may lead to a complicated entanglement of the magnetic and vibrational degrees of freedom. It is therefore a subtle problem to describe the low energy excitations of the spin-Peierls phase accurately, and various approaches are discussed in the literature [49].

It follows from the arguments given above that any quasi one-dimensional antiferromagnet should be unstable towards the spin-Peierls transition at low temperatures. However, there are only few materials known where this is indeed observed. In most quasi one-dimensional antiferromagnets, Néel order is established at a critical temperature T_N. The state is then no longer one-dimensional, but rather exhibits two or three-dimensional order and does not feature any instability based on the spin-Peierls mechanism.

Most materials that are known to show the spin-Peierls transition are organic, the first known example being TTF-CuBDT [50]. This is due to the fact that organic materials tend to have soft lattice vibrations such that a Peierls-type of distortion will be less costly. Secondly, the distance between neighboring chains is typically long in organic materials. This weakens interchain exchange couplings that may favor Néel order. On the other hand, strain interactions that will couple a local distortion at one point of the lattice to another distortion at a distant point may be thought of as long ranged [4]. The Peierls temperature scale T_{sp} is therefore much less affected by the greater interchain distance.

In the last decade, however, the anorganic compound $CuGeO_3$ [51] has caught much attention for being the first inorganic material showing spin-Peierls behavior. Table 2.1 compares the energy scales of TiOCl to those of TTF-CuBDT and $CuGeO_3$. It is interesting to note that the scales observed in TiOCl are larger by half an order of magnitude. On the other hand, a peculiarity of $CuGeO_3$ is that, unlike in TTF-CuBDT or TiOCl, a seizable next-nearest-neighbor exchange $J' > 0$ is present [52]. A positive J' may by itself already favor dimerization at low temperatures, as will be discussed in later chapters of this thesis. This effect will conspire with spin-lattice couplings to drive the system into a dimerized low temperature phase, and provides some intuitive explanation why a spin-Peierls transition is observed in this anorganic material.

Such effects are absent in TiOCl, where the good fit to the Bonner-Fisher curve suggests that no significant J' is present. Nonetheless, the susceptibility presented

[4] A. Millis, private communication

in 2.3 shows one-dimensional behavior at high temperatures and a transition into a gapped phase at low temperatures. It is clear from this that the low temperature phase is not Néel ordered. Therefore, it stands to reason that the observed transition at T_{c1} is a spin-Peierls instability.

A structural property that may indeed suppress Néel order in TiOCl is the frustration of the interchain geometry. This would be the case is the magnetic chains are running along the b-direction of the crystal, as shown in Figs. 2-3a), 2-17. In this case, the spin chains run along the diagonals of a distorted square lattice, which frustrates Néel ordering. On the other hand, the dimerization from chain to chain is also frustrated in the sense explained in Fig. 2-17. There, the lattice is divided into two sublattices consisting of different sets of next-nearest neighbor chains. Each chain may choose one of two distinct dimerized states that are related by a lattice translation and which are distinguished by the sign of the order parameter (2.14). The sign of this order parameter is defined arbitrarily for each of the two sublattices. Figs. 2-17a) and b) show two different configurations of two dimerized nearest neighbor chains. The first chain is in identical states in a) and b) whereas the sign of the order parameter of the second chain is flipped between a) and b). It is obvious that the two configurations have the same energy. Thus the energy does not depend on the relative sign of the order parameters between neighboring chains, and the ground state will be infinitely degenerate if only nearest neighbor chain couplings are taken into account. In this sense, the dimerization is frustrated in TiOCl.

This is to be contrasted with a non-frustrated situation such as a regular square lattice with spin chains along the *edges* (Fig. 2-18). Here, the energy is sensitive to the relative sign of the order parameter between neighboring chains, and this will always favor one of the two-dimensional dimer orders shown in Figs. 2-18 a) and b).

2.5 Evidence from other experiments

The structural changes of the lattice geometry that are associated with a dimer-transition have been observed by so far unpublished x-ray scattering experiments [54]. There, a doubling of the unit cell in the b-direction of the crystal has been

	J	J'/J	T_{sp}	Refs.
TTF-CuBDT	$77K$	$\ll 1$	$12K$	[50]
$CuGeO_3$	$160K$	.36	$14K$	[51, 52, 53]
TiOCl	$660K$	$\ll 1$	$65K$	[29]

Table 2.1: Some spin Peierls materials. Shown are the nearest neighbor exchange J, the ratio J'/J where J' is the next-nearest neighbor exchange, and the spin-Peierls transition temperature T_{sp}. The term "$\ll 1$" in the third column means that a satisfactory fit of the susceptibility to the Heisenberg model can be achieved without the introduction of J'.

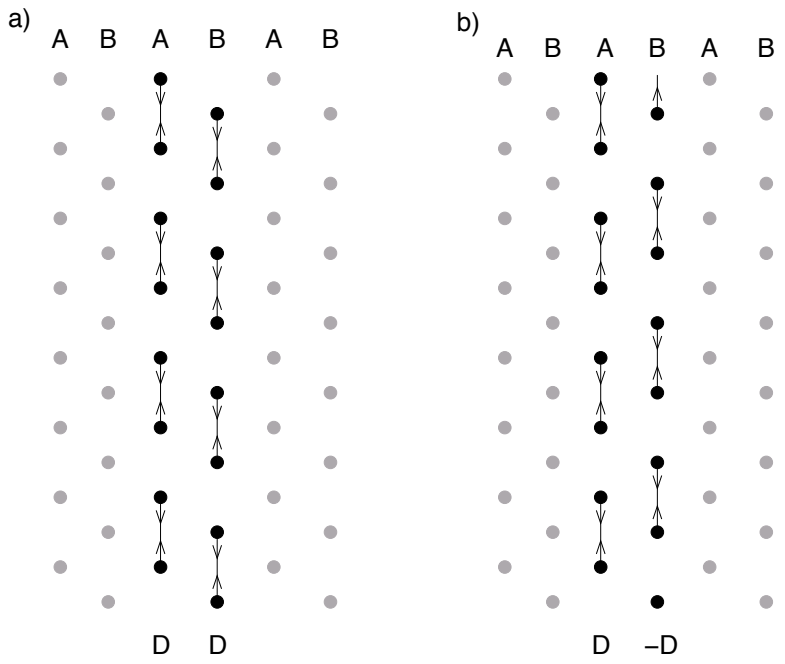

Figure 2-17: Frustration of dimerization in TiOCl. The lines denote singlet pairs. The lattice distortion is indicated only by means of little arrows. The two configurations in a) and b) are energetically identical.

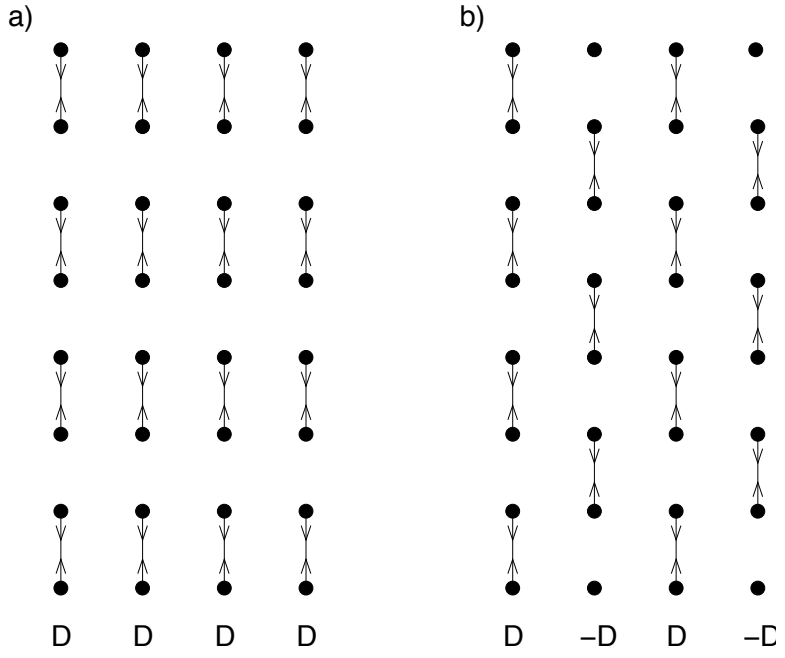

Figure 2-18: Non-frustrated dimer patterns on a square lattice. Nearest neighbor chain couplings will always favor one of the two dimer orders shown in a) and b)

observed below the temperature T_{c1} of the first order transition displayed by the susceptibility data (Fig. 2-10). This agrees with the prediction of the LDA+U band structure and suggests that the frustrated linear chains of Fig. 2-3a) are indeed favored over the zig-zag chains of Fig. 2-3 b), which run along the a-direction and are not frustrated. A doubling of the unit cell in a first order like transition is also confirmed by recent NMR-measurements [55], where doublets appear below T_{c1} in the Cl and Ti NMR-lineshapes. The NMR-data does not give any direct evidence about the directionality of the spin chains. Interestingly, however, a pseudogap manifests itself as a change of slope of the quantity $1/T_1T$ already above T_{c1}, at a temperature $T^* = 130K$. Here, T_1 is the lattice relaxation rate. Furthermore, a continuous phase transition is seen at $T_{c2} = 94 \pm 2K$: Below T_{c2} the single Ti and Cl lines evolve into a broad continuum, out of which two separate lines emerge at T_{c1}. A possible interpretation of this behavior is that a regime of one-dimensional fluctuations with dimer character is already present between T_{c1} and T_{c2}. In this regime, the coupling of spin and lattice degrees of freedom is already important and local one-dimensional order should be present. This leads to the gradual suppression of the susceptibility in this regime and the observed deviation from the Bonner-Fisher curve below T^*. Note that the temperature T_{c2}, which was identified as the critical temperature of a second order transition by NMR, could be observed as an inflection point in the susceptibility data (Fig. 2-10).

The anisotropy of the g-tensor was measured by recent ESR experiments [56]. It turns out that the c-axis is a principal axis of the g-tensor. This is consistent with the assumption that the spins reside in the d_{xy}-orbitals that form the linear chains of Fig. 2-7a). It is not consistent with a picture based on d_{xy} or d_{yz}-orbitals, unless symmetric superpositions of these orbitals are formed. However, this would not likely give rise to quasi one-dimensional physics. Furthermore, it was found that the ESR line width ΔH and the components of the g-tensor depend on temperature in a relatively strong and unexpected way. This was attributed in [56] to the coupling of the Ti-spins to orbital and/or lattice degrees of freedom.

An anomalous temperature dependence was also reported for the phonon spectrum observed in recent Raman scattering experiments [57]. There a broad continuum evolves into several sharp components above T_{c1}, which goes along with a pronounced softening of several of the observed peaks. This evolution terminates at T_{c1}, below which the phonon spectrum consists of several sharp and temperature independent lines. The magnetic part of the Raman spectrum exhibits a structure that is richer than expected for a non-frustrated linear spin chain [58]. There exist two broad peaks at energies of $2J$ and $3J$, where the $2J$ peak has a substructure consisting of modulations at a characteristic energy that corresponds roughly to the energy of two of the phonon modes. This, too, was interpreted as a hint at the important role of spin-phonon couplings in TiOCl. A key to explaining much of this rich behavior may be the understanding of the role played by geometrical frustration in a quasi-one-dimensional material with a spin-Peierls transition. Frustration may also allow for the first order character of the transition at T_{c1}, as will be argued in the next section. In any case, geometrical frustration is a feature which distinguishes TiOCl from other materials where a spin-Peierls like transition has been observed, in addition to the

comparatively large energy scale (Table 2.1).

2.6 A Ginzburg-Landau theory of a first order frustrated dimer transition

The first order character of the dimer transition at T_{c1} calls for further explanation. In the few previously known spin-Peierls compounds, such as $CuGeO_3$ or TTF-CuBDT, the transition is reasonably well described by a mean-field theory of a single spin chain coupled to three-dimensional phonons [59]. This mean-field theory predicts a universal ratio of $2\Delta_s/T_c = 3.53$ where Δ_s is the spin gap. In addition, the mean-field theory predicts a second order transition rather than first order. These predictions are indeed met quite well by $CuGeO_3$, where a spin gap of $\Delta_s \approx 24K$ has been observed [53], leading to a ratio of $2\Delta_s/T_c \approx 3.43$.

In TiOCl this prediction fails utterly, where NMR-data suggests a spin gap in the low-temperature phase as large as $\Delta_s \approx 430K$. Using $T_{c1} = 67K$ as the transition temperature, this gives rise to the very large ratio $2\Delta_s/T_{c1} \approx 13$. However, in TiOCl the failure of the standard mean-field approach is already clear from the first order character of the transition.

As explained above, the situation in TiOCl is special because of its frustrated interchain geometry (Figs. 2-17, 2-19a). Here, the standard mean-field theory is very likely to underestimate strong fluctuations in the chain direction. This may well suppress T_c. As will be shown below, the frustration makes a further distortion of the lattice necessary, in addition to the distortion associated with the dimerization. This additional distortion should involve a relative shift between neighboring chains in the dimerized phase (e.g. as shown in Fig. 2-19b), that will lift the degeneracy of the states shown in Fig. 2-17.

All this can be captured by a simple Ginzburg-Landau theory. We assume for now that dimers on the same sublattice (A or B) will lock in phase (Fig. 2-19). The dimerization on the two sublattices is then described by two order parameters, D_1 for sublattice A and D_2 for sublattice B. In Fig. 2-19 a) the dimerization is such that the center lines of dimers (dashed for sublattice A and dashed-dotted for B) are not affected, and remain the same as in the undimerized phase. As noted before, each chain can be paired up in dimers in two distinct ways, which are represented by the choice of sign for the order parameters D_1, D_2 : A change of sign of D_1 will move the dimer pattern on sublattice A up by one lattice constant, which is shown in the chain labeled A' in Fig. 2-19a). The symmetry of the lattice is such that any random choice of signs for D_1 and D_2 will always lead to the same free energy, as long as only nearest neighbor chain couplings are considered. In this sense, the dimerization is frustrated between neighboring chains.

So far it has been assumed that the two sublattices remain frozen with respect to one another, apart from the dimerization. However, this assumption is not justified, for in the presence of a non-zero dimerization as shown in Fig. 2-19a) there is no symmetry that would prevent a relative shift between the two sublattices. Such a

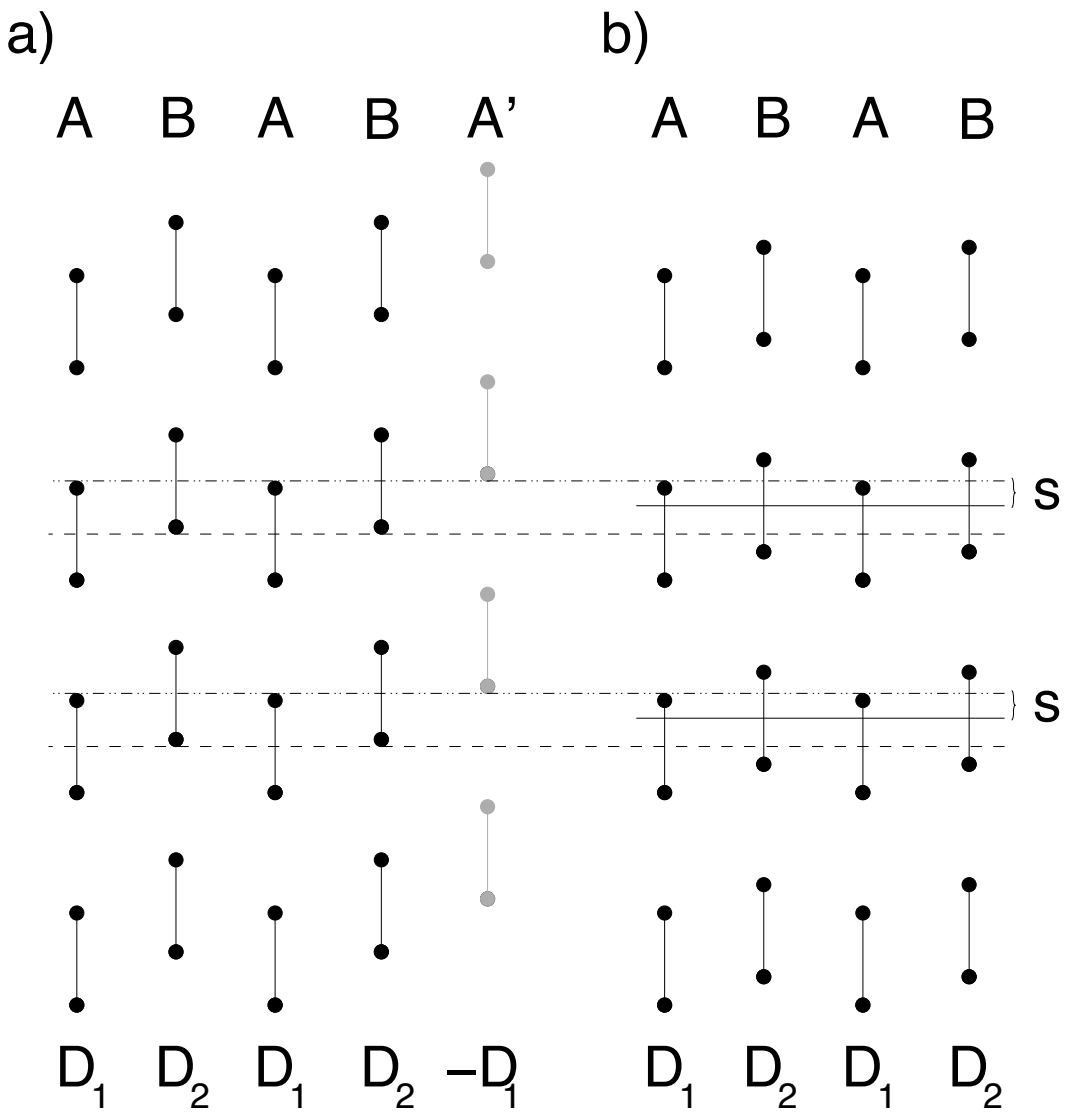

Figure 2-19: Ginzburg-Landau order parameters a) Dimerized chains before inter-chain shift ($s = 0$). b) Shifted chains ($s \neq 0$)

shift has been introduced in (Fig. 2-19 b) and is denoted by s. Note that this shift would cause an electric dipole moment and should be observable by experiments. We now construct a Ginzburg-Landau function of the 3 parameters D_1, D_2, s. It is easily seen that $F(D_1, D_2, s)$ must have the following symmetries:

$$F(D_1, D_2, s) = F(-D_1, -D_2, s) = F(-D_1, D_2, -s) = F(D_1, -D_2, -s) \tag{2.15}$$
$$F(D_1, D_2, s) = F(D_2, D_1, s) \tag{2.16}$$

Up to fourth order, the only analytic terms consistent with these symmetries are:

$$\begin{aligned} F(D_1, D_2, s) = \quad & a\left(D_1^2 + D_2^2\right) + bs^2 + c\, D_1 D_2\, s \\ & + d\left(D_1^4 + D_2^4\right) + e\, D_1^2 D_2^2 + f\left(D_1^2 + D_2^2\right) s^2 + g\, s^4 + \ldots \end{aligned} \tag{2.17}$$

In this equation, the frustration of the lattice is evident from the fact that the only terms coupling D_1 and D_2 that are sensitive to their signs do also couple to s. There is only one such term at this order, whose coefficient is c. Since this term is linear in s, the value of the shift s will inevitably be non-zero in the dimerized phase.

At high temperatures the system is in a disordered phase and $D_1 = D_2 = s = 0$. Hence the coefficients a and b are both positive. b will always be positive, since the shift s in Fig. 2-19b) will only be favorable because of dimerization (i.e non-zero values of D_1 and D_2) and not because the lattice is otherwise unstable. The point where the disordered phase becomes unstable is hence characterized by $a = 0$. This will give rise to a second order transition, unless a global minimum has already formed elsewhere, such that the disordered phase becomes metastable already before $a = 0$. In the latter case the transition is first order. Hence, the criterion for a first order transition to take place is whether F has negative values when a vanishes. If it does, the disordered point is clearly no longer a global minimum. If, on the other hand, F is still non-negative when $a = 0$, then the disordered point is still a global minimum, and the minimum will move away gradually from this point when the temperature is further lowered (i. e. as a becomes negative). It turns out that it will depend on the detailed values of the coefficients of (2.17) which case applies, since the only third order term present is a product of all three order parameters.

The detailed analysis goes as follows: Let now $a = 0$, and assume that F has negative values (first order transition). The c-term must then certainly outweigh the b-term, since all terms except the c-term are positive definite:

$$bs^2 + c\, D_1 D_2\, s > 0 \quad \Rightarrow \quad |s| < \frac{c}{b} D_1 D_2 \tag{2.18}$$

It then follows that all terms in (2.17) are of the same order except the last two, which are negligible. We introduce r as the ratio between $D_1 D_2$ and s:

$$s = r D_1 D_2 \tag{2.19}$$
$$\Rightarrow F = D_1^2 D_2^2 \left(br^2 + cr + e\right) + d\left(D_1^4 + D_2^4\right) + \cdots \tag{2.20}$$

At this point, we may clearly set $D_1 = D_2 \equiv D$ in order to minimize the last expression:

$$F = D^4 \left(b \left(r - \frac{c}{2b} \right)^2 + 2d + e - \frac{c^2}{4b} \right) \tag{2.21}$$

Apparently, F has non-zero values when

$$c^2 > 4b(2d + e) \tag{2.22}$$

holds. (2.22) is the criterion for a first order transition to take place.

Hence, the third order term in the Ginzburg-Landau function, which is induced by frustration, is not powerful enough to *guarantee* a first order transition. However, is makes a first order transition *possible* which would not be the case without frustration.

This analysis has assumed that next-nearest neighbor chains lock in place. However, one may also think about a scenario where next-nearest neighbor chains lock *out of phase*. The corresponding dimer pattern would then be that formed by the last 3 chains in Fig. 2-19a) labeled ABA'. Such a configuration would not be very sensitive to a shift s between the two sublattices. However, if instead a *shear* of the entire lattice is introduced, the analysis is completely analogous to the one presented above for next-nearest-neighbor in-phase locking. The two cases can be distinguished experimentally, since a shear would not cause an electric dipole moment, as opposed to the shift of Fig. 2-19b).

2.7 Conclusions

The LDA+U band structure and the new susceptibility data presented here are consistent with elementary crystal field considerations and indicate the existence of spin-$\frac{1}{2}$ chains in TiOCl. Above $130K$, the susceptibility of TiOCl is well described by a nearest-neighbor-exchange Heisenberg model with $J = 660K$. Also, a straightforward extension of this model gives quantitative agreement with the susceptibility of Sc-impurity doped samples. The abrupt drop of the susceptibility at $T_{c1} = 65K$ has been interpreted as a transition into a spin-Peierls state.

The LDA band structure features energetically isolated Ti-t_{2g} bands at the Fermi surface that have only very small admixtures of O and Cl orbitals. In the LDA+U calculation, a single tight-binding like d_{xy} band is lowered suggesting that the Ti spins reside in essentially unhybridized d_{xy}-orbitals and are forming chains along the b-direction of the crystal. This is in agreement with recent x-ray experiments [54] which have observed a dimerization along the b-axis below T_{c1}. Moreover, the fact that the spin chains run along the b-axis of the crystal offers some explanation for certain quantitative discrepancies between the experimental data and the standard mean-field theory of the spin-Peierls transition. The resulting interchain geometry is frustrated, and interchain coupling effects which eventually will lock dimers in the low temperature phase are likely to be weak. The first order character of the phase

transition at T_{c1} can be justified by Ginzburg-Landau arguments provided that such frustration is present.

The frustration of the b-chain scenario makes TiOCl unique among materials with a spin-Peierls transition. In addition, the energy scales J and T_{c1} observed in TiOCl are large compared to those of other spin-Peierls compounds (Table 2.1). When mobile carriers are introduced, this comparatively large energy scale may help to avoid carrier localization effects. This makes TiOCl an attractive candidate for hole doping. If holes are mobile in the chain direction, one may be able to study the physics of a one-dimensional dimer liquid. Then scenarios are possible that bear much resemblance with the RVB scenario and may lead to unconventional superconductivity. The strong interplay between magnetic and vibrational degrees of freedom may provide an additional complication, but the interchain frustration may still justify a quasi one-dimensional treatment of the problem. These ideas have motivated the research described in the following chapter.

Chapter 3

The tJJ'-model in one dimension

It is a good morning exercise for a research scientist to discard a pet hypothesis every day before breakfast. It keeps him young.

Konrad Lorenz

3.1 Doped dimerized spin chains: A path to superconductivity ?

The behavior of mobile holes in a one-dimensional dimerized spin chain is a theoretically interesting problem because of its similarity to the resonating valence bond scenario in two dimensions. Intuitively, one may argue that in a dimerized system there naturally exists an amplitude for pair formation. Upon introduction of holes, the dimer pairs could become mobile and phase coherence may be established. This idea has been previously proposed in the literature [60]. The resulting superconductivity would be in close analogy with the RVB scenario [15] discussed in the introduction. On the other hand, one dimensional models of correlated fermions are often much more tractable than similar models in two dimensions.

One can distinguish between two rough physical pictures of hole doping into a dimerized chain (Fig. 3-1). In the first scenario (Fig. 3-1a)) the dimer order remains long ranged even after hole doping. The dimers tend to reside on every second link of the lattice as in the symmetry broken undoped state, and holes tend to pair on the empty sites in between. This situation can be modeled by a Hamiltonian whose spin part features explicit dimerization such as (2.13) and whose charge part is given by a tJ-type of hopping term [61]. Note that this case bears some resemblance to doped ladder models [62]. Indeed strong superconducting correlations have been proposed for dimer-models with explicit symmetry breaking [61, 63].

A second possibility is that the holes enter the chain as domain walls between different dimer phases (Fig. 3-1b). Then the long range order of dimers is destroyed, but the singlet gap remains. It is this case which closely resembles Anderson's RVB scenario, where the dimers are in a true liquid state of unbroken translational symmetry. However, the pictures presented in Fig. 3-1 are based on the limit of large J/t,

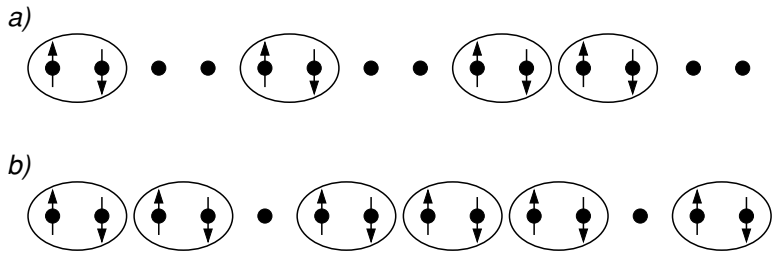

Figure 3-1: Frozen and mobile dimers a) doping into frozen dimer state. Ovals represent singlet pairs. b) mobile dimers with domain walls.

where J and t are the energy scales associated with magnetic exchange and hopping, as before. Only in this limit, it may be justified to think of the dimers as strongly bound entities. In physical systems, on the other hand, J/t is usually a fraction of unity. In this regime, the hole kinetic energy is dominant and it is less clear intuitively if the dimer picture discussed above applies. Below, this question will be studied in the context of the tJJ'-model in one dimension.

Apart from the availability of exact techniques such as numerical diagonalization and Bethe ansatz integrability, the most powerful tool in the study of one-dimensional systems is the precise knowledge of a low energy effective theory: the Luttinger liquid [45]. Similar to the Fermi liquid paradigm in three-dimensional Fermi systems, the Luttinger liquid has so far been found to describe all gapless degrees of freedom in one-dimensional systems. In the following section, the basic Luttinger liquid phenomenology will be briefly reviewed in order to establish basic notation and to state some elementary and well known results. Extensive reviews will be referenced where appropriate.

3.2 The Luttinger Liquid: A Review

3.2.1 The Tomonaga-Luttinger model

The Tomonaga-Luttinger Hamiltonian describes a gas of two species of interacting fermions in a one-dimensional system of size L:

$$H_{TL} = H_0 + H_2 + H_4 \tag{3.1}$$

$$H_0 = \sum_{r,k,s} v_F(rk - k_F) : c^\dagger_{rks} c_{rks} : \tag{3.2}$$

$$H_2 = \frac{1}{L} \sum_{q,s,s'} \left(g_{2||}(q)\delta_{s,s'} + g_{2\perp}(q)\delta_{s,-s'} \right) \rho_{+,s}(q)\rho_{-,s'}(-q) \tag{3.3}$$

$$H_4 = \frac{1}{2L} \sum_{r,q,s,s'} \left(g_{4||}(q)\delta_{s,s'} + g_{4\perp}(q)\delta_{s,-s'} \right) : \rho_{r,s}(q)\rho_{r,s'}(-q) : \tag{3.4}$$

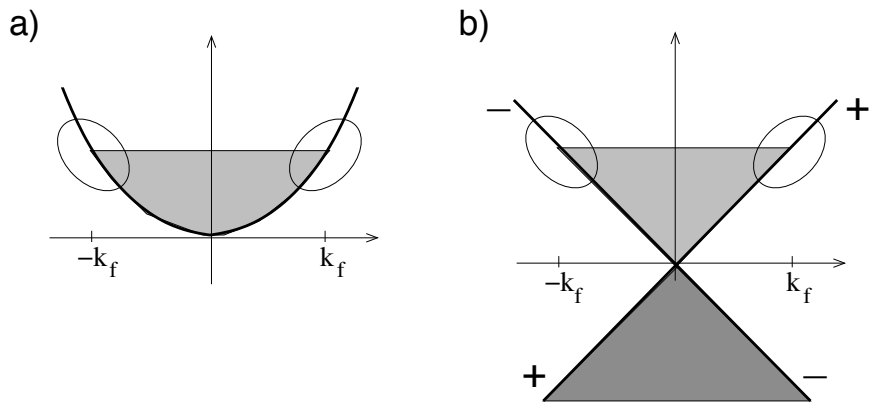

Figure 3-2: Mapping to the Tomonaga-Luttinger model. a) Non-interacting Fermi sea in one dimension. Interactions are assumed to be confined to small regions around the Fermi points (ovals). b) Ground state of the non-interacting part of the Luttinger model H_0. The shaded area represents occupied regions in momentum space. The dark grey area corresponds to "positron" states which are not present in the Hilbert space of a).

Here, the $c^\dagger_{rks}$ are fermion ladder operators that annihilate spin-$\frac{1}{2}$ particles of momentum k and spin projection $s = \{\uparrow, \downarrow\}$ on one of the two branches $r = \pm$ in Fig. 3-2b). The two branches each extend to $k = \pm\infty$, which is commonly referred to as fermion doubling. Hence, at each momentum k there exists a state on the "+"-branch and a state on the "−"-branch, where the linear dispersion in (3.2) assures that for $k > 0$ the "+"-branch has positive energies and the "−"-branch has negative energies and vice versa for $k < 0$. Hence, at some finite Fermi vector $k_f > 0$, all negative energy states are completely filled and are sometimes referred to as "positron states" (in analogy with massless QED), whereas the right Fermi point at $+k_f$ resides on the "+"-branch and the left Fermi point at $-k_f$ lies on the "−"-branch. Therefore, the particles on the "+"-branch are referred to as "right movers" and those on the "−"-branch are referred to as "left movers". The colon stands for normal ordering of operators defined by [1]

$$: \mathcal{O} : \equiv \mathcal{O} - \langle \mathcal{O} \rangle_0 \tag{3.5}$$

where $<>_0$ denotes the expectation value in the non-interacting ground state shown in Fig. 3.1b). Normal ordering is introduced in order to avoid references to the ill-defined total number of particles of the Luttinger model [2]. This also enters the definition of the density operators $\rho_{r,s}(q)$:

[1] This definition deviates from the standard fermion normal ordering for products of more than two fermions. The definition (3.5), however, is most suited to regularize the theory.

[2] The term "Luttinger"-model implies that no finite cutoff is introduced for the unphysical positron branches. Such a cutoff was used by Tomonaga. Throughout this thesis Luttinger's point of view is adopted, which makes the normal ordering procedure necessary. Regularization by means of a cutoff is reviewed in [64].

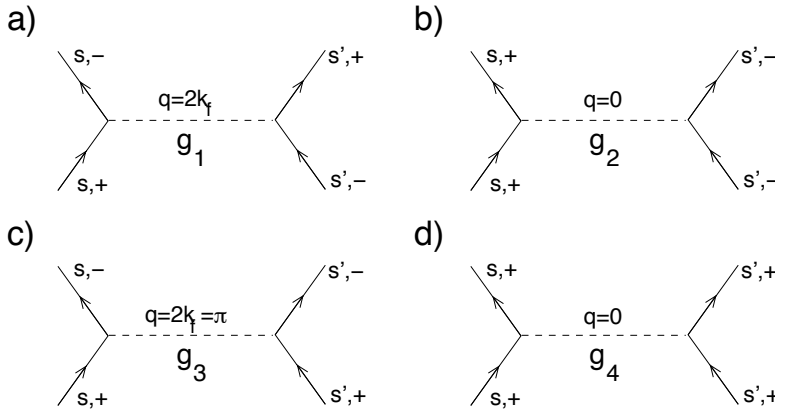

Figure 3-3: Processes in the generalized Tomonaga-Luttinger model. a) Backward scattering. b) Forward scattering involving particles on different branches. c) Umklapp scattering, only possible for commensurate band fillings $k_f = \pi/2$. d) Forward scattering involving particles on the same branch.

$$\rho_{r,s}(q) \equiv \sum_k : c^\dagger_{r,k+q,s} c_{r,k,s} : \tag{3.6}$$

The normal ordering procedure assures that operators are finite when acting on the Hilbert space which is generated by all states that differ from the non-interacting ground state only by a finite (but arbitrary) number of particle hole excitations.

The Luttinger model (3.1)-(3.4) was originally proposed as a description for a system of interacting fermions in one dimension with finite range interactions in the limit of 1.) weak interaction and 2.) high densities. This can be understood by comparison of Figs. 3.1a) and 3.1b). Figs. 3.1a) shows a non-interacting one-dimensional Fermi sea. When weak interactions are added, only scattering processes of particles close to the Fermi points have to be considered which cost very little energy (oval areas). The Luttinger model can represent the physics close to the Fermi points accurately, since there the dispersion of the real system is approximately linear, and the presence of the unphysical "positron states" matters little since they are far away from the Fermi surface. However, in H_{TL} only those low energy processes with very small momentum transfer $q \approx 0$ are represented. Other low energy processes at $q \approx 2k_f$ that scatter particles from one Fermi point to another (Fig. 3-3) are not present in the Luttinger model, and the number of particles on each branch is conserved. The neglect of these processes can be justified, at least naively, by considering the limit of high density or large k_f, such that $2k_f$ is much larger than the range of the interaction in momentum space. A weakly interacting Fermi system that meets these criteria can then straightforwardly be mapped onto the Luttinger model, which is exactly soluble.

In the more general situation of a Fermion system whose interactions are not weak on the scale of the band width, the mapping onto the Luttinger model appears to be imperfect, due to its neglect of band curvature effects and scattering processes where particles hop from one Fermi point to another and a momentum $q \approx 2k_f$ is exchanged. Processes of the latter sort can be written as follows and may be added

to H_{TL}:

$$H_1 = \frac{1}{L}\sum_{q,s,s'}\left(g_{1||}(q)\delta_{s,s'} + g_{1\perp}(q)\delta_{s,-s'}\right) : c^\dagger_{-,k+q,s}c_{+,k,s}c^\dagger_{+,k'-q,s'}c_{-,k',s'} : \tag{3.7}$$

$$H_3 = \frac{1}{L}\sum_{q,s,s'}\left(g_{3||}(q)\delta_{s,s'} + g_{3\perp}(q)\delta_{s,-s'}\right) c^\dagger_{+,k+q,s}c^\dagger_{+,k'+2\pi-q,s'}c_{-,k',s'}c_{-,k,s} + h.c. \tag{3.8}$$

The study of the phase diagram diagram of the more general Hamiltonian $\sum_{i=1}^4 H_i$ is known as "g-ology" in the literature. H_1 exchanges two particles at opposite Fermi points and is commonly referred to as backward scattering. It is easily seen that the term proportional to $g_{1||}$ may be rewritten as a contribution to $g_{2||}$. Hence, complications due to backward scattering arise only from the $g_{1\perp}$-terms and do not exist in spinless problems. H_3 is known as umklapp scattering which moves two particles from one branch to the other. It does not occur in models with full translational symmetry, but only occurs in effective theories of lattice models since it conserves momentum only up to a reciprocal lattice vector. Furthermore, H_3 is relevant only in models where $4k_f$ is close to a reciprocal lattice vector, since only in this case umklapp processes of this sort can connect the two Fermi points and are therefore important in the low energy sector. At incommensurate band fillings, Umklapp processes may generally be dropped.

The simplifications implicitly made in the Luttinger Hamiltonian, particularly the neglect of backward and umklapp scattering, make it not seem obvious that this model is related to the low-energy effective theory of any gapless microscopic one-dimensional model, even in the weak coupling limit. From renormalization group studies, however, it turns out that H_1 and H_3 are either irrelevant at weak coupling, or are expected to open up gaps in the spectrum of the model [43]. As a consequence, H_{TL} can indeed be expected to be the correct effective theory for all weak coupling-models in one dimension, whenever both spin and charge degrees of freedom are gapless.

In 1980, it was conjectured by Haldane that the universality of the Luttinger model goes beyond the weak coupling case [45]. He proposed that *all* gapless degrees of freedom of interacting particles in one dimension are described by a low energy effective theory of the form (3-2)-(3.4) with certain renormalized couplings. These effective couplings in general cannot be inferred in a straightforward way from the bare couplings of the microscopic theory; this is possible only in the weak coupling limit. However, Haldane has shown that all the relevant effective parameters can be inferred from spectral properties of the model, and thus can in principle be extracted by numerical or even analytic means. It has been demonstrated by Haldane that the resulting Luttinger liquid phenomenology is indeed consistent with various exactly solvable models [45, 65], and survives when band curvature effects are added to the Luttinger model [66]. Since then, this "Luttinger liquid theory" has been tested and verified in a great number of cases. It has so far been found to apply to all gapless degrees of freedom in one-dimensional systems, similar to Fermi liquid theory in three dimensions.

The exact solubility of the Luttinger model gives access to a rich and well understood phenomenology of one-dimensional systems, including thermodynamics, correlations functions and transport. This phenomenology will be vital to the subsequent parts of this thesis, and is reviewed extensively in [67, 68]. In the following, a quick review of the exact solution of the Luttinger model will be given.

3.2.2 The collective density mode solution of the model

The Luttinger model (3-2)-(3.4) has first been solved by Mattis and Lieb and then on a higher level of rigor by Heidenreich et al. [69] and Haldane [66]. The following brief summary will follow the notation of the review [67]. For simplicity, we will let

$$\begin{aligned} g_{2||,\perp}(q) &\equiv g_{2||,\perp}(0) = \text{const.} \\ g_{4||,\perp}(q) &\equiv g_{4||,\perp}(0) = \text{const.} \end{aligned} \tag{3.9}$$

Although the model is still soluble without these assumptions, all universal properties are related to the couplings at $q = 0$. Hence little could be gained at this point by keeping the q-dependence of the couplings. With the assumptions (3.9), the interactions become contact interactions in real space.

The solution of the problem now proceeds by realizing that at $q \neq 0$ the density operators obey Bose commutation relations:

$$[\rho_{r,s}(q), \rho_{r',s'}(-q')] = \delta_{r,r'}\delta_{s,s'} \sum_k \left(c^\dagger_{r,k+q,s} c_{r,k+q',s} - c^\dagger_{r,k+q-q',s} c_{r,k,s} \right) \tag{3.10}$$

For $q \neq q'$ this vanishes, as a shift of the summation variable easily shows. However, at $q = q'$ a subtlety arises because each branch of the Luttinger model is filled with an infinite number of "positron" states. There, each individual term in (3.10) is infinite while the sum of the two terms in the bracket still gives rise to a finite quantity. It is then not permissible to shift the summation variable, and one obtains

$$[\rho_{r,s}(q), \rho_{r',s'}(-q')] = -\delta_{r,r'}\delta_{s,s'}\delta_{q,q'} \frac{L}{2\pi} rq \tag{3.11}$$

Eq. (3.11) is easily verified for the non-interacting ground state of the Luttinger model, and with hardly more effort one sees that it is valid for *any* state that differs from the non-interacting ground state only by a finite number of particle-hole excitation, hence on the entire basis of the Hilbert space we consider. For $q > 0$, one can thus introduce boson creation operators via

$$b^\dagger_{r,s}(q) \;=\; \sqrt{\frac{2\pi}{qL}}\, \rho_{r,s}(rq) \tag{3.12}$$

satisfying

$$\left[b_{r,s}(q), b^\dagger_{r,s}(q') \right] \;= \delta_{r,r'}\delta_{s,s'}\delta_{q,q'} \tag{3.13}$$

Apparently, the interactions (3.3) and (3.4) are already in boson form and the remaining challenge is to write the kinetic energy (3.2) in terms of bosons. To this end, one observes that

$$\left[H_0, b^\dagger_{r,s}(q)\right] = v_f\, r\, q\, b^\dagger_{r,s}(q) \tag{3.14}$$

This suggests that the following identity holds

$$\begin{aligned} H_0 &= \sum_{r,s,q>0} v_f\, q\; b^\dagger_{r,s}(q) b_{r,s}(q) + \text{const} \\ &= \frac{\pi v_f}{L} \sum_{r,s,q\neq 0} :\rho_{r,s}(q)\rho_{r,s}(-q): + \text{const.} \end{aligned} \tag{3.15}$$

This equation is indeed satisfied and is known as Kronig's identity [70]. It is obvious from equation (3.14) that (3.15) and (3.2) yield the same energy for any state obtained by acting on the non-interacting ground state with an arbitrary number of boson creation operators $b^\dagger_{r,s}(q)$. To complete the proof of the identity, one must show that every state in the Hilbert space can be accessed this way, i. e. that the $b^\dagger_{r,s}(q)$'s generate a complete basis when acting on the ground state of H_0. To prove this, it is sufficient to show that (3.15) has a unique ground state in the full fermion Hilbert space.

However, the discussion was so far implicitly limited to a sector of the fermion Hilbert space with a *fixed* number of particles on each of the four branches labeled by r, s. In the fermionic Hilbert space, it is possible to consider excitations that involve changes of the number of particles in each branch. Indeed, the "const." term in (3.15) depends on these particle numbers, which are conserved by the boson operators and cannot be expressed in terms of them, for they are related to the $q = 0$ term which is absent in the definition of the bosons and in (3.15). Indeed, one has

$$:\rho_{r,s}(0)\rho_{r,s}(0): = \; N^2_{r,s} \tag{3.16}$$

where $N_{r,s}$ is the number of particles on the r, s- branch measured relative to an arbitrarily chosen ground state at some finite k_f. $N_{r,s}$ is thus a finite quantity. The importance of a proper treatment of these $q = 0$ modes and their inclusion into the boson Hamiltonian has been stressed by Haldane. Only when the $q = 0$ limit is accurately represented by the boson Hamiltonian, non-trivial relations between Luttinger liquid parameters and thermodynamic properties of the model follow [45], as will be discussed in 3.2.5.

The diagonalization is now readily performed by the introduction of quantities corresponding to charge and spin degrees of freedom, preserving the commutation relations (3.11):

$$\rho_r(q) = \frac{1}{\sqrt{2}}\left[\rho_{r,\uparrow}(q) + \rho_{r,\downarrow}(q)\right], \qquad N_{r,\rho} = \frac{1}{\sqrt{2}}\left[N_{r,\uparrow} + N_{r,\downarrow}\right]$$
$$\sigma_r(q) = \frac{1}{\sqrt{2}}\left[\sigma_{r,\uparrow}(q) - \sigma_{r,\downarrow}(q)\right], \qquad N_{r,\sigma} = \frac{1}{\sqrt{2}}\left[N_{r,\uparrow} - N_{r,\downarrow}\right] \tag{3.17}$$

We may now rewrite the Luttinger Hamiltonian in the following form (using $\nu = \rho, \sigma$):

$$H_{TL} = H_0 + H_2 + H_4 \tag{3.18}$$
$$H_0 = \frac{\pi v_f}{L} \sum_{\nu,r} \left(\sum_{q\neq 0} : \nu_r(q)\nu_r(-q) : + N_{r,\nu}^2 \right) \tag{3.19}$$
$$H_2 = \frac{2}{L} g_{2\nu} \sum_{\nu} \left(\sum_{q\neq 0} \nu_+(q)\nu_-(-q) + N_{+\nu}N_{-\nu} \right) \tag{3.20}$$
$$H_4 = \frac{1}{L} g_{4\nu} \sum_{\nu,r} \left(\sum_{q\neq 0} : \nu_r(q)\nu_r(-q) : + N_{r,\nu}^2 \right) \tag{3.21}$$

where couplings

$$g_{i\rho} = \frac{1}{2}\left(g_{i\|} + g_{i\perp}\right) \quad , \quad g_{i\sigma} = \frac{1}{2}\left(g_{i\|} - g_{i\perp}\right) \tag{3.22}$$

have been introduced. It is apparent that H_4 is already of the same form as H_0, and hence the only difficulty comes from H_2. This may be resolved by the canonical transformation

$$\tilde{\nu}_r(q) \equiv \nu_r(q)\cosh(\xi_\nu) + \nu_{-r}(q)\sinh(\xi_\nu) \tag{3.23}$$
$$\text{where} \qquad K_\nu \equiv e^{2\xi_\nu} = \sqrt{\frac{\pi v_f + g_{4\nu} - g_{2\nu}}{\pi v_f + g_{4\nu} + g_{2\nu}}} \tag{3.24}$$

by means of which the Hamiltonian takes the final form

$$H_{TL} = \frac{\pi}{L} \sum_{\nu} \left(\sum_{r,q\neq 0} v_\nu : \tilde{\nu}_r(q)\tilde{\nu}_r(-q) : + \frac{1}{2}\left(v_{N\nu} N_\nu^2 + v_{J\nu} J_\nu^2 \right) \right) \tag{3.25}$$

$$\tag{3.26}$$

where
$$v_\nu = \sqrt{\left(v_f + \frac{g_{4\nu}}{\pi} \right)^2 - \left(\frac{g_{2\nu}}{\pi} \right)^2} \tag{3.27}$$

$$N_\nu = N_{+\nu} + N_{-\nu} \quad , \quad J_\nu = N_{+\nu} - N_{-\nu} \tag{3.28}$$

$$v_{N\nu} = v_\nu / K_\nu = v_f + \frac{g_{4\nu} + g_{2\nu}}{\pi} \tag{3.29}$$

$$v_{J\nu} = v_\nu \, K_\nu = v_f + \frac{g_{4\nu} - g_{2\nu}}{\pi} \tag{3.30}$$

The final form (3.25) of the Luttinger Hamiltonian is formally almost identical to the non-interacting Hamiltonian (3.19), except that now six different velocity parameters appear which are all equal to v_f in the non-interacting case. The collective density mode operators $\tilde{\nu}_r(q)$ satisfy the commutation relations (3.11) and are thus proportional to boson creation and annihilation operators. The corresponding collective modes are linearly dispersing with velocities v_ρ in the charge sector and v_σ in the spin sector. Spin and charge sector are completely decoupled. Each of these sectors features a conserved charge N_ν and a conserved current J_ν. Excitations involving changes in these two quantum numbers are characterized by different velocity parameters $v_{N\nu}$ and $v_{J\nu}$, respectively. Note that only in the non-interacting case, where all these velocities are trivially the same, *both* the collective mode picture with spin-charge separation as well as a Fermi liquid picture based on quasi-particles apply; for in this case, (3.25) may easily mapped back onto the non-interacting fermion Hamiltonian (3.2), and one could in principle map back and forth between these pictures. However, whenever interactions are present and the six velocity parameters are *not* the same, a mapping onto non-interacting fermions is not possible. Then only the bosonic collective mode picture applies, and the system is obviously not a Fermi liquid, which is most evident from the fact that the gapless spin and charge modes can have different velocities v_ν. This implies that any amount of interaction will destroy the Fermi liquid in one dimension, which already followed from the line of arguments given in (2.4.1).

Note that the three velocity parameters characterizing each sector $\nu = \rho, \sigma$ of the Luttinger model are not completely independent, but satisfy the relations

$$v_\nu^2 = v_{N\nu} v_{J\nu} \tag{3.31}$$

It is not obvious from (3.25) that this relation has to be satisfied by any physical model whose low energy effective theory is of the form (3.25). One might think that relation (3.31) is an artifact of the restrictive choice of interactions considered in the Luttinger model, and that other types of interactions such as (3.7), (3.8) could give rise to renormalization that lead to a violation of (3.31). Is was pointed out by

Haldane [45] that this is not so, but any choice of velocity parameters that violates (3.31) is unphysical. This becomes more apparent when the Hamiltonian (3.25) is expressed in terms of *local* bosonic fields, which will be done in the next section.

3.2.3 Bosonization and phase variables

The solution (3.25) reveals everything about the thermodynamics of the Luttinger model. It reveals little about its correlation functions, as it is not obvious how to express the local Fermi operators

$$\Psi_{r,s}(x) = \frac{1}{\sqrt{2\pi}} \sum_k e^{ikx} c_{rks} \tag{3.32}$$

in terms of the bosonic degrees of freedom introduced in the previous section. To achieve a bosonization of the above operator, one needs to introduce *local* bosonic fields. In order to motivate the proper definition of these quantities, it is useful to first solve the problem of how to rewrite the Hamiltonian (3.25) as a harmonic theory of local bosonic fields, then interpret these fields in terms of the local fermion density and use them to construct the fermion operators (3.32). [3]

Again, we first focus on the non-interacting part H_0 of the Hamiltonian, eq. (3.19). First we define ladder operators both for positive and negative momenta:

$$a_\nu^\dagger(q) = \sqrt{\frac{2\pi}{|q|L}} \begin{cases} \nu_+(q) \ , \ q > 0 \\ \nu_-(q) \ , \ q < 0 \end{cases} \tag{3.33}$$

such that

$$H_0 = v_f \sum_\nu \left(\sum_{q \neq 0} |q| \, a_\nu^\dagger(q) a_\nu(q) + \frac{\pi}{2L} \left(N_\nu^2 + J_\nu^2 \right) \right) \tag{3.34}$$

Now, it is a standard task in elementary quantum field theory to introduce a mode expansion for a local real field $\Phi_\nu(x)$, such that the linear spectrum of (3.34) can be reproduced by a harmonic field theory in terms of $\Phi_\nu(x)$ and its canonically conjugate momentum $\Pi_\nu(x)$ (see, e.g., [71]):

[3] In most of the original literature and virtually all reviews this program is inverted, probably for historical reasons. In the opinion of the author this does not lead to a very intuitive path.

$$\Phi_\nu(x) = \sqrt{\frac{2\pi}{L}} \sum_{q\neq 0} \frac{i}{2} \frac{\mathrm{sign}(q)}{\sqrt{|q|}}\, e^{iqx-\alpha|q|/2} \left(a_\nu(q) + a_\nu^\dagger(-q)\right) - \frac{\pi}{L} N_\nu\, x$$
$$= -\frac{2\pi i}{L} \sum_{q\neq 0} \frac{e^{-iqx-\alpha|q|/2}}{2q} \left(\nu_+(q) + \nu_-(q)\right) - \frac{\pi}{L} N_\nu\, x \tag{3.35}$$

$$\Pi_\nu(x) = \sqrt{\frac{1}{2\pi L}} \sum_{q\neq 0} \mathrm{sign}(q) \sqrt{|q|}\, e^{iqx-\alpha|q|/2} \left(a_\nu(q) - a_\nu^\dagger(-q)\right) + \frac{J_\nu}{L} \tag{3.36}$$

$$= \frac{1}{L} \sum_{q\neq 0} e^{-iqx-\alpha|q|/2} \left(\nu_+(q) - \nu_-(q)\right) + \frac{J_\nu}{L} \tag{3.37}$$

$$[\Phi_\nu(x), \Pi_{\nu'}(x')] = i\delta_{\nu,\nu'}\delta(x-x') \tag{3.38}$$

Here, α is an infinitesimal which has been introduced for regularization purposes. In the end, the $\alpha \to 0$ limit is always taken. The above definitions are standard, except for the $q = 0$ modes which do not have a corresponding ladder operator but are again represented by the operators N_ν, J_ν. Their coefficients were chosen such that both $\partial_x \Phi_\nu(x)$ as well as $\Pi_{\nu'}(x')$ are "continuous" at $q = 0$ when $\nu_r(q = 0)$ is identified with $N_{\nu,r}$.

With these definitions, the following identity for the non-interacting Hamiltonian H_0 holds:

$$H_0 = \frac{1}{2\pi} \sum_\nu \int dx\; v_f \left\{ \pi^2 \Pi_\nu^2(x) + \left(\frac{\partial \Phi_\nu(x)}{\partial x} \right)^2 \right\} \tag{3.39}$$

It was shown in the previous section that even the interacting problem can be mapped onto a theory of non-interacting linearly dispersing bosons, hence it makes sense that the full problem can also be cast into a form such as (3.39). One might want to go through the same steps that let to eq. (3.39), this time using the "renormalized" operators $\tilde{\nu}_r$ instead of the ν_r. However, this would lead to field definitions that depend on the interaction. Clearly, is is desirable to express both the Hamiltonian as well as the fermion operators (3.32) in terms of bosonic fields that are interaction independent, such as (3.35) and (3.37). One therefore proceeds by expressing the remainder of the Hamiltonian in terms of the fields defined above:

$$H_2 = \frac{1}{2\pi}\sum_\nu \int dx\ \frac{g_{2\nu}}{\pi}\left\{\pi^2\Pi_\nu^2(x) - \left(\frac{\partial\Phi_\nu(x)}{\partial x}\right)^2\right\} \tag{3.40}$$

$$H_4 = \frac{1}{2\pi}\sum_\nu \int dx\ \frac{g_{4\nu}}{\pi}\left\{\pi^2\Pi_\nu^2(x) + \left(\frac{\partial\Phi_\nu(x)}{\partial x}\right)^2\right\} \tag{3.41}$$

Hence the full Hamiltonian reads:

$$\begin{aligned} H_{TL} &= H_0 + H_2 + H_4 \\ &= \frac{1}{2\pi}\sum_\nu \int dx\ \left\{v_{J\nu}\pi^2\Pi_\nu^2(x) + v_{N\nu}\left(\frac{\partial\Phi_\nu(x)}{\partial x}\right)^2\right\} \end{aligned} \tag{3.42}$$

As expected, the full Luttinger Hamiltonian can still be expressed in terms of a harmonic field theory of linearly dispersing collective spin– and charge modes whose velocities are given by $v_\nu = \sqrt{v_{N\nu}v_{J_\nu}}$. In the present form, it is natural that each sector of the theory (spin and charge) is characterized by two free parameters and not three, and that whenever the three velocities (of each sector) in (3.25) do not satisfy relation (3.31), a mapping to a field theory of precisely the form (3.42) is not possible. Physically, relation (3.31) guarantees that both density and current response functions are continuous as $q \to 0$, as has been argued by Haldane [45].

The field $\Phi_\rho(x)$ is related to the local density $\rho(x)$ via:

$$\rho(x) \equiv \sum_{r,s}\rho_{r,s} = \sqrt{2}\left[\rho_+(x) + \rho_-(x)\right] = -\frac{\sqrt{2}}{\pi}\partial_x\phi_\rho(x) \tag{3.43}$$

where the $\sqrt{2}$ comes from (3.17). Similarly

$$\sigma(x) \equiv \sum_{r,s}s\rho_{r,s} = \sqrt{2}\left[\sigma_+(x) + \sigma_-(x)\right] = -\frac{\sqrt{2}}{\pi}\partial_x\phi_\sigma(x) \tag{3.44}$$

for the spin density. The meaning of these equations is the the $\Phi_\nu(x)$ must be thought of as "kink" fields, which jumps by $-\sqrt{2}/\pi$ at points where a charge or a spin, respectively, is localized. Based on this notion, a complete phenomenological derivation of all the results in this section can be given [72]. Similarly, one can define a field $\Theta_\nu(x)$, such that

$$\Pi_\nu(x) = \frac{1}{\pi}\partial_x \Theta_\nu(x) \tag{3.45}$$

$$\text{hence:} \quad \Theta_\nu(x) \equiv \pi \int_{-\infty}^{x} dx' \Pi_\nu(x')$$

$$= \frac{2\pi i}{L} \sum_{q\neq 0} \frac{e^{-iqx-\alpha|q|/2}}{2q} \left(\nu_+(q) - \nu_-(q)\right) + \frac{\pi}{L} J_\nu \, x \tag{3.46}$$

and the Hamiltonian (3.42) may be reexpressed as

$$H_{TL} = \frac{1}{2\pi} \sum_\nu \int dx \, \left\{ v_{J\nu} \left(\frac{\partial \Theta_\nu(x)}{\partial x} \right)^2 + v_{N\nu} \left(\frac{\partial \Phi_\nu(x)}{\partial x} \right)^2 \right\} \tag{3.47}$$

The field $\Theta_\nu(x)$ satisfies the commutation relation

$$[\Phi_\nu(x), \Theta_{\nu'}(x')] = i\frac{\pi}{2} \, \delta_{\nu,\nu'} \, \mathrm{sign}(x' - x) \tag{3.48}$$

from which (3.38) follows upon differentiation, as well as

$$[\nu(x), \Theta_{\nu'}(x')] = -\frac{\sqrt{2}}{\pi} \partial_x \left[\Phi_\nu(x), \Theta_{\nu'}(x')\right] = i\sqrt{2} \, \delta_{\nu,\nu'} \, \delta(x - x') \tag{3.49}$$

Hence up to a factor of $\sqrt{2}$, the phase fields $\Theta_\nu(x)$ are conjugate to the spin and charge density, respectively. This property allows us to construct the fermion operators (3.32). $\Psi_{r,s}(x)$ destroys a fermion on branch r with spin s at position x. Therefore, this operator must shift the charge density by $-\delta(x - x')$, whereas the spin density must be shifted by $-s\delta(x - x')$. This can be achieved by

$$\Psi_{r,s}(x) \propto \exp\left(\frac{i}{\sqrt{2}} \left[\Theta_\rho(x) + s\Theta_\sigma(x)\right] \right) \tag{3.50}$$

However, the above relation is by no means complete, since it does not depend on r yet, and the operator on the right commutes for different x. This can be corrected by a Jordan-Wigner type of factor:

$$\exp\left(-i\pi \int_{-\infty}^{x} dx \rho_{r,s}(x) \right) = \exp\left(-\frac{i}{\sqrt{2}} \left[r\Phi_\rho(x) + sr\Phi_\sigma(x) \right] \right) \tag{3.51}$$

The number inside the exponent is the number of particles on the r, s- branch which is located to the left of position x, just like in the familiar Jordan-Wigner transformation on a lattice [48]. The exponents in (3.50) and (3.51) may be added, since a proper use of the Baker-Hausdorff-identity would only give rise to an (infinite) c-number which is unspecified up to this point:

$$\Psi_{r,s}(x) \propto \exp\left(-\frac{i}{\sqrt{2}} \left[r\Phi_\rho(x) - \Theta_\rho(x) + s\left\{ r\Phi_\sigma(x) - \Theta_\sigma(x) \right\} \right] \right) \tag{3.52}$$

Now, the right hand side anticommutes for identical branches, but still commutes for different branches. Also, one must note that $\Psi_{r,s}(x)$ will change the quantum number $N_{r,s}$, which the bosonic fields in (3.52) are not capable of, as mentioned earlier. All this can be fixed by the introduction of unitary Klein operators, which change the numbers $N_{r,s}$ by one and anticommute for different branches. More precisely, the Klein operators $U_{r,s}$ are defined via commutation relations:

$$\left\{U_{r,s}, U^\dagger_{r',s'}\right\} = 2\delta_{r,r'}\delta_{s,s'} \qquad \text{where} \quad U_{r,s}, U^\dagger_{r,s} = \mathbf{1} \tag{3.53}$$

$$\left\{U_{r,s}, U_{r',s'}\right\} = 0 \quad \text{for} \quad (r,s) \neq (r',s') \tag{3.54}$$

$$\left[N_{r,s}, U_{r',s'}\right] = \delta_{r,r'}\delta_{s,s'}U_{r',s'} \tag{3.55}$$

$$\left[U_{r,s}, \nu_r(q \neq 0)\right] = 0 \tag{3.56}$$

This may be used to establish the following identity

$$\Psi_{r,s}(x) = \lim_{\alpha\to 0} \frac{e^{irk_f x}}{\sqrt{2\pi\alpha}} U^\dagger_{r,s} \exp\left(-\frac{i}{\sqrt{2}}\left[r\Phi_\rho(x) - \Theta_\rho(x) + s\left\{r\Phi_\sigma(x) - \Theta_\sigma(x)\right\}\right]\right) \tag{3.57}$$

In this complete form, the bosonization identity was first derived by Heidenreich et al. [69] and Haldane [66]. Their approach which has been sketched here is referred to as constructive bosonization, since it leads to an exact operator identity valid on the entire Hilbert space of the Luttinger model, including sectors with non-zero N_ν and J_ν. Constructive bosonization is reviewed in [64, 67, 73, 74, 75]. Besides this route, there exists an alternative "field theoretic bosonization". The latter is less rigorous, because of ambiguities concerning the cutoff-procedure and because it misses the Klein factors entirely, unless they are put in by hand[4]. In most practical cases, the Klein factors will drop out of the calculation because of their unitarity property and since the operators $\Psi_{r,s}(x)$, $\Psi^\dagger_{r,s}(x)$ usually come in pairs. However, the Klein factors can be crucial in problems of weakly coupled one-dimensional systems.

Perhaps unfortunately, the field theoretic approach to bosonization is somewhat more popular in the literature than the constructive one. The field theoretic approach is reviewed in [76, 77, 78].

3.2.4 Correlation functions

The bosonization identity (3.57) along with the harmonic Hamiltonian (3.47) now allows various correlation functions of physical interest to be calculated. It turns out that in a Luttinger liquid correlations generally decay with non-universal, interaction dependent power-laws. Let $\mathcal{O}(x)$ be a local operator whose correlation functions are to be calculated. These will be of the following generic form:

[4]This was obviously done here, too. However, e.q. (3.57) can be put on a completely firm basis using constructive bosonization. The reader is referred to the referenced literature.

$$\Big\langle \mathcal{O}(x)\,\mathcal{O}(0)\Big\rangle \propto \frac{\cos(2nk_f x)}{|x|^\theta} \tag{3.58}$$

Here, n is an integer and the correlation exponent θ will depend on the interactions of the model via the Luttinger parameter K_ρ:

$$K_\rho = \sqrt{\frac{v_{J\rho}}{v_{N\rho}}} \tag{3.59}$$

(cf. (3.29), (3.30)). Eq. (3.58) holds at all length scales for the Luttinger model. In a microscopic model, however, whose low energy effective theory is given by the Luttinger liquid, eq. (3.58) gives only the asymptotic behavior for $|x|$ much larger than any microscopic length scale. The small $|x|$ behavior will depend on model dependent microscopic details. The same is true for the overall coefficient in (3.58) which is cutoff ($\alpha-$) dependent in the Luttinger model, and in any given model will again depend on microscopic details. However, the correlation exponent θ is determined solely by the low energy properties of the model, as will be demonstrated below. In the following, a few operators of special interest will be given in the bosonized form, and their correlation exponents can be read of Table 3.1. The explicit evaluation of the correlation functions (3.58) is straightforward by means of the quadratic Hamiltonian (3.47), and is reviewed for example in [67].

The operator for the total density $\rho_{tot}(x)$ reads

$$\rho_{tot}(x) = \sum_s \Big(\Psi^\dagger_{+,s}(x) + \Psi^\dagger_{-,s}(x)\Big)\Big(\Psi_{+,s}(x) + \Psi_{-,s}(x)\Big) \tag{3.60}$$

and has a piece that oscillates at a wave vector $2k_f$, defining the $2k_f$–charge density wave (CDW) operator

$$\begin{aligned}\mathcal{O}_{CDW}(x) &= \sum_s \Psi^\dagger_{+,s}(x)\Psi_{-,s}(x) \\ &= \frac{1}{\pi\alpha}\exp\Big(-2ik_f x + \sqrt{2}i\Phi_\rho(x)\Big)\cos\Big(\sqrt{2}\Phi_\sigma(x)\Big) \quad ,\end{aligned} \tag{3.61}$$

whose correlations may dominate over those of the non-oscillatory piece of the density[5]. Similarly, $2k_f$–spin density wave operators may be defined:

$$\begin{aligned}\mathcal{O}_{SDW,z}(x) &= \sum_s s\Psi^\dagger_{+,s}(x)\Psi_{-,s}(x) \\ &= \frac{i}{\pi\alpha}\exp\Big(-2ik_f x + \sqrt{2}i\Phi_\rho(x)\Big)\sin\Big(\sqrt{2}\Phi_\sigma(x)\Big) \quad ,\end{aligned} \tag{3.62}$$

Finally, one may define operators corresponding to singlet and triplet superconducting

[5]The non-oscillatory part of the density has correlations that decay with a universal power $\theta = 2$ and are hence never the most dominant correlations at large distances (Table 3.1).

pairing:

$$\mathcal{O}_{SS}(x) = \frac{1}{\sqrt{2}} \sum_s s\Psi_{-,s}(x)\Psi_{+,-s}(x)$$
$$= \frac{1}{\sqrt{2}\pi\alpha} \exp\left(\sqrt{2}i\Theta_\rho(x)\right) \cos\left(\sqrt{2}\Phi_\sigma(x)\right) \tag{3.63}$$

$$\mathcal{O}_{TS,0}(x) = \frac{1}{\sqrt{2}} \sum_s \Psi_{-,s}(x)\Psi_{+,-s}(x)$$
$$= \frac{1}{\sqrt{2}\pi\alpha} \exp\left(\sqrt{2}i\Theta_\rho(x)\right) \sin\left(\sqrt{2}\Phi_\sigma(x)\right) \tag{3.64}$$

Naturally, there are three triplet pairing operators, where only the one is displayed that creates an $S_z = 0$ triplet state. Similarly, there are three components to the spin-density wave operator. However, here we only consider the isotropic case, where all three components of these operator triplets have the same correlation functions. When the details are worked out, this corresponds to the case $K_\sigma = 1$, and for all other values of K_σ the spin density wave and triplet superconducting correlations will not be isotropic. Hence, in a model with isotropic interactions there are only two possibilities for the spin sector: Either it scales to the Luttinger fixed point with $K_\sigma = 1$, or it flows to strong coupling, in which case the spin sector will be gapped. The charge parameter K_ρ, however, can take any value at the Luttinger fixed point.

The term "Luttinger liquid" has so far been used to describe a system whose spin and charge degrees of freedom are both gapless and are described by the low energy effective theory (3.47). However, due to spin-charge separation, such a system really consists of two independent liquids, one corresponding to spin and one corresponding to charge degrees of freedom. It may well be that the Luttinger liquid picture breaks down for only one of the two sectors, while the other one is still described by the corresponding part of the Hamiltonian (3.47). For example, it may occur that the spin sector is gapped and is described by a gapped sine-Gordon field theory, which contains additional relevant anharmonic operators, whereas the charge part remains

	θ, no spin-gap	θ, with spin-gap
CDW	$1 + K_\rho$	K_ρ
SDW	$1 + K_\rho$	∞
SS	$1 + 1/K_\rho$	$1/K_\rho$
TS	$1 + 1/K_\rho$	∞

Table 3.1: Correlation exponent θ of various correlation functions in a Luttinger liquid. The first column assumes the isotropic gapless case $K_\sigma = 1$ (see text). In the spin gapped case, the entry "∞" denotes that the corresponding correlations decay exponentially.

gapless and is described by the harmonic theory derived in the previous section. Then, all aspects that refer to only charge degrees of freedom are still described by the same Luttinger liquid phenomenology, and one may still regard the charge sector of the model as a (spinless) Luttinger liquid. All these cases are summarized in Table 3.1 (Refs. [43, 67]).

One notes that when $K_\rho > 1$, pairing correlations dominate over density wave correlations at large distances, and vice versa for $K_\rho < 1$. From (3.24) these cases correspond to attractive and repulsive forward scattering interactions, respectively, while $K_\rho = 1$ characterizes a non-interacting Fermi sea. This basic picture still holds when a spin gap is present, except that spin density wave and triplet pairing correlations decay exponentially. Here, the competition is therefore solely between CDW and SS correlations.

Note that no true long range order can ever be established in a one-dimensional system even at $T = 0$, unless a *discrete* broken symmetry is involved. The Luttinger liquid therefore does not describe a true superconductor, nor a true charge density wave state for any finite value of K_ρ. On the other hand, gaps may open up in the spectrum of 1d systems without any symmetry breaking, and *algebraically* decaying order is usually present in more than one order parameter simultaneously. These orders are competing when higher dimensional couplings are present. One may consider an array of weakly coupled one-dimensional chains or quantum wires. At sufficiently high temperatures, the interchain couplings are irrelevant and the individual chains behave to a good approximation like isolated one-dimensional systems with competing orders[6]. However, as the temperature is lowered, interchain couplings will enhance the systems tendency to order and give rise to a finite transition temperature T_c into a state where higher dimensional order is present and the Luttinger liquid physics is thereby destroyed. At T_c a dimensional crossover takes place, where the interchain couplings become relevant and will lock the relative phases of a certain order parameter between chains, thereby establishing long range order both within the chains and in the perpendicular direction. This will be the fate of all real quasi-one-dimensional systems, since true one-dimensionality is an idealization and higher dimensional couplings always exist.

Which type of order is established at T_c (i.e. SS, CDW etc...) in a quasi one-dimensional system depends on both the relative strength of various competing orders in the decoupled idealized one-dimensional system, as well as on the nature of the interchain couplings. In most cases, however, the competition is won by the order parameter whose correlations would decay the slowest at large distances in the absence of interchain effects.

[6]Power-law correlations exist only at $T = 0$ in a one-dimensional system. However, the correlations which dominate at long distances for $T = 0$ will also dominate at finite temperature when length scales of order v/T are considered, where v is a characteristic velocity.

3.2.5 Calculating correlation functions from spectral properties

The benefit of knowing a low energy effective theory such as the Luttinger liquid is that *both* the long distance correlation functions as well as the low energy thermodynamic and spectral properties of a system can be expressed in terms of a few parameters that entirely characterize the effective theory. To perform the mapping between a microscopic model and its low energy effective theory means to calculate these few parameters from the microscopics. Conveniently, this can be done by calculating thermodynamic and spectral properties of the microscopic model, which in 1d systems can be carried out either numerically, or sometimes analytically by means of the Bethe ansatz. (This will usually still require some numerical tasks). A direct calculation of correlation functions is impossible for most microscopic models. However, the Luttinger liquid parameters calculated from the low energy spectrum do also determine the behavior of correlation functions at large distances, provided that the system can indeed be described as Luttinger liquid. In the isotropic case, all relevant correlation exponents can be expressed in terms of the single Luttinger parameter K_ρ (Table 3.1). On the other hand, it was shown above that K_ρ can be calculated given any two of the three "velocities" of the Luttinger liquid [45]:

$$K_\rho = \sqrt{\frac{v_{J\rho}}{v_{N\rho}}} = \frac{v_\rho}{v_{N\rho}} = \frac{v_{J\rho}}{v_\rho} \tag{3.65}$$

The collective charge mode velocity v_ρ characterizes the linear dispersion of the charge modes and is hence related to the low energy spectrum in an obvious manner. Is is slightly less obvious how to conveniently extract the parameters $v_{N\rho}$ and $v_{J\rho}$. Yet from (3.25) it is apparent that these parameters determine the response of the ground state energy when an overall change in density and current is imposed on the system. Indeed, it is follows straightforwardly from (3.25) that a change in the average density $\Delta\rho$ will cause the following change in the ground state energy:

$$\Delta E_0 = \frac{\pi}{4} L v_{N\rho} (\Delta\rho)^2 \tag{3.66}$$

where again an additional factor of $1/2$ comes from (3.17). This implies that $v_{N\rho}$ can be obtained from the ground state energy as function of particle density via

$$\begin{aligned} v_{N\rho} &= \frac{2}{\pi L} \frac{\partial^2 E}{\partial \rho^2} \\ &\equiv \frac{2}{\pi \rho^2 \kappa} \end{aligned} \tag{3.67}$$

where the compressibility κ of the system has been introduced. Hence, the physical meaning of $v_{N\rho}$ is that it is essentially the inverse compressibility of the system.

For $v_{J\rho}$ on the other hand, one would in principle need to calculate the ground state as function of the quantum number J_ρ, which is related to the current. Physically,

it is equivalent to consider the system on a ring with periodic boundary conditions penetrated by a magnetic flux $L\phi$. Such a flux can be represented by a constant vector potential

$$A(x) \equiv \phi \tag{3.68}$$

Such a vector potential may be removed by a gauge transformation, under which the fermion operators (3.32) transform as (taking the unit charge to be $e \equiv 1$)

$$\Psi_{r,s}(x) \longrightarrow e^{i\phi x}\Psi_{r,s}(x) \tag{3.69}$$

which is independent of r and s. From the bosonization identity (3.57) this is equivalent to letting

$$\Theta_\rho(x) \longrightarrow \Theta_\rho(x) + \sqrt{2}\phi x \tag{3.70}$$

which is consistent with the interpretation that the field $\Theta_\rho(x)$ is essentially the phase conjugate to the local charge density. The Hamiltonian (3.47) then transforms as

$$H_{TL} \longrightarrow H_{TL} + \frac{v_{J\rho}}{2\pi}\int_0^L dx\, \left(2\sqrt{2}\,\frac{\partial\Theta\rho(x)}{\partial x}\,\phi + 2\phi^2\right) \tag{3.71}$$

Since $\int dx\, \frac{\partial\Theta\rho(x)}{\partial x} = \pi J_\rho$ [7], the ground state energy transforms as

$$E \longrightarrow E + \sqrt{2}v_{J\rho}J_\rho\phi + v_{J\rho}\frac{L}{\pi}\phi^2 \tag{3.72}$$

It follows that $v_{J\rho}$ can be inferred from the ground state energy E as function of ϕ via

$$v_{J\rho} = \frac{\pi}{2L}\,\frac{\partial^2}{\partial\phi^2}E\bigg|_{\phi=0} \tag{3.73}$$

As an aside, the current operator of a system can generally be written as the functional derivative of the Hamiltonian with respect to the vector potential $A(x)$. By (3.68) and (3.71), this gives for $\phi = 0$:

$$j(x) = \frac{\partial H}{\partial A(x)} = v_{J\rho}\frac{\sqrt{2}}{\pi}\frac{\partial\Theta\rho(x)}{\partial x} \tag{3.74}$$

Note that the current is indeed proportional to $v_{J\rho}$ and thus has nothing to do with the collective mode velocity v_ρ. In this sense $v_{J\rho}$ plays the role of a renormalized Fermi velocity [45]. In particular, in a system with a Galilean invariance the current operator is directly proportional to the momentum operator in the limit $q \to 0$, and is independent of interactions. Hence $v_{J\rho}$ will not be renormalized by interactions at all and will be equal to the Fermi velocity of the non-interacting system. An example of a Galilei invariant system would be a one-dimensional electron gas with density-density interactions, which will always give rise to $g_{2\nu} = g_{4\nu}$. Indeed, this leads to

[7] This implies the boundary condition $\Theta_\rho(L) - \Theta_\rho(0) = \pi J_\rho$ for the field Θ_ρ, showing that the current (3.75) is associated with a topological "winding number".

$v_{J\nu} = v_f$ in (3.30).

Finally, it follows from (3.74) that the quantum number J_ρ corresponds to a global current

$$I_{tot} = \int_0^L dx\, j(x) = \sqrt{2} v_{J\rho} J_\rho \quad . \tag{3.75}$$

Being the coefficient of a squared phase gradient proportional to the current in (3.47), the parameter $v_{J\rho}$ can be regarded as the charge stiffness of the Luttinger liquid. In one-dimension, however, a non-zero value of the stiffness defined in the above sense does not imply long range order in the phase variable Θ_ρ. Furthermore, by means of (3.73) it can be shown that $v_{J\rho}$ is proportional to the Drude weight of the conductivity, and hence to the inverse of the charge carrying mass [79, 80, 81].

3.3 The numerical phase diagram of the tJJ'–model

Following the motivation given in section 3.1 we wish to study a one-dimensional lattice model of spin-$\frac{1}{2}$ fermions that fulfills the following requirements:

1. The Hamiltonian has the full translational symmetry of the lattice.

2. When the band is half filled (one particle per site), the model dimerizes spontaneously, i. e. the dimer order parameter (2.14) has a non-zero expectation value.

3. Doping holes into the half filled band will lead to a liquid state with restored translational symmetry, but the spins remain gapped.

Note that for simplicity, we demand all these properties from a model of merely electronic degrees of freedom, whereas the spin-Peierls transition in real systems is triggered by an interplay between electronic and lattice degrees of freedom. However, the nature of the mechanism that gives rise to the dimerization played no particular role in the arguments given in section 3.1. The phenomenology discussed there is interesting enough in its on right to be studied in the context of a purely electronic model, even if phonons should alter the physics. However, it has been argued for pure spin systems that a problem with spin-phonon couplings can be mapped onto a frustrated spin chain by means of flow equations [82]. Though this can be strictly justified only in the idealized situation of a very fast lattice, it gives rise to the conjecture that at least in a purely one-dimensional situation the physics of a spin-phonon system is related to that of a frustrated spin chain. Indeed, as will be discussed below, a frustrated spin chain can also be in a dimerized state at $T = 0$, since a discrete symmetry may be broken even in a purely one-dimensional system. This motivates the choice of the one-dimensional tJJ'-model:

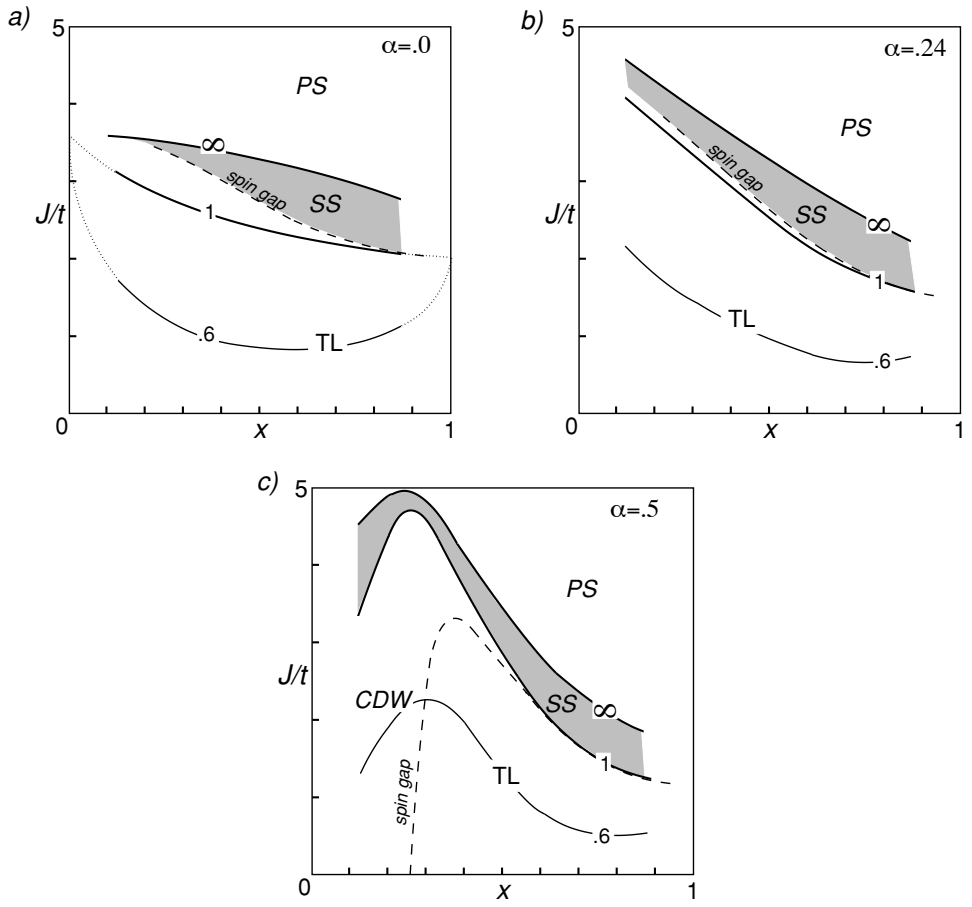

Figure 3-4: Sketch of the zero temperature phase diagram of the tJJ'-model as determined numerically in Ref.[83] for $\alpha = 0$ (a), $\alpha = .24$ (b) and $\alpha = .5$ (c). Contours are labeled by values of K_ρ. The shaded region marks the domain of dominant singlet superconducting correlations. The dotted lines in (a) were proposed in Ref. [84].

$$H = -t\mathcal{P}\sum_i (c^\dagger_{i,\sigma} c_{i+1,\sigma} + h.c.)\mathcal{P} + J\sum_i (S_i \cdot S_{i+1} - \frac{1}{4} n_i n_{i+1}) \\ + J'\sum_i (S_i \cdot S_{i+2} - \frac{1}{4} n_i n_{i+2}) + V\sum_i n_i n_{i+1} \tag{3.76}$$

Again, $\mathcal{P}$ enforces the constraint of no doubly occupied sites as discussed below (1.2). The first two terms are identical to the tJ-model (1.2) in one dimension, and a next-nearest neighbor coupling J' has been added. Both the nearest- and next-nearest-neighbor couplings J and J' are assumed positive throughout this thesis. In addition, a nearest neighbor interaction V has been included for later convenience. For $V = 0$ the zero temperature phase diagram of (3.76) has been obtained numerically [83, 84, 85] for various values of the parameter $\alpha \equiv J'/J$. The results are sketched in

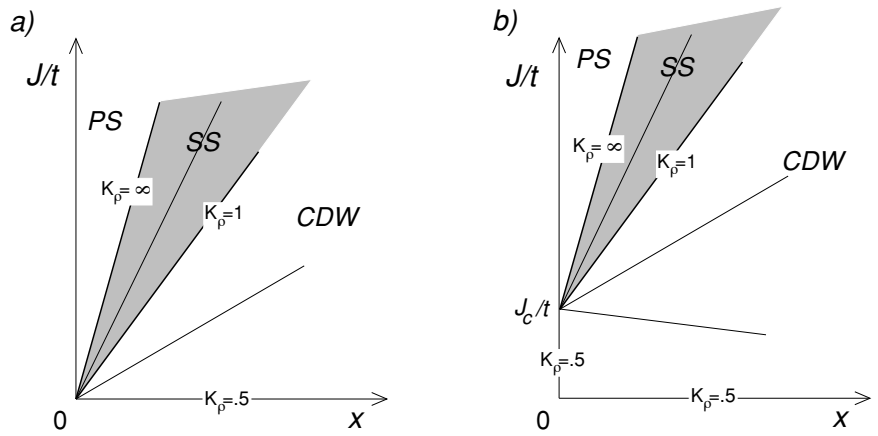

Figure 3-5: Two possible scenarios for the phase diagram for $\alpha > \alpha_c$ at small doping and J/t. a) $J_c = 0$ all contours of K_ρ flow into the origin. b) Finite J_c. Contours flow into a critical point [$x = 0$, $J_c > 0$].

Fig. 3-4). These phase diagrams have been determined by exact diagonalization of clusters of up to $L = 16$ sites using the methods described in 3.2.5. That is, the Luttinger parameter K_ρ has been obtained form the charge mode velocity v_ρ and the "compressibility parameter" $v_{N\rho}$. Contours of constant values of K_ρ are shown.

All phase diagrams show a Tomonaga-Luttinger liquid (TL) region below the dashed line labeled "spin gap", where both spin and charge degrees of freedom are gapless. Above the dashed line there is a spin gapped liquid phase which is subdivided into a regime of dominant singlet superconducting (SS) correlations (shaded grey) and, where present, a regime of dominant charge-density-wave correlations (CDW). These regions are readily identified form the respective value of K_ρ and the cases shown in Table 3.1. That is, the crossover between the (SS) region and the (CDW) region in the spin-gapped phase is given by the $K_\rho = 1$ contour.

In addition, the liquid phase is bounded by a line where K_ρ diverges. There, the compressibility of the system is infinite, and the liquid phase becomes unstable towards phase separation (PS). In this region of the phase diagram, the ground state of the system has a phase boundary between a hole-rich and an electron rich phase.

At zero doping ($x = 0$) eq. (3.76) reduces to a pure spin Hamiltonian. It is well known that the undoped spin chain undergoes a phase transition at a critical value of $\alpha_c \approx .24$ (Refs. [86, 87]) above which the ground state is dimerized and doubly degenerate with a gap in the spin excitation spectrum [88, 89]. For $\alpha > \alpha_c$ this spin gap remains present over a finite range of doping for any value of J/t, as was shown in Ref. [85]. In this regime, the Hamiltonian (3.76) hence satisfies all the criteria formulated in the beginning of this section, and probably can be regarded the simplest and most elementary model that does this.

Fig. 3-4c) shows the phase diagram at $\alpha = .5$. Apparently, this case differs qualitatively from the cases $\alpha = 0$ (a)) and $\alpha = \alpha_c$ (b)) at small doping. For one, a spin gap is present at any J/t. Secondly, it appears from the numerics as if all K_ρ

contours, including the phase separation boundary $K_\rho = \infty$, flow to small values of J/t at small x (cf. Refs. [85, 83]). This behavior gives rise to considerable overlap of the pairing region $K_\rho > 1$ with the spin gap region even at small doping. One expects that all K_ρ contours will focus on a single critical point $[x = 0, J_c/t]$, as was proposed in Ref. [84] for the tJ-model ($J' = 0$, Fig. 3-4a)

A possibility that seems consistent with the numerics at $\alpha = .5$ is that $J_c = 0$, i.e. all contours flow into the origin of the phase diagram (Fig. 3-5 a). In this case, a sufficiently small amount of doping would always lead to phase separation, and upon further doping one would enter a region of dominant SS correlations. Alternatively, J_c could be finite (Fig. 3-5 b) but possibly smaller than its value at $\alpha = 0$, which is between $3t$ and $4t$ (Fig. 3-4 a). This would imply that the above phenomenology of phase separation and superconductivity at small doping occurs only for $J > J_c$, while for $J < J_c$ the liquid phase is stable at any doping x. In the latter case, one would expect the Luttinger parameter K_ρ to approach the value $1/2$ in the dilute hole limit $x \to 0$, which is the value corresponding to non-interacting spinless degrees of freedom[8]. This behavior is clearly exemplified by the numerical phase diagram of the tJ-model (Fig. 3-4a). Note that both scenarios sketched in Fig. 3-5 assume that the phase separation boundary intersects the $x=0$–axis with positive slope, which is suggested by the numerics (yet unessential in case b)).

The numerics do not indicate which of the two scenarios in Fig. 3-5 applies to the tJJ'-model at $\alpha > \alpha_c$. The primary goal of the remainder of this thesis is to provide analytic insight into this question. The result will be strongly in favor of scenario b), where the stability of the liquid phase is demonstrated perturbatively for sufficiently small J/t, and the free spinless soliton picture for the charge degrees of freedom is confirmed in detail in the limit $x \to 0$. The latter is a manifestation of spin charge-separation that has been shown to occur in many integrable models (e.g. [90]), but which is usually hard to firmly demonstrate for non-integrable systems such as the tJJ'-model.

3.4 Mathematical formulation of the problem

We begin our analysis by casting the Hamiltonian (3.76) into a language where the holes play the role of domain walls between broken segments of an infinite spin chain [9] (Fig. 3-6). We consider a lattice of L sites with a number of N_e electrons and $N_h = L - N_e$ holes. Denoting the i'th spin on the lattice by S_i we may regard the spins as residing on a "squeezed" lattice where the hole sites have been dropped from the system and the label i of the spin S_i is a site label in this squeezed space, as in Fig. 3-6). We also introduce interstitial sites for the squeezed spin lattice whose labels $j = i + 1/2$ differ from those of the spin sites by $1/2$. Each interstitial site may accommodate a number $n_j = 0, 1...$ of holes. A faithful representation of the Hilbert

[8] This can easily be seen by evaluating any of the expression (3.65) for a gas of non-interacting spinless particles in one dimension

[9] I thank F.D.M. Haldane for pointing out to me this possibility

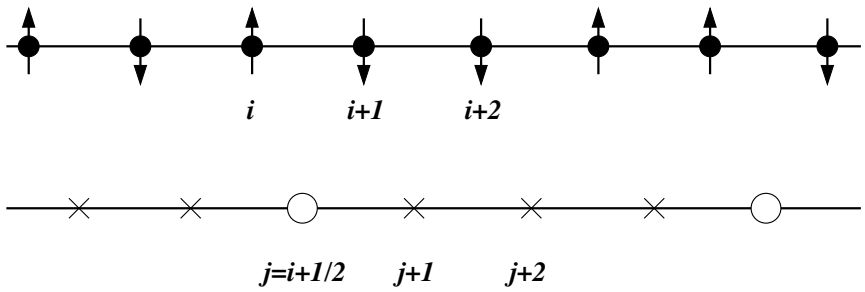

Figure 3-6: Domain wall representation of the Hilbert space. The upper chain represents the spin sector with sites labeled by i. The holes live on a lattice of interstitial sites labeled by j. Crosses represent "empty" interstitial sites, circles represent holes between two spins.

space of (3.76) is given by states labeled by

$$\begin{aligned} \Big| \ldots, \sigma_i, n_{i+\frac{1}{2}}, \sigma_{i+1}, \ldots \Big\rangle &\equiv |\ldots \sigma_i \ldots\rangle \, |\ldots n_j \ldots\rangle \\ \sum_j n_j &= N_h \\ i &= 1 \ldots N_e \\ j &= \frac{1}{2} \ldots N_e + \frac{1}{2} \end{aligned} \tag{3.77}$$

where $\sigma_i = \pm\frac{1}{2}$ denotes the z-component of the spin S_i. This language turns out to be particularly convenient when one introduces a large nearest neighbor hole repulsion, i. e. if we let $V = \infty$ in (3.76), such that it is forbidden for two holes to occupy neighboring sites. In the present language this means that the occupancy of the hole cluster labeled by j is now restricted to be $n_j = 0, 1$. This modification of the model will be irrelevant in the dilute hole limit which we are interested in. One may now choose to formulate the hole dynamics either in terms of hard-core boson operators or spinless fermion operators. For convenience, we introduce fermion ladder operators c_j, $c_j^\dagger$, where the action of $c_j^\dagger$ can be described by cutting the spin chain open at the interstitial site j, introducing a hole at this position and multiplying the state by an appropriate fermion phase. The hole kinetic energy is then simply given by

$$H_c = -\sum_j \Big(t \, c_j^\dagger c_{j+1} + h.c. \Big) \tag{3.78}$$

(3.78) can be thought of as the $J = J' = 0$ limit of the Hamiltonian. In the other limit of interest, namely the limit of zero doping $x = N_h/L$, the Hamiltonian becomes that of a pure spin chain:

$$H_s = J \sum_i \left(X_{i,i+1} + \alpha X_{i,i+2} \right)$$
$$\text{where} \qquad X_{i,i'} = S_i \cdot S_{i'} - \frac{1}{4} \tag{3.79}$$

where we work at constant $\alpha = J'/J$ from now on, and assume that $\alpha > \alpha_c$, such that the small doping regime is spin gapped. The combined Hamiltonian

$$H_0 = H_s + H_c, \tag{3.80}$$

where the spin and charge parts are still completely decoupled, will serve as a starting point for the perturbation theory proposed in this chapter. In order to correctly reproduce matrix elements of the Hamiltonian (3.76), couplings between the spin sector and the charge sector must be introduced:

$$H = H_0 + H_{sc} + H'_{sc} \tag{3.81}$$
$$H_{sc} = -J \sum_j n_j \gamma_j \tag{3.82}$$
$$H'_{sc} = J\alpha \sum_i X_{i-1,i+1} n_{i-\frac{1}{2}} n_{i+\frac{1}{2}} \tag{3.83}$$

where

$$\gamma_{i+\frac{1}{2}} = (1-\alpha) X_{i,i+1} + \alpha (X_{i-1,i+1} + X_{i,i+2}) \tag{3.84}$$

Here, H_{sc} is a correction which couples spin and charge by adjusting nearest neighbor bonds and removing next-nearest neighbor bonds in the squeezed spin space in the vicinity of a hole. Certain corrections of the latter sort are redundant whenever two holes are next - nearest neighbors in real space – or nearest neighbors in the present formalism – and this is corrected by H'_{sc}. Formally, H_{sc} and H'_{sc} are suppressed by powers of both J/t *and* x, and hence can be regarded as small compared to H_0. The strategy is hence to treat the spin-charge coupling terms $H_{sc} + H'_{sc}$ as a perturbation. Caution, however, will be necessary since the hole kinetic energy H_c is very small, or order tx^2, and the small energy denominators that appear in perturbation theory must be treated with care. Below this method will be applied to the spin gapped regime $\alpha > \alpha_c$ and will be found to be a valid procedure in second order perturbation theory, in the sense that corrections are indeed small in the limit considered here. The general systematics of this at higher order perturbation theory are elucidated in appendix A.

In the next section it will be shown that the approach described above gives rise to a perturbative expansion of the ground state energy which may be used to analyze the phase diagram of (3.76) in the vicinity of the origin, where the fate of the various phases is uncertain from numerics for $\alpha > \alpha_c$ (Fig. 3-4c). The procedure proposed here bears some resemblance to that used by Xiang et al. to study the tJ-model in a

first order perturbative approach [91].

3.5 Perturbative analysis of the model

As argued in section 3.2.5, it is generally possible in gapless one-dimensional systems to derive basic features of the phase diagram from spectral properties by means of Luttinger liquid theory [45]. In particular, by working with the first of relations (3.65) we can calculate the crucial Luttinger parameter K_ρ and hence all correlation exponents of the model from only the ground state energy E as a function of the density and a phase ϕ as defined in section 3.2.5:

$$K_\rho = \sqrt{\frac{v_{J\rho}}{v_{N\rho}}} \tag{3.85}$$

where:

$$v_{N\rho} = \frac{2}{\pi L}\frac{\partial^2 E}{\partial x^2} \tag{3.86}$$

$$v_{J\rho} = \frac{\pi}{2L}\frac{\partial^2 E}{\partial \phi^2}\bigg|_{\phi=0} \tag{3.87}$$

Here, $v_{N\rho}$ has been reexpressed in terms of the hole density $x = 1 - \rho$. The strategy in now to evaluate both the numerator and the denominator in (3.85) perturbatively.

We now proceed by imposing periodic boundary conditions on the charge sector and the spin sector of the system (3.81)-(3.83) separately. This is apparently not the same as imposing periodic boundary conditions in real space, since momenta are now quantized in units of $2\pi/N_e$ rather than $2\pi/L$. Note that there is a unique and well defined map between the state space introduced in (3.77) and the Hilbert space of the tJJ' model only for a finite system with *open* boundary conditions. Indeed, imposing open boundary in real space *is* equivalent to imposing them in the spin sector and the charge sector separately. However, going from open to periodic boundary conditions is not expected to matter for large system sizes. The unperturbed Hamiltonian H_0 then has two separately conserved momenta, and we denote its ground state by

$$|\sigma_0, \psi_0\rangle \equiv |\sigma_0\rangle\,|\psi_0\rangle \tag{3.88}$$

where $|\sigma_0\rangle$ is the ground state of the spin Hamiltonian H_s on a ring of N_e spin sites. Although for $\alpha > \alpha_c$ the ground state of H_s has a broken translational symmetry and is doubly degenerate, we will assume that $|\sigma_0\rangle$ is a symmetric superposition of the two symmetry broken ground states and thus has zero lattice momentum. Likewise $|\psi_0\rangle$ is a non-interacting Fermi sea of N_h spinless Fermions hopping on N_e sites with periodic boundary conditions. The unperturbed ground state energy we write as

$$E_0 = E_{\sigma_0} + E_{\psi_0} = E_{\sigma_0} - N_e \frac{2t}{\pi} \sin(k_f) \tag{3.89}$$

$$\text{where} \quad k_f = \pi \frac{N_h}{N_e} = \frac{\pi x}{1-x} \tag{3.90}$$

and E_{σ_0}, E_{ψ_0} are the ground state energy of H_s and the spinless fermion kinetic energy, respectively. We will focus the analysis on the limit $x \to 0$ where J/t is small but fixed. In this limit one can argue that the ground state energy of (3.81) has an asymptotic expansion of the form

$$E = E_{\sigma_0} + L(Ax + Bx^2 + Cx^3 + \dots) \tag{3.91}$$

The coefficients $A, B \dots$ will depend on J/t. At the leading order, they can in principle be inferred from the spinless fermion kinetic energy in (3.89). Formally, however it will be more convenient to work with an expansion of the form

$$E = E_{\sigma_0} + N_e \left(\tilde{A} \left(\frac{k_f}{\pi} \right) + \tilde{B} \left(\frac{k_f}{\pi} \right)^2 + \tilde{C} \left(\frac{k_f}{\pi} \right)^3 + \dots \right) \tag{3.92}$$

The coefficients in (3.91) and (3.92) will in general not be the same, due to the non-linear dependence of k_f on x in (3.90). However, since $N_e = L(1-x)$, the $\tilde{A}$ term in (3.92) is linear in x, and hence

$$A = \tilde{A}, \quad B = \tilde{B} \tag{3.93}$$

We will now proceed by evaluating the above series order by order in perturbation theory, treating the spin-charge coupling terms $H_{sc} + H'_{sc}$ perturbatively as outlined above. We write

$$\begin{aligned} E &= E_0 + E_1 + E_2 + \dots + E_k + \dots \\ A &= A_0 + A_1 + A_2 + \dots + A_k + \dots \\ &\vdots \end{aligned} \tag{3.94}$$

and similarly for all other coefficients, where the label k denotes a term arising at k'th order perturbation theory. We have:

$$A_0 = -2t \quad B_0 = 0 \quad C_0 = \frac{\pi^2}{3} t \tag{3.95}$$

From (3.85)-(3.87), (3.91) it follows that at small x, J/t

$$K_\rho \approx \frac{\pi}{2}\sqrt{\frac{A_{\phi\phi}\, x}{2B + 6C\, x}} \approx \frac{\pi}{2}\sqrt{\frac{A_{0,\phi\phi}\, x}{2B + 6C_0\, x}} = \frac{1}{2}\sqrt{\frac{tx}{B/\pi^2 + tx}} \tag{3.96}$$

where $A_{\phi\phi}$ denotes the second derivative with respect to the phase ϕ introduced above, and $A_0(\phi) = -2t\cos(\phi)$ was used. In the second line of eq. (3.96), all terms proportional to x have been replaced by their $J = 0$ values. However, the term linear in B is not suppressed by powers of x but vanishes at $J = 0$ and hence can be expected to be suppressed by powers of J/t. It will be crucial to decide whether the B-coefficient acquires a non-zero value in the presence of non-zero J, or remains zero to all orders in J/t. Note in particular that if B acquires a finite negative value due to the spin-charge couplings, K_ρ will diverge as $x \to 0$ even at small J/t. This would then lead to the scenario of Fig. 3-5 a), where strong superconducting fluctuations and phase separation at the divergence occur at any value of J/t as $x \to 0$.

On the other hand, if B is zero or positive, the liquid phase will be stable for small x and J/t, and dominant superconducting correlations will be absent in the vicinity of the origin of the phase diagram. In this case, one would expect that $B = 0$ to all orders in perturbation theory, since for $B > 0$ one would have $K_\rho \to 0$ as $x \to 0$ which seems inconsistent with the numerical phase diagram. Also, $K_\rho = 0$ is a somewhat unlikely pathological limit of Luttinger liquid theory, where the coefficient of the conjugate momentum of the charge field in (3.42) becomes negligible and the charges freeze into a classical state. This again seems unlikely in the absence of long-rage interactions, which one may assume especially in the presence of a spin gap. As argued initially, one would rather expect the charges to behave as non-interacting spinless solitons in the dilute limit, and Luttinger liquid physics then implies that K_ρ assumes the value $\frac{1}{2}$ in this limit, provided that no instability intervenes (Fig. 3-5b)). This then requires that the coefficient $A_{\phi\phi}$ and C in (3.96) are not independent, but have a constant ratio independent of J.

Hence, only two cases need to be distinguished which are the only ones consistent with the numerical phase diagram for $\alpha > \alpha_c$, Luttinger liquid theory and general expectations from the study of integrable models [45, 90]:

1. $B < 0$, leading to a phase separation instability in the dilute hole limit for any value of J/t, and

2. $B \equiv 0$, $6C \equiv \pi^2 A_{\phi\phi}$ for any J/t, corresponding to a stable liquid as $x \to 0$ and small J/t, where the charges act as a dilute gas of non-interacting spinless solitons.

It will be shown in the following that the second case applies.

At first order perturbation theory the energy corrections factorize into mean-field

like products, since spin and charge are not correlated in the ground state wave function (3.88). We have

$$\begin{aligned} E_1 &= \langle \sigma_0, \psi_0 | H_{sc} + H'_{sc} | \sigma_0, \psi_0 \rangle \\ &= -N_e J \langle n_j \rangle_0 \langle \gamma_j \rangle_0 + N_e J\alpha \langle X_{i-1,i+1} \rangle_0 \langle n_j n_{j+1} \rangle_0 \\ &= -L \langle \gamma_j \rangle_0 \; Jx + LJ\, O(x^4) \qquad (3.97) \\ \text{hence:} \qquad A_1 &= -\langle \gamma_j \rangle_0 J \qquad (3.98) \end{aligned}$$

where $<>_0$ denotes the expectation value with respect to $|\sigma_0>$ or $|\psi_0>$ when no ambiguity is possible. Note that the contribution of H'_{sc} is of order x^4. The smallness of this term as $x \to 0$ reflects the fact that the holes obey the Pauli principle which suppresses the probability of two holes being near each other. One observes that already at this order, H'_{sc} does not renormalize any of the coefficients in (3.91) which are of interest here. H'_{sc} will thus be dropped from the subsequent discussion. To determine leading corrections to B and C, one needs to go to second order:

$$E_2 = -\sum_{|\sigma,\psi\rangle}{}' \frac{\langle \sigma_0, \psi_0 | H_{sc} | \sigma, \psi \rangle \langle \sigma, \psi | H_{sc} | \sigma_0, \psi_0 \rangle}{E_\psi - E_{\psi_0} + E_\sigma - E_{\sigma_0}} \qquad (3.99)$$

where the sum goes over a complete set of unperturbed eigenstates and the prime excludes the ground state (3.88) from the sum. We now rewrite H_{sc} as

$$H_{sc} = -\frac{J}{N_e} \sum_q n_q \gamma_{-q} \qquad (3.100)$$

where Fourier transforms

$$\begin{aligned} n_q &\equiv \sum_j e^{iqj} n_j = \sum_k c^\dagger_{k+q} c_k \\ \gamma_q &\equiv \sum_j e^{iqj} \gamma_j \end{aligned} \qquad (3.101)$$

have been introduced. Using the fact that the intermediate states in (3.99) can be chosen to be momentum eigenstates, we have

$$E_2 = -\frac{J^2}{N_e^2} \sum_q \sum_{|\sigma,\psi\rangle}{}' \frac{\langle \psi_0 | n_{-q} | \psi \rangle \langle \psi | n_q | \psi_0 \rangle \langle \sigma_0 | \gamma_q | \sigma \rangle \langle \sigma | \gamma_{-q} | \sigma_0 \rangle}{E_\psi - E_{\psi_0} + E_\sigma - E_{\sigma_0}} \qquad (3.102)$$

It is necessary to distinguish between terms with zero momentum exchange between spin and charge and those with $q \neq 0$. We write:

$$E_2 = E_2^0 + E_2' \qquad (3.103)$$

where E_2^0 contains all $q = 0$ terms and E_2' contains all the rest. At $q = 0$, $n_q = \sum n_j = N_h$ commutes with the Hamiltonian, hence there can be no virtual charge excitation and the charge matrix element is diagonal, $|\psi >= |\psi_0 >$:

$$E_2^0 = -\left(\frac{k_f}{\pi}\right)^2 J^2 \sum_{\sigma}{}' \frac{\langle\sigma_0|\,\gamma_{q=0}\,|\sigma\rangle\,\langle\sigma|\,\gamma_{q=0}\,|\sigma_0\rangle}{E_\sigma - E_{\sigma_0}} \tag{3.104}$$

Note that virtual states without spin excitations do not enter (3.102), since $|\sigma >= |\sigma_0 >$ would imply $q = 0$ and again the charge part vanishes unless also $|\psi >= |\psi_0 >$, which is excluded from the sum. Thus for $\alpha > \alpha_c$ the energy denominator in (3.102) is bounded from below by the spin gap Δ which will dominate over charge excitation energies of order tx^2 very close to the Fermi surface. This assures that the perturbative expansion is well behaved in the limit $x \to 0$ (see appendix A).

For $q \neq 0$ we note that n_q excites only single particle-hole excitations. We can thus convert the sum over these terms into a double integral over a hole momentum k_1 and a particle momentum k_2:

$$E_2' = -N_e \int_{-k_f}^{k_f} \frac{dk_1}{2\pi} \int_{k_f}^{2\pi - k_f} \frac{dk_2}{2\pi}\, f(k_1, k_2) \tag{3.105}$$

where

$$f(k_1, k_2) = \frac{J^2}{N_e} \sum_{|\sigma\rangle}{}' \frac{\langle\sigma_0|\,\gamma_{k_2-k_1}\,|\sigma\rangle\,\langle\sigma|\,\gamma_{k_1-k_2}\,|\sigma_0\rangle}{\epsilon(k_2) - \epsilon(k_1) + E_\sigma - E_{\sigma_0}} \tag{3.106}$$

and $\epsilon(k) = -2t\cos(k)$ is the free fermion dispersion. For later convenience, we also introduce the function

$$\begin{aligned} F(q) &= \frac{1}{2}\left(f(\frac{q}{2}, -\frac{q}{2}) + f(-\frac{q}{2}, \frac{q}{2})\right) \\ &= \frac{J^2}{2N_e}\left(\sum_{|\sigma\rangle}{}' \frac{\langle\sigma_0|\,\gamma_{-q}\,|\sigma\rangle\,\langle\sigma|\,\gamma_q\,|\sigma_0\rangle}{E_\sigma - E_{\sigma_0}} + (q \to -q)\right) \end{aligned} \tag{3.107}$$

where the symmetry of $\epsilon(k)$ was used.

The leading correction to the energy at second order perturbation theory is a contribution to the A coefficient in (3.91):

$$\begin{aligned} A_2 &= \frac{\pi}{N_e}\frac{\partial}{\partial k_f} E_2' \Big|_{k_f=0} \\ &= -\int_0^{2\pi} \frac{dk}{2\pi}\, f(0, k) \end{aligned} \tag{3.108}$$

To leading order in J/t the integral over momenta may be carried out to give a

quantity defined in terms of the pure spin chain H_s. This will demonstrate that the present expansion is well behaved, but the evaluation of A_2 will be deferred to the next section in order to continue with the analysis of the crucial B coefficient. Its correction at this order reads:

$$\begin{aligned} B_2 &= \frac{\pi^2}{2N_e}\left(\frac{\partial^2}{\partial k_f^2}E_2^0 + \frac{\partial^2}{\partial k_f^2}E_2'\right)\Bigg|_{k_f=0} \\ &= -F(0) + \frac{\pi^2}{2N_e}\frac{\partial^2}{\partial k_f^2}E_2'\Bigg|_{k_f=0} \end{aligned} \tag{3.109}$$

Again, the contribution from E_2' is evaluated by straightforward differentiation of (3.105). Only boundary terms survive, as all derivatives of the integrand vanish by symmetry when the limit $k_f \to 0$ is taken, using the 2π-periodicity of f in the second argument. We find:

$$B_2 = -F(0) + \frac{1}{2}\left(F(2k_f) + F(2\eta)\right)\Big|_{k_f\to 0} \tag{3.110}$$

At this point an infinitesimal η was introduced since terms with zero momentum transfer are really excluded in the sum defining E_2'. However, it can be argued that the function $F(q)$ is continuous at $q = 0$ and hence B_2 vanishes. Note that this is the effect of a non-trivial cancellation between $q = 0$ processes and processes with $q \to 0$. A physical argument for the continuity of $F(q)$ can be given if one interprets $F(q)$ as the second order energy response of a pure spin chain due to a periodic perturbation. The details of this argument are given in appendix B. Hence, by (3.110)

$$B_2 = 0 \tag{3.111}$$

A similar analysis can be carried out in third order perturbation theory, where contributions to the B coefficient cancel in a similar manner. This analysis is given in appendix C. It is therefore very likely that indeed

$$B = 0 \tag{3.112}$$

to all orders in perturbation theory, and thus for small J/t the liquid remains stable in the limit $x \to 0$ even in the case $\alpha \approx .5$ (Fig. 3-4c). The scenario of Fig. 3-5 a) is thereby ruled out.

The physical implication of (3.112) is that indeed the holes act as spinless fermions whose interaction is short ranged, and is irrelevant in the dilute limit. The Pauli principle severely suppresses the wave function when two holes approach each other. The range of this suppression is larger in one dimension than for dimensions greater than one, since in higher dimensions a curvature of the wave function is less costly at small distances. Therefore, in one dimension this effect is strong enough in order to prevent a short range interaction from generating a term of order x^2 in the energy.

As argued initially, in the scenario of Fig. 3-5 b) one has $K_\rho \to 1/2$ as $x \to 0$

for $J < J_c$ due to the non-interacting character of the dilute hole gas. It was shown above that this behavior does not only require $B = 0$, but also imposes a constraint fixing the ratio of the coefficients $C \sim v_{N\rho}$ and $A_{\phi\phi} \sim v_{J\rho}$, although both these quantities individually will depend on J/t. This non-trivial behavior may be verified perturbatively as well, as we shall now see.

Note that $B = 0$ leads to $C = \tilde{C}$ in (3.91) and (3.92), such that

$$C_2 = \frac{\pi^3}{6N_e} \frac{\partial^3}{\partial k_f^3} E_2' \Big|_{k_f=0} \tag{3.113}$$

In this case boundary terms such as those displayed in (3.110) do not contribute, since these vanish by symmetry as $k_f \to 0$ when another derivative is acting on them. Instead, we have now again a "bulk" contribution analogous to that in (3.108):

$$C_2 = -\frac{1}{6}\frac{\pi}{2} \int_0^{2\pi} dk \, \frac{\partial^2}{\partial k_f^2} f(k_f, k) \Big|_{k_f=0} \tag{3.114}$$

This expression is to be compared to the coefficient $A_{2,\phi\phi}$. In the presence of a magnetic flux $L\phi$, a phase twist ϕ will modify all hopping matrix elements via $t \to t\, e^{i\phi}$ in (3.78) and leads to the following replacement of the free hole dispersion in the function $f(k_1, k_2)$ in (3.106):

$$\begin{aligned} \epsilon(k) &\longrightarrow \quad \epsilon_\phi(k) = -2t \cos(k + \phi) \\ f(k_1, k_2) &\longrightarrow f_\phi(k_1, k_2) \end{aligned} \tag{3.115}$$

Hence from (3.108)

$$A_{2,\phi,\phi} = \frac{\partial^2}{\partial \phi^2} A_2 \Big|_{\phi=0} = -\int_0^{2\pi} \frac{dk}{2\pi} \; \frac{\partial^2}{\partial \phi^2} f_\phi(0, k) \Big|_{\phi=0} \tag{3.116}$$

However, using the fact that

$$f_\phi(0, k) = f(\phi, k + \phi) \tag{3.117}$$

holds, it follows by shifting the integration variable and comparison with (3.114) that

$$6C_2 = \pi^2 A_{2,\phi\phi} \tag{3.118}$$

is indeed satisfied. Again, an analogous relation is derived at third order perturbation theory in appendix C, and this suggests that indeed

$$6C = \pi^2 A_{\phi\phi} \tag{3.119}$$

to all orders. Hence, although the parameters $v_{N\rho}$ and $v_{J\rho}$ in (3.85) each receive nontrivial corrections, their ratio is fixed to leading order in x such that K_ρ always approaches $\frac{1}{2}$ in the limit $x \to 0$. Luttinger liquid theory then implies that the dilute

holes share all the universal properties of a gas of non-interacting spinless particles. It seems likely that this picture will hold in the entire regime $J < J_c$ as in Fig. 3-5 b), whereas for $J > J_c$ small doping will give rise to phase separation.

3.6 Explicit evaluation of coefficients

In the previous section it has been shown that the perturbative approach is consistent in all details with a picture where the charge degrees of freedom behave as non-interacting spinless solitons in the dilute limit, and are effectively decoupled from the spin dynamics. The second order expressions that have been derived involve complicated sums over both spin and charge degrees of freedom. It will now be shown that the expressions for A_2 and C_2 can be evaluated more explicitly, to leading order in J/t, in terms of quantities that are derived from a pure spin chain problem. In this way explicit asymptotic expansions are obtained for the ground state energy and the compressibility parameter $v_{N\rho}$, showing that second order corrections are suppressed by non-trivial powers of J/t compared to the leading orders. Also, these quantities are related to the single hole energy and mass renormalization, which will be clarified in the next section.

It must be stressed once more that the results presented here are valid in the limit $x^2 \ll J/t$. In this limit the low lying charge excitations are dominated by the curvature near the band bottom of the bare dispersion $\epsilon(k)$, and their contribution to the energy denominator in (3.105) is dominated by that of the gapped spin excitations. In the opposite limit $J/t \ll x^2$ the perturbation theory presented here is still valid, yet a crossover will take place and the asymptotic expansion (3.91) will not hold (see appendix A).

With this in mind, the first and second order energy corrections are dominated by the following terms:

$$\begin{aligned} E_1/L &\simeq A_1 x = -\langle \gamma_j \rangle_0 \, Jx \\ E_2/L &\simeq A_2 x \end{aligned} \tag{3.120}$$

It will now be shown that the second order term is indeed suppressed by powers of J/t compared to the first order term, which is of order Jx. To achieve a systematic expansion of A_2 in J/t we rewrite (3.108) in the form

$$A_2 = -\int_0^{2\pi} \frac{dk}{2\pi} \int dE \frac{A(k,E)}{\epsilon(k) - \epsilon(0) + E - E_{\sigma_0}} \tag{3.121}$$

where we have introduced a spectral function

$$
\begin{aligned}
A(k,E) &= \frac{J^2}{N_e}\sum_{\sigma}{}' \left|\langle\sigma_0\left|\gamma_k\right|\sigma\rangle\right|^2 \delta(E_\sigma - E) \\
&\equiv \sum_n K_n(E)\, e^{ikn}
\end{aligned}
\tag{3.122}
$$

and its energy dependent Fourier coefficients $K_n(E)$. In terms of the latter we may write

$$
A_2 = -\frac{1}{2t}\int dE \sum_n K_n(E) \int_0^{2\pi} \frac{dk}{2\pi} \frac{e^{ikn}}{1+\frac{E-E_{\sigma_0}}{2t} - \cos(k)} \tag{3.123}
$$

The k-integral is readily performed to give

$$
\begin{aligned}
A_2 &= -\frac{1}{2t}\int dE \sum_n K_n(E) \frac{\left(1+\Delta-\sqrt{(1+\Delta)^2-1}\right)^{|n|}}{\sqrt{(1+\Delta)^2-1}} \\
&\text{where} \quad \Delta \equiv \frac{E-E_{\sigma_0}}{2t}
\end{aligned}
\tag{3.124}
$$

The matrix elements defining $K_n(E)$ will decay rapidly when E is a few times J and hence we may expand (3.124) in powers of Δ. Keeping only the leading term this yields

$$
\begin{aligned}
A_2 &\simeq -\frac{1}{2t}\int dE \sum_n K_n(E) \frac{1}{\sqrt{\frac{E-E_{\sigma_0}}{t}}} \\
&\simeq -\frac{t}{2}\Gamma_{\frac{1}{2}} \left(\frac{J}{t}\right)^{\frac{3}{2}}
\end{aligned}
\tag{3.125}
$$

where the coefficient $\Gamma_{\frac{1}{2}}$ is a quantity defined only in terms of eigenstates of the doped spin chain. For later convenience we define the more general function:

$$
\begin{aligned}
\Gamma_p &= J^{p-2}\int dE\, \frac{A(q=0,E)}{(E-E_{\sigma_0})^p} \\
&= \frac{1}{N_e}\sum_{|\sigma\rangle}{}' \frac{\langle\sigma_0|\,\gamma_{q=0}\,|\sigma\rangle\,\langle\sigma|\,\gamma_{q=0}\,|\sigma_0\rangle}{\left(\frac{E_\sigma - E_{\sigma_0}}{J}\right)^p}
\end{aligned}
\tag{3.126}
$$

Hence, it is apparent from (3.120) and (3.125) that

$$
\frac{E_2}{E_1} \sim \left(\frac{J}{t}\right)^{\frac{1}{2}} \tag{3.127}
$$

indicating the convergence of our perturbative approach for small J/t. In appendix A, the convergence and expansion parameters of this series in various limits will be further commented on. Note that the non-analytic nature of the expansion originates from the gaplessness of the charge degrees of freedom and the existence of a regime where the spin gap dominates the energy denominator in (3.121).

Similarly, in second order perturbation theory the compressibility parameter $v_{N\rho}$ reads to leading order in x:

$$v_{N\rho} \simeq \left(4\pi t + \frac{12}{\pi} C_2\right) x \tag{3.128}$$

By means of (3.114) the evaluation of C_2 goes analogous to that of A_2 and we get:

$$\begin{aligned} C_2 &\simeq -\frac{\pi^2}{12} \Gamma_{\frac{3}{2}} \sqrt{Jt} \\ v_{N\rho} &\simeq \pi t \left(4 - \Gamma_{\frac{3}{2}} \sqrt{\frac{J}{t}}\right) x \end{aligned} \tag{3.129}$$

Eq. (3.126) has been evaluated numerically at $\alpha = .5$ for $p = \frac{1}{2}, \frac{3}{2}$, and $\Gamma_{\frac{1}{2}} = .2502(2)$, $\Gamma_{\frac{3}{2}} = .474(3)$ have been found (Fig. 3-7). Hence, although the compressibility $\kappa \sim v_{N\rho}^{-1}$ increases with J, no unstable value of J can be inferred that lies within the validity of our perturbation theory.

3.7 Single spin-polaron picture

In this section, a variational picture of the polaronic effects of a single hole on its spin environment will be developed for small J/t in the special case $\alpha = .5$. The perturbation theory presented in the previous section for a finite carrier concentration may be applied to the problem of doping a single hole into the infinite spin chain as well, such that we will be able to compare variational and perturbative results. In second order perturbation theory, the energy of a single hole at momentum k reads:

$$E_p(k) = -2t\cos(k) - \langle \gamma_j \rangle_0 \; J - \int_0^{2\pi} \frac{dk_2}{2\pi} \; f(k, k_2) \tag{3.130}$$

where the contribution E_{σ_0} from the spin background has not been included. At $k = 0$ we immediately see by comparison with (3.95), (3.98) and (3.108) that

$$E_p \equiv E_p(k=0) = A_0 + A_1 + A_2 \equiv A \tag{3.131}$$

holds for the single polaron energy in second order perturbation theory. Likewise, for the renormalized mass of the spin-polaron we have, comparing to eqs. (3.95) and (3.114):

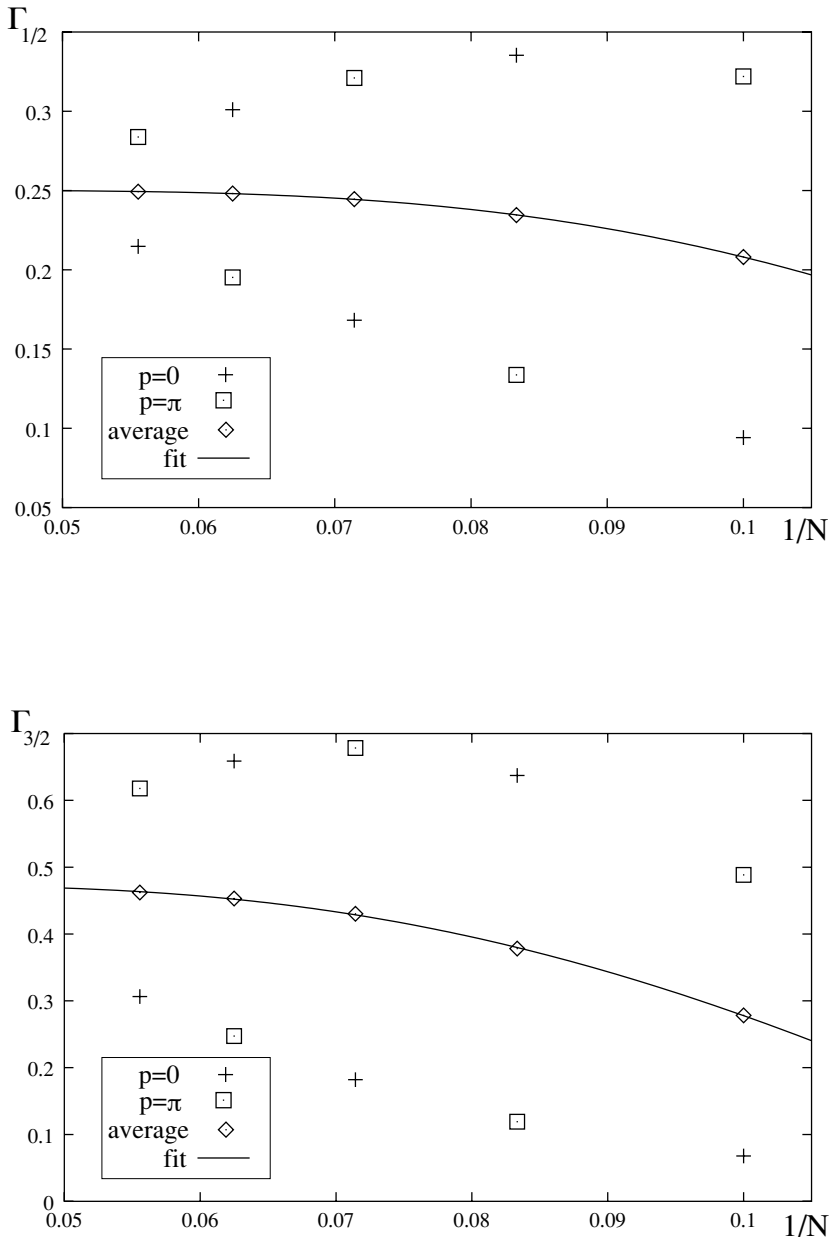

Figure 3-7: Numerical determination of $\Gamma_{\frac{1}{2}}$ and $\Gamma_{\frac{3}{2}}$ by exact diagonalization of H_s for $\alpha = \frac{1}{2}$. System sizes of up to $N = 18$ have been diagonalized. Results are plotted for the two degenerate ground states with momenta $p = 0$ (crosses) and $p = \pi$ (squares). The extrapolated values have been determined by fitting their averages (diamonds) to the function $f(N) = a + b\,\exp(-cN)$.

$$m^{-1} \equiv \frac{\partial^2}{\partial k^2} E_p \Big|_{k=0} = \frac{6}{\pi^2} (C_0 + C_2) \equiv \frac{6}{\pi^2} C \tag{3.132}$$

at this order. We may therefore rewrite the ground state energy of the system at finite doping (3.91) as

$$\begin{aligned} E &= E_{\sigma_0} + L \left(E_p x + \frac{\pi^2}{6m} x^3 + \dots \right) \\ &= E_{\sigma_0} + N_e \int_{-k_f}^{k_f} \frac{dk}{2\pi} E_p(k) \ + O(k_f^4) \end{aligned} \tag{3.133}$$

Hence up to third order in x the ground state energy of the system is apparently given by the energy of non-interacting spinless particles with a dispersion $E_p(k)$, where interaction effects enter only beyond this order. This further confirms the picture established in the previous sections.

We now focus on the Majumdar-Gosh point $\alpha = .5$, where the ground state of the spin Hamiltonian H_s is known exactly [92]. It consists of a direct product of uncorrelated singlet pairs:

$$|MG\rangle = \prod_i \frac{1}{\sqrt{2}} \Big(|\uparrow\downarrow\rangle - |\downarrow\uparrow\rangle \Big)_{2i,2i+1} \tag{3.134}$$

This very simple product of dimers can be thought of as the prototype of a dimerized wave function, where spin-spin correlations are ultra-short ranged in that they vanish identically over distances greater then one site. Apart from the exact ground state, some excited states are also known exactly for the $\alpha = .5$ spin chain [93], but the lowest excitations have been characterized only variationally [80]. Moreover, the existence of a spin gap can be proven rigorously [94]. Note that we use $|MG>$ to denote one of the two doubly degenerate symmetry broken ground states, whereas $|\sigma_0>$ has been used to denote their symmetric superposition. At $\alpha = .5$, the results for the single polaron energy and mass eqs. (3.131) and (3.132) take the concrete form

$$\begin{aligned} E_p &= -t \left(2 - \frac{9}{16} \frac{J}{t} + .125 \left(\frac{J}{t} \right)^{\frac{3}{2}} \right) \\ m^{-1} &= t \left(2 - .237 \sqrt{\frac{J}{t}} \right) \end{aligned} \tag{3.135}$$

We may write the ground state of the unperturbed Hamiltonian H_0 as a superposition

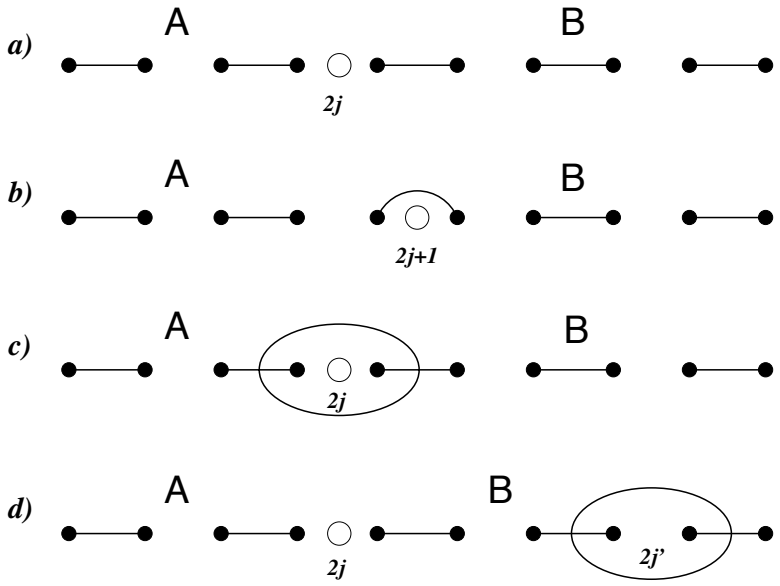

Figure 3-8: States used in the construction of the variational wave function. "A" and "B" label different dimer phases. a)+b) Single hole basis states forming the ground state of the non-interacting Hamiltonian H_0 (eq. (3.136)). Lines denote the singlet pairs in (3.134). c) A pair of triplets excited by the presence of the hole. The oval denotes a singlet formed by two triplet states on the links adjacent to the hole, as displayed in (3.137). d) States used to form the variational wave function (3.138).

of states depicted in Fig. 3-8a)+b):

$$|\Omega_0\rangle = \frac{1}{\sqrt{N_e}} \sum_j |j\rangle_c \, |MG\rangle_s \tag{3.136}$$

where $|j\rangle_c$ denotes a state with a hole at the interstitial site j and "c" and "s" refer to the spin sector and the charge sector of the state. Note that although it is not obvious in Fig. 3-8, which is a depiction of the "squeezed" domain wall representation of the Hilbert space (3.77), the hole interpolates between two different dimer phases labeled A and B that correspond to the two degenerate ground states of the spin Hamiltonian. Therefore, the states (3.136) do describe solitons.

When the interaction H_{sc} is taken into account, a hole in the state $|2j\rangle_c$ will excite a spin configuration where the two dimers adjacent to the hole are in triplet states, and the two triplets form a singlet (Fig. 3-8c)). More precisely, the oval in Fig. 3-8c) denotes the following spin state:

$$\left| i \bullet\!\!-\!\!\bigcirc\!\!-\!\!\bullet_{j\ k}\!\!-\!\!\bullet\, l \right\rangle =$$

$$\frac{1}{\sqrt{3}}\Big(|\uparrow\uparrow\rangle_{ij} \otimes |\downarrow\downarrow\rangle_{kl} + |\downarrow\downarrow\rangle_{ij} \otimes |\uparrow\uparrow\rangle_{kl} \tag{3.137}$$

$$- \frac{1}{2}\Big(|\uparrow\downarrow\rangle + |\downarrow\uparrow\rangle \Big)_{ij} \otimes \Big(|\uparrow\downarrow\rangle + |\downarrow\uparrow\rangle \Big)_{kl} \Big)$$

We may now denote such a triplet pair excitation which is centered around the hole site $2j$ by $|2j\rangle_s$. Similarly, the hole state $|2j+1\rangle_c$ will excite the spin states $|2j\rangle_s$ and $|2j+2\rangle_s$. Clearly, a variational wave function will need admixtures of states such as shown in Fig. 3-8c). However, in the vicinity of the hole the kinetic energy H_c is the dominant part of the Hamiltonian, and it will allow the hole to move away from the excited triplet states as shown in Fig. 3-8d). To optimize the kinetic energy, it is hence necessary to include the more general states of Fig. 3-8d) into the wave function. We therefore write down the following trial wave function for a state with one hole at momentum k:

$$|t_k\rangle = \frac{1}{\sqrt{N_e}} \sum_j e^{ikj} |j\rangle_c \otimes \left(|MG\rangle_s + a \sum_{2j'} e^{-|j-2j'|\beta + i(j-2j')\delta} |2j'\rangle_s \right) \tag{3.138}$$

Hence $|t_k\rangle$ lives in the subspace of all states that can be reached by acting once with the perturbation H_{sc} on the zeroth order wave function (3.136) and then acting an arbitrary number of times with the hopping operator H_c. Note also that indeed certain exact excited states of a Majumdar-Gosh spin chain are given in terms of the tightly bound triplet excitations shown in eq. (3.137) and Fig. 3-8 (Ref. [93]). The following matrix elements are needed to evaluate the energy of the state (3.138):

$$\begin{aligned}
{}_s\langle MG\,|-\gamma_j|\,2j'\rangle_s &= \frac{\sqrt{3}}{8} J\left(\delta_{j,2j'} + \delta_{j-1,2j'} + \delta_{j+1,2j'}\right) && (3.139)\\
{}_s\langle 2j'\,|-\gamma_j|\,2j'\rangle_s &= \frac{9}{16} J - (-1)^j \frac{3}{16} J \\
&\quad + \frac{1}{4} J\left(\delta_{j,2j'} - \delta_{j-1,2j'} - \delta_{j+1,2j'}\right) && (3.140)\\
{}_s\langle 2j'\,|H_s|\,2j'\rangle_s &= {}_s\langle MG\,|H_s|\,MG\rangle_s + J \\
&= -\frac{3}{4} J N_e \;+\; J && (3.141)
\end{aligned}$$

In addition, both γ_j and H_s do not have off-diagonal matrix elements among the states $|2j\rangle_s$. This leads to the following expectation values:

$$\begin{aligned}
\langle t_k|H_c|t_k\rangle &= -2t\cos(k) - 4t|a|^2\xi_3\cos(k+\delta) && (3.142a)\\
\langle t_k|H_s|t_k\rangle &= -\frac{3}{4} J N_e \langle t_k|t_k\rangle + J|a|^2(\xi_1+\xi_2) && (3.142b)\\
\langle t_k|H_{sc}|t_k\rangle &= \frac{9}{16} J \langle t_k|t_k\rangle \\
&\quad + \frac{\sqrt{3}}{16} J\left(1 + 2e^{-\beta}\cos(\delta)\right)(a+a^*) + O(J|a|^2) && (3.142c)\\
\langle t_k|t_k\rangle &= 1 + |a|^2(\xi_1+\xi_2) && (3.142d)
\end{aligned}$$

where the constants ξ_1 and ξ_2 are proportional to the weight of spin excited states with the hole on even positions and odd positions, respectively, and ξ_3 arises from

hopping between even and odd sites in the presence of a spin excitation:

$$\begin{aligned}
\xi_1 &= \frac{1}{2}\sum_{j'} e^{-2\beta|2j'|} = \frac{1}{4\beta} + \frac{1}{3}\beta + \dots \\
\xi_2 &= \frac{1}{2}\sum_{j'} e^{-2\beta|2j'-1|} = \frac{1}{4\beta} - \frac{1}{6}\beta + \dots \\
\xi_3 &= \frac{1}{4}\sum_{j'} e^{-\beta|2j'|}\left(e^{-\beta|2j'-1|} + e^{-\beta|2j'+1|}\right) = \frac{1}{4\beta} - \frac{1}{24}\beta + \dots
\end{aligned} \tag{3.143}$$

Terms of order $J|a|^2$ were only kept in (3.142) when they are multiplied by $\xi_i \sim 1/\beta$. It is apparent from (3.142a) that $\delta = -k$ has to be chosen, and from (3.142c) that a is real and negative. Keeping only leading terms, this leads to the variational energy function

$$\begin{aligned}
E_p^{var}(k;a,\beta) &\equiv \langle t_k|H_c + H_s + H_{sc}|t_k\rangle \,/\, \langle t_k|t_k\rangle \\
&= -2t\cos(k) + \frac{9}{16}J + \frac{1}{2}ta^2\beta - t\frac{a^2}{\beta}(1-\cos(k)) \\
&\quad + J\frac{a^2}{2\beta} + \frac{\sqrt{3}}{8}Ja\,(1+2\cos(k))
\end{aligned} \tag{3.144}$$

where again the bulk contribution of the spin chain was not included. We first minimize this function for $k = 0$ and find for the variational parameters at the stationary point

$$\beta_0 = \sqrt{\frac{J}{t}} \tag{3.145a}$$

$$a_0 = -\frac{3\sqrt{3}}{16}\sqrt{\frac{J}{t}} \tag{3.145b}$$

By (3.145a), the size of the spin-polaron cloud is proportional to $(J/t)^{-\frac{1}{2}}$ in agreement with (3.130) where the dominant contributions to the integral come from the region where k_2^2 is of the order of the spin gap. The variational energy of the spin-polaron at $k = 0$ is thus

$$E_p^{var} \equiv E_p^{var}(k=0;a_0,\beta_0) = -t\left(2 - \frac{9}{16}\frac{J}{t} + \frac{27}{256}\left(\frac{J}{t}\right)^{\frac{3}{2}}\right) \tag{3.146}$$

This is indeed of the same form as (3.135) where the first two terms are reproduced exactly, as they are mean-field like in character. Moreover, the coefficient of the last term is about .105 and hence matches the one obtained by perturbative and numerical methods in (3.135) within roughly 15%.
The appearance of a mass term proportional to $\sqrt{J/t}$ as in (3.135) may also be

understood from this variational approach. It is seen in (3.144) that a term of order $a^2/\beta \sim \sqrt{J}$ is no longer precisely canceled at finite k. The reason for this is that at finite k time reversal symmetry is absent and a non-zero value of the parameter δ introduced in (3.138) is generally allowed. We have tuned δ such that the polaronic corrections in the kinetic energy (3.142a) do not have the same k-dependence as the leading term. This is giving rise to a a^2/β term at finite k. It leads to the variational mass

$$\begin{aligned}(m^{var})^{-1} &= \frac{\partial^2}{\partial k^2} E_p^{var}(k; a_0, \beta_0)\Big|_{k=0} \\ &= t\left(2 - \frac{27}{256}\sqrt{\frac{J}{t}} + \dots\right)\end{aligned} \tag{3.147}$$

Here, the dependence of a and β on k^2 need not be taken into account because of stationarity. The coefficient of the second term happens to be the same as the one showing up in (3.146), which is now off by about a factor of 2 when compared to the mass shown in (3.135). This may be attributed to the variational character of the state (3.138), since the mass comes from a subdominant term proportional to k^2. However, the correct dependence on J as well as the right order of magnitude are again obtained. This leads to the conclusion that the wave function (3.138) provides a quite accurate picture of the large polaronic cloud in the limit of small J/t, especially at $k = 0$.

In view of the original motivation to examine the stability of the liquid phase of the tJJ' model as $x \to 0$ at small J/t, it is interesting to think about the possibility of the formation of bound hole states. It is generally expected that either at the critical value for the onset of phase separation, J_c/t, or at an even smaller critical value $J_c'/t < J_c/t$ bound states of two holes will exist[10] (see also Ref. [84]). In the latter case, one would have $K_\rho \to \frac{1}{2}$ as $x \to 0$ for $0 < J < J_c'$ and, $K_\rho \to 1$ for $J_c' < J < J_c$ corresponding to a non-interacting dilute gas of bound pairs of spinless particles. In contrast, the scenario of Fig. 3-5b) assumes that any finite or infinite number of particles will form a bound state above J_c, whereas no bound states at all exist below J_c. The present analysis is restricted to very small J/t and cannot distinguish these two cases, while it can rule out the scenario of Fig. 3-5a). In any case, however, two holes should be able to bind in the phase separated regime.

The existence of such bound states can be discussed on a qualitative level based on the variational spin-polaron picture proposed in this section. To form a bound state, the single polaron wave functions must significantly overlap, hence the size of a bound state will be of order $r \sim (J/t)^{-\frac{1}{2}}$. The potential energy gain will be of order $(J/t)^{\frac{3}{2}}$ since the mean field term of order J in (3.146) will not be affected by pair formation. However, the kinetic energy cost of such a state is of order $1/r^2 \sim J/t$ and is dominant. Hence, one can conclude that bound states of holes will require finite J/t of order 1 or greater, in agreement with the picture of free single hole-like charge

[10] F. D. M. Haldane, private communication

degrees of freedom established in the above.

3.8 Conclusions

We have examined the tJJ'-model in one dimension, in the regime of small x and J/t by perturbative and variational approaches. This parameter regime is most challenging to numerical methods, and earlier numerical studies did not allow a firm conclusion as to whether a phase separation instability and a phase of dominant singlet superconducting fluctuations extend down to values of $J/t < 1$ in the case $\alpha = J'/J \approx .5$, where a spin gap is present at small doping.

Using an approach where couplings between spin and charge degrees of freedom are treated as a perturbation, a detailed analysis of the model in second (and third, appendix C) order perturbation theory has been presented, showing that no instability is present at small J/t. Instead, using Luttinger liquid arguments and by studying the dispersion of a single hole immersed into the correlated spin system, it has been demonstrated that the hole degrees of freedom precisely behave as free spinless solitons in the dilute limit, despite their microscopic coupling to the non-trivial spin background. This behavior conforms to Luttinger liquid physics, where spin and charge are separate degrees of freedom, and couplings between them are regarded as irrelevant in a renormalization group sense. While this point of view is generally accepted for one-dimensional systems, in microscopic one-dimensional lattice models it usually may be firmly demonstrated only at special integrable points [45, 90]. The method that was established in section 3.5 provides a perturbative framework for such a demonstration in a non-integrable model over a range of parameters. Moreover, it allows the calculation of non-trivial quantities such as the leading corrections to the single hole energy and mass renormalization, which depend on non-analytic powers of J/t. The numerical calculation of the coefficients in this expansion still requires an exact diagonalization of a pure spin problem. These results were used for a comparison to a variational approach. Proposing a variational wave function where the hole is surrounded by a polaronic cloud of tightly bound pairs of triplet excitations it has been possible to confirm the perturbative results for the dependence of the single polaron energy and mass on J/t, as well as the order of magnitude of the coefficients. In particular, the second order perturbative energy corrections are in close quantitative agreement with the variational result. Based on these findings, it has been argued that for the parameter $\alpha = .5$ the onset of phase separation at small doping as well as the formation of bound states require J/t to be at least of order 1.

The theory of the tJJ'-model presented here is limited to small values of J/t. It has turned out that this region does not overlap a region of dominant superconducting correlations, which at $\alpha = .5$ might exists at moderate values of J/t and small doping from numerics. It would be very interesting to obtain a realistic value for the critical coupling J_c/t corresponding to the onset of phase separation at $x = 0$ (Fig. 3-5a) for $\alpha \approx .5$. This will be the minimum value of J/t at which strong superconducting correlations occur in the tJJ'-model for small doping x, and may give rise to some estimate for the range of J/t in which superconductivity is to be expected in a doped

dimerized quasi-one-dimensional spin-$\frac{1}{2}$ system.

However, in a real system interchain effects will play an important role when true long range order is established. These interchain couplings can either favor dimer locking, or a superconducting dimer liquid. In particular when dimer locking is frustrated such as in TiOCl, superconducting long range order may be favored even if pairing correlations are subdominant in the isolated spin chains. This possibility calls for further analysis, which is beyond the scope of the present thesis.

3.9 Appendix A: Convergence and crossover behavior of the perturbative expansion

In the following, the general behavior at k'th order of the perturbative expansion applied in this chapter will be briefly illustrated. At order k, one will encounter terms in the expansion of the ground state energy analogous to (3.105) (c.f. also eqs. (3.162), (3.163)):

$$E_k \sim \int_{-k_f}^{k_f} dh_1 \ldots \int_{-k_f}^{k_f} dh_m \int_{k_f}^{2\pi-k_f} dp_1 \ldots \int_{k_f}^{2\pi-k_f} dp_n \sum_{\sigma_1 \ldots \sigma_{k-1}} \underbrace{\frac{J^k M\left(h_1 \ldots h_m; p_1 \ldots p_n; \sigma_1 \ldots \sigma_{k-1}\right)}{\left(\epsilon(p_1) - \epsilon(h_1) + E_{\sigma_1} - E_{\sigma_0}\right)\left(\quad\right)\ldots\left(\quad\right)}}_{k-1 \text{ factors}} + \ldots \tag{3.148}$$

The phase space consists of m-hole momenta and n-particle momenta. It is enough to consider the case $m+n=k$. There will be terms with fewer integrals also, but they are multiplied by additional powers of x such as (3.104).

We focus on the regime $k_f^2 \ll J/t$ first. Since $\epsilon(k) \approx \text{const} + tk^2$, the integrand does not significantly depend on the hole momenta, such that each of the hole integrals will give rise to a factor of x. The integral over particle momenta p_i will be dominated by the region where all momenta are within a range of $\sqrt{\Delta_s/t}$ of the Fermi points, where $\Delta_s \sim J$ is the spin gap. In this regime, all of the $k-1$ factors in the denominator are dominated by the spin gap and are of order Δ_s. Hence we obtain the following estimate for the term displayed in (3.148)

$$(3.148) \sim x^m \left(\Delta_s/t\right)^{n/2} \frac{J^k}{\Delta_s^{k-1}} \sim \; x^m \left(\sqrt{J/t}\right)^n J \tag{3.149}$$

The leading contribution to E_k in the limit $x^2 \ll J/t$ will thus be a term of order

$$E_k \sim \; x \left(\sqrt{J/t}\right)^{k-1} J \tag{3.150}$$

Eq. (3.150) shows that subsequent orders in perturbation theory are always sup-

pressed by powers of $\sqrt{J/t}$, as we verified explicitly up to second order (cf. (3.127)). Note that relations (3.149) and (3.150) are valid asymptotically in a given limit, they do not imply the existence of an analytic expansion in powers of x and $\sqrt{J/t}$. Rather, the E_k's are quite complicated functions of x and J. Relation (3.150) will hold until $x^2/J \sim 1/t$, and upon further increase of this ratio a crossover will take place. We may however write down an asymptotic expansion in x:

$$\begin{aligned} E_k &= L\left(A_k(J)x + B_k(J)x^2 + C_k(J)x^3 + D_k(J)x^4 \dots\right) \\ E &= \text{const.} + E_1 + E_2 + \dots \end{aligned} \tag{3.151}$$

as we did in second order perturbation theory. Recall from (3.125), (3.129) that $A_2 \sim (J/t)^{3/2}$, $C_2 \sim (J/t)^{1/2}$ while $B_2 = 0$. Formally, however, B_2 is of order J. This implies that in general $\sqrt{tx^2/J}$ is the expansion parameter of the series (3.151).

In the opposite limit $J \ll tx^2$ it is easily seen from (3.148) that now $E_k \sim J^k$ holds. In this limit it is not necessary, though still permissible, to include the spin chain part H_s in the unperturbed Hamiltonian H_0. Instead one may apply degenerate perturbation theory in the spin couplings, which gives rise to an asymptotic expansion in J:

$$E = \text{const} + L\left(a(x)J + b(x)J^2 + c(x)J^3 + d(x)J^4 \dots\right) \tag{3.152}$$

This method has been applied in Ref. [85] to calculate the intersection of the spin gap phase boundary with the x-axis. Note that in (3.152) x need not be small, whereas in (3.151) both J/t and x^2t/J have to be small. However, due to the limitation $J \ll tx^2$, eq. (3.152) cannot be used to address the nature of the phase diagram in the dilute hole limit.

3.10 Appendix B: The continuity of the function $F(q)$

In this appendix a physical argument is given for the continuity of the function $F(q)$, which leads to the crucial cancellation in (3.110). This question is more subtle than it may seem, and the following argument would require more scrutiny in the gapless case $\alpha < \alpha_c$. We restrict ourselves to the spin gapped case, as we have done throughout this thesis. Recall the definition of $F(q)$ from (3.107):

$$F(q) = \frac{J^2}{2N_e}\left(\sum_{|\sigma\rangle}{}' \frac{\langle\sigma_0|\,\gamma_{-q}\,|\sigma\rangle\,\langle\sigma|\,\gamma_q\,|\sigma_0\rangle}{E_\sigma - E_{\sigma_0}} + (q \to -q)\right) \tag{3.153}$$

Physically, the continuity of $F(q)$ can be seen by interpreting this function as the second order energy response of a pure spin chain due to a periodic perturbation.

More precisely, we consider the following auxiliary spin chain problem:

$$\begin{aligned} H_q(\lambda) &= H_s + \lambda\, J \sum_j \cos(qj)\gamma_j \\ &= H_s + \frac{\lambda}{2}\, J\,(\gamma_q + \gamma_{-q}) \end{aligned} \tag{3.154}$$

where H_s is as defined in (3.79). Let $\mathcal{E}_q(\lambda)$ denote the ground state energy per site of this problem. Then it is easily seen from second order perturbation theory and the definition (3.153) that at $q = 0$

$$F(0) = -\frac{1}{2}\,\mathcal{E}''_{q=0} \tag{3.155}$$

holds, where the prime denotes a derivative with respect to λ taken at $\lambda = 0$. On the other hand, at $q \neq 0$ the same argument gives

$$F(q \neq 0) = -\,\mathcal{E}''_q \tag{3.156}$$

Note the factor of 2 difference between (3.155) and (3.156). Despite this apparent difference between the cases $q = 0$ and $q \neq 0$, it is $\mathcal{E}''_q$ which is discontinuous at $q = 0$, not $F(q)$, as the following argument shows: In the vicinity of a site j the ground state of $H_q(\lambda)$ will have great overlap with the ground state of $H_{q=0}(\lambda(j))$ as $q \to 0$, where $\lambda(j) \equiv \lambda\cos(qj)$. In other words, as $q \to 0$ it should be justified to replace the oscillating perturbation in $H_q(\lambda)$ by a flat perturbation in a sufficiently large local region around each site j. The size of this region can still be chosen to be $\ll 1/q$. One can thus argue that up to powers of q the ground state energy will be given by a sum over local contributions $\mathcal{E}_{q=0}(\lambda(j))$:

$$\begin{aligned} \mathcal{E}_{q\to 0}(\lambda) &= \frac{1}{N_e}\sum_j \mathcal{E}_{q=0}(\lambda(j)) \approx \frac{1}{N_e}\int_0^{N_e} dx\; \mathcal{E}_{q=0}\big(\lambda\cos(qx)\big) \\ &= \frac{1}{N_e}\int_0^{N_e} dx\left(\mathcal{E}_{q=0} + \lambda\cos(qx)\mathcal{E}'_{q=0} + \frac{1}{2}\lambda^2\cos^2(qx)\mathcal{E}''_{q=0} + \dots\right) \\ &\approx\; \mathcal{E}_{q=0} + \frac{1}{4}\lambda^2\mathcal{E}''_{q=0} \end{aligned} \tag{3.157}$$

From (3.156), (3.155) it then follows that

$$F(q \to 0) = -\frac{1}{2}\mathcal{E}''_{q=0} = F(0) \tag{3.158}$$

Note that the local point of view taken here is better justified in the gapped case, where any local perturbation decays exponentially in space.

3.11 Appendix C: Third order perturbative corrections

Below it will be shown that the general results $B = 0$ and $6C = \pi^2 A_{\phi\phi}$, which where proven within second order perturbation theory in the main body of this chapter (eqs. (3.111) and (3.118)), still hold when third order corrections are taken into account. This is particularly illuminating in view of the non-trivial cancellation (3.110) in the inverse compressibility at $x = 0$, which guarantees the stability of the liquid for small J/t. It will be seen that such a cancellation was not a coincidence at second order perturbation theory, but does occur at third order as well.

The third order correction to the ground state energy reads (see e.g. [95]):

$$
\begin{aligned}
E_3 = & \sum_{|\sigma_1,\psi_1\rangle}{}' \sum_{|\sigma_2,\psi_2\rangle}{}' \frac{\langle\sigma_0,\psi_0|\, H_{sc}\,|\sigma_2,\psi_2\rangle\,\langle\sigma_2,\psi_2|\, H_{sc}\,|\sigma_1,\psi_1\rangle\,\langle\sigma_1,\psi_1|\, H_{sc}\,|\sigma_0,\psi_0\rangle}{\left(E_{\psi_2}-E_{\psi_0}+E_{\sigma_2}-E_{\sigma_0}\right)\left(E_{\psi_1}-E_{\psi_0}+E_{\sigma_1}-E_{\sigma_0}\right)} \\
& - \sum_{|\sigma,\psi\rangle}{}' \frac{\langle\sigma_0,\psi_0|\, H_{sc}\,|\sigma,\psi\rangle\,\langle\sigma,\psi|\, H_{sc}\,|\sigma_0,\psi_0\rangle}{\left(E_{\psi}-E_{\psi_0}+E_{\sigma}-E_{\sigma_0}\right)^2}\,\langle\sigma_0,\psi_0|\, H_{sc}\,|\sigma_0,\psi_0\rangle \\
= & -\frac{J^3}{N_e^3}\sum_{q_1,q_2}\sum_{|\sigma_1,\psi_1\rangle}{}'\sum_{|\sigma_2,\psi_2\rangle}{}' \\
& \frac{\langle\psi_0|\, n_{-q_1-q_2}\,|\psi_2\rangle\,\langle\psi_2|\, n_{q_2}\,|\psi_1\rangle\,\langle\psi_1|\, n_{q_1}\,|\psi_0\rangle\,\langle\sigma_0|\,\gamma_{q1+q2}\,|\sigma_2\rangle\,\langle\sigma_2|\,\gamma_{-q2}\,|\sigma_1\rangle\,\langle\sigma_1|\,\gamma_{-q1}\,|\sigma_0\rangle}{\left(E_{\psi_2}-E_{\psi_0}+E_{\sigma_2}-E_{\sigma_0}\right)\left(E_{\psi_1}-E_{\psi_0}+E_{\sigma_1}-E_{\sigma_0}\right)} \\
& + \frac{J^3}{N_e^2}\frac{k_f}{\pi}\sum_{q}\sum_{|\sigma,\psi\rangle}{}' \frac{\langle\psi_0|\, n_{-q}\,|\psi\rangle\,\langle\psi|\, n_{q}\,|\psi_0\rangle\,\langle\sigma_0|\,\gamma_{q}\,|\sigma\rangle\,\langle\sigma|\,\gamma_{-q}\,|\sigma_0\rangle}{\left(E_{\psi}-E_{\psi_0}+E_{\sigma}-E_{\sigma_0}\right)^2}\,\langle\sigma_0|\,\gamma_{q=0}\,|\sigma_0\rangle
\end{aligned}
$$

$\equiv$

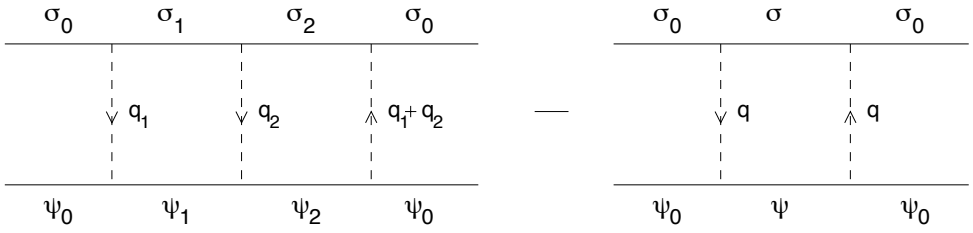

(3.159)

The last line is an obvious diagrammatic representation of the two terms. It must be cautioned, however, that this graph is not to be interpreted as a Feynman diagram in standard time dependent many-body perturbation theory. First of all, the spin sector of our model is lacking an obvious equivalent of Wick's theorem. Also, both terms do have an equal number of factors in the denominator, although they seem to have a different number of propagators in this simplified notation.

Again, at third order perturbation theory in H_{sc} we can still have only a single particle-hole excitation in the virtual state, since each virtual state must have a direct

matrix element with the ground state. As done below eq. (3.99), one can convert the sums over charge states into integrals over particle and hole momenta. However, one must again pay special attention to matrix elements in (3.159) with zero momentum transfer between spin and charge. Those matrix elements are diagonal in the charge sector, as explained below (3.103), and therefore their contribution is non-negligible despite the smaller corresponding phase space. We hence write :

$$E_3 = E_3^1 + E_3^2 + E_3^3 + E_3^4 + E_3^5 + E_3^6 + E_3^7 \tag{3.160}$$

where each term is defined in Table 3.2. The most general term is E_3^1 with non-zero momentum transfer at each vertex. At the first vertex, a particle at a position k_1 in the non-interacting Fermi sea is excited to a momentum k_2 outside the Fermi sea. At the second vertex, either the particle at k_2 or the hole at k_1 may hop. At the third vertex, the particle-hole pair is recombined. Hence there are two parts to E_3^1:

$$E_3^1 = E_3^{1a} + E_3^{1b} \tag{3.161}$$

$$E_3^{1a} = -N_e \int_{-k_f}^{k_f} \frac{dk_1}{2\pi} \int_{k_f}^{2\pi-k_f} \frac{dk_2}{2\pi} \int_{k_f}^{2\pi-k_f} \frac{dk_3}{2\pi}\, f_a(k_1,k_2,k_3) \tag{3.162}$$

$$E_3^{1b} = +N_e \int_{-k_f}^{k_f} \frac{dk_1}{2\pi} \int_{k_f}^{2\pi-k_f} \frac{dk_2}{2\pi} \int_{-k_f}^{k_f} \frac{dk_3}{2\pi}\; f_b(k_1,k_2,k_3) \tag{3.163}$$

where:

$$f_a(k_1,k_2,k_3) = \frac{J^3}{N_e} \sum_{\sigma_1,\sigma_2}{}' \frac{\langle\sigma_0|\,\gamma_{k_3-k_1}\,|\sigma_2\rangle\,\langle\sigma_2|\,\gamma_{k_2-k_3}\,|\sigma_1\rangle\,\langle\sigma_1|\,\gamma_{k_1-k_2}\,|\sigma_0\rangle}{\big(\epsilon(k_3)-\epsilon(k_1)+E_{\sigma_2}-E_{\sigma_0}\big)\big(\epsilon(k_2)-\epsilon(k_1)+E_{\sigma_1}-E_{\sigma_0}\big)} \tag{3.164}$$

$$f_b(k_1,k_2,k_3) = \frac{J^3}{N_e} \sum_{\sigma_1,\sigma_2}{}' \frac{\langle\sigma_0|\,\gamma_{k_2-k_3}\,|\sigma_2\rangle\,\langle\sigma_2|\,\gamma_{k_3-k_1}\,|\sigma_1\rangle\,\langle\sigma_1|\,\gamma_{k_1-k_2}\,|\sigma_0\rangle}{\big(\epsilon(k_2)-\epsilon(k_3)+E_{\sigma_2}-E_{\sigma_0}\big)\big(\epsilon(k_2)-\epsilon(k_1)+E_{\sigma_1}-E_{\sigma_0}\big)} \tag{3.165}$$

	q_1	q_2	$q_3 = -q_1 - q_2$	q
E_3^1	$\neq 0$	$\neq 0$	$\neq 0$	
E_3^2	0	$\neq 0$	$\neq 0$	
E_3^3	$\neq 0$	$\neq 0$	0	
E_3^4	$\neq 0$	0	$\neq 0$	
E_3^5	0	0	0	
E_3^6				$\neq 0$
E_3^7				0

Table 3.2: Definition of various partial sums of (3.159). Columns show which vertices have zero momentum transfer between spin and charge sector. The last two rows refer to the second term in (3.159).

Here, E_3^{1a} is the part where the particle is hopping twice, and E_3^{1b} is the part where the second step consists of a hole hopping within the Fermi sea. The change of sign in the definition of E_3^{1b} is due to the fact that two particles in the Fermi sea are exchanged. Most of the remaining partial sums are now straightforwardly expressed in terms of the functions f_a and f_b:

$$E_3^2 = -N_e \frac{k_f}{\pi} \int_{-k_f}^{k_f} \frac{dk_1}{2\pi} \int_{k_f}^{2\pi - k_f} \frac{dk_2}{2\pi}\ f_a(k_1, k_1, k_2) \tag{3.166}$$

$$E_3^3 = -N_e \frac{k_f}{\pi} \int_{-k_f}^{k_f} \frac{dk_1}{2\pi} \int_{k_f}^{2\pi - k_f} \frac{dk_2}{2\pi}\ f_a(k_1, k_2, k_1) \tag{3.167}$$

$$E_3^4 = -N_e \frac{k_f}{\pi} \int_{-k_f}^{k_f} \frac{dk_1}{2\pi} \int_{k_f}^{2\pi - k_f} \frac{dk_2}{2\pi}\ f_b(k_1, k_2, k_1) \tag{3.168}$$

$$E_3^5 = -N_e \left(\frac{k_f}{\pi}\right)^3 f_a(0,0,0) \tag{3.169}$$

$$E_6^6 = N_e \frac{k_f}{\pi} \int_{-k_f}^{k_f} \frac{dk_1}{2\pi} \int_{k_f}^{2\pi - k_f} \frac{dk_2}{2\pi}\ \frac{J^3}{N_e} \sum_{\sigma}{}' \frac{\langle\sigma_0|\,\gamma_{k_2-k_1}\,|\sigma\rangle\,\langle\sigma|\,\gamma_{k_1-k_2}\,|\sigma_0\rangle}{\left(\epsilon(k_2) - \epsilon(k_1) + E_{\sigma_1} - E_{\sigma_0}\right)^2}\ \langle\sigma_0|\,\gamma_{q=0}\,|\sigma_0\rangle \tag{3.170}$$

$$E_6^7 = N_e \left(\frac{k_f}{\pi}\right)^3 \frac{J^3}{N_e} \sum_{\sigma}{}' \frac{\langle\sigma_0|\,\gamma_{q=0}\,|\sigma\rangle\,\langle\sigma|\,\gamma_{q=0}\,|\sigma_0\rangle}{\left(\epsilon(k_2) - \epsilon(k_1) + E_{\sigma_1} - E_{\sigma_0}\right)^2}\ \langle\sigma_0|\,\gamma_{q=0}\,|\sigma_0\rangle \tag{3.171}$$

Note that since $f_a(k_1, k_2, k_2) = f_b(k_1, k_2, k_1)$, one may in principle choose freely between f_a and f_b in eqs. (3.166)-(3.169). The reason for the above choices will become apparent below (see eqs.(3.174)). We now write, as we did before

$$E_3 = L\left(A_3 x + B_3 x^2 + C_3 x^3 + \dots\right) \tag{3.172}$$

It will now be shown that

$$B_3 = \frac{\pi^2}{2N_e} \frac{\partial^2}{\partial k_f^2} E_3 \bigg|_{k_f=0} = 0 \tag{3.173}$$

To this end, we group the partial sums defined above as follows:

$$E_3^a = E_3^{1a} + E_3^2 + E_3^3 \tag{3.174a}$$

$$E_3^b = E_3^{1b} + E_3^4 + E_3^6 \tag{3.174b}$$

$$E_3^c = E_3^5 + E_3^7 \tag{3.174c}$$

We will show that for all $\tau = a, b, c$:

$$B_3^\tau \equiv \frac{\pi^2}{2N_e}\,\frac{\partial^2}{\partial k_f^2} E_3^\tau \bigg|_{k_f=0} = 0 \tag{3.175}$$

This is trivial for B_3^c, since $E_3^3 \propto k_f^3$. We will now turn to B_3^b. It is convenient to redefine the function f_b such that it includes terms coming from the second term in (3.159):

$$\begin{aligned}\tilde{f}_b(k_1,k_2,k_3) = \frac{J^3}{N_e}\,{\sum_{\sigma_1,\sigma_2}}' \,\frac{\langle\sigma_0|\,\gamma_{k_2-k_3}\,|\sigma_2\rangle\,\langle\sigma_2|\,\gamma_{k_3-k_1}\,|\sigma_1\rangle\,\langle\sigma_1|\,\gamma_{k_1-k_2}\,|\sigma_0\rangle}{\big(\epsilon(k_2)-\epsilon(k_3)+E_{\sigma_2}-E_{\sigma_0}\big)\big(\epsilon(k_2)-\epsilon(k_1)+E_{\sigma_1}-E_{\sigma_0}\big)} \\ - \frac{J^3}{N_e}\,{\sum_{\sigma}}' \,\frac{\langle\sigma_0|\,\gamma_{k_2-k_1}\,|\sigma\rangle\,\langle\sigma|\,\gamma_{k_1-k_2}\,|\sigma_0\rangle}{\big(\epsilon(k_2)-\epsilon(k_1)+E_{\sigma_1}-E_{\sigma_0}\big)^2}\,\langle\sigma_0|\,\gamma_{k_3-k_1}\,|\sigma_0\rangle\end{aligned} \tag{3.176}$$

Note that the additional second term is non-zero only for $k_1 = k_3$, i. e. in the case where the middle one of the three vertices in the first term has $q = 0$. The effect of this new term is to regularize the terms with $\sigma_1 = \sigma_2$ in the first sum, where the middle piece is a diagonal matrix element from which the respective ground state expectation value is subtracted by the second sum.

E_3^b is now conveniently written as:

$$\begin{aligned}E_3^b = &+ N_e \int_{-k_f}^{k_f}\frac{dk_1}{2\pi}\int_{k_f}^{2\pi-k_f}\frac{dk_2}{2\pi}\int_{-k_f}^{k_f}\frac{dk_3}{2\pi}\;\;\tilde{f}_b(k_1,k_2,k_3) \\ &- N_e\,\frac{k_f}{\pi}\int_{-k_f}^{k_f}\frac{dk_1}{2\pi}\int_{k_f}^{2\pi-k_f}\frac{dk_2}{2\pi}\;\tilde{f}_b(k_1,k_2,k_1)\end{aligned} \tag{3.177}$$

In the first integral, the replacement $f_b \to \tilde{f}_b$ is justified since the additional terms in (3.176) have no weight in this integral. The second term correctly reproduces the sum of E_3^3 and E_3^6.

When taking the second derivative with respect to k_f, it is clear that the two derivatives have to act on the k_1 and k_3 integral in the first term, and on the k_1-integral and the overall factor of k_f in the second term. Other contributions vanish in the limit $k_f \to 0$. We hence get:

$$\begin{aligned}B_3^b &= \frac{\pi^2}{2N_e}\,\frac{\partial^2}{\partial k_f^2} E_3^b \bigg|_{k_f=0} = 0 \\ &= \frac{1}{4\pi}\int_0^{2\pi} dk_2\,\Big(\tilde{f}_b(\eta,k_2,-\eta)+\tilde{f}_b(-\eta,k_2,\eta)-2\,\tilde{f}_b(0,k_2,0)\Big)\end{aligned} \tag{3.178}$$

Here, as in the second order treatment, an infinitesimal η was introduced for all terms coming from the first integral in (3.177). More accurately, this integral represents the

partial sum defining E_3^{1b} and by definition does not include terms with zero momentum transfer, and in particular terms with $k_1 = k_3$. Such terms only enter the second part in (3.177) and give rise to the last term in (3.178). Again, the processes with $q = 0$ and $q \to 0$ apparently cancel each other precisely in (3.178), as it has been found at second order, provided that $\tilde{f}_b$ is a continuous function at $k_1 = k_3$. However, even more so than at second order, the need to clarify this point is obvious from (3.176), where the case $k_1 = k_3$ plays a very special role: Firstly, one can have $\sigma_1 = \sigma_2$ in the first term of (3.176) in this case. This leads to diagonal matrix elements which are much larger than off-diagonal matrix elements in the thermodynamic limit. Secondly, the additional term in (3.176) is non-zero only at $k_1 = k_3$. It will be shown in the following that this is precisely what is needed to regularize the diagonal contributions and to render $\tilde{f}_b$ continuous at $k_1 = k_3$.

A proof of this statement is more difficult here that it is at second order perturbation theory, where it could be proven by analyzing a mere spin problem (appendix B). In (3.178) there is still an integral over a free momentum to be carried out, and hence the charge dispersion will not vanish from the energy denominator. A first intuitive test for the continuity of $\tilde{f}_b$ can be made by assuming that the main contribution to (3.178) comes from small momenta k_2, where the charge part is negligible in the denominator of (3.176). For simplicity, we further assume that each factor in the energy denominator may be replaced by the spin gap Δ_s. We may then use the completeness of the σ states and have within this approximation:

$$\begin{aligned}
\tilde{f}_b(k_1, k_2, k_3) \sim & \frac{1}{N_e} \frac{J^3}{\Delta_s^2} \langle \sigma_0 | \gamma_{k_2 - k_3} \left[\mathbf{1} - |\sigma_0\rangle \langle \sigma_0| \right] \gamma_{k_3 - k_1} \left[\mathbf{1} - |\sigma_0\rangle \langle \sigma_0| \right] \gamma_{k_1 - k_2} |\sigma_0\rangle \\
& - \frac{1}{N_e} \frac{J^3}{\Delta_s^2} \langle \sigma_0 | \gamma_{k_2 - k_1} \left[\mathbf{1} - |\sigma_0\rangle \langle \sigma_0| \right] \gamma_{k_1 - k_2} |\sigma_0\rangle \langle \sigma_0 | \gamma_{k_3 - k_1} |\sigma_0\rangle \\
\equiv & \frac{1}{N_e} \frac{J^3}{\Delta_s^2} \langle \sigma_0 | \gamma_{k_2 - k_3} \gamma_{k_3 - k_1} \gamma_{k_1 - k_2} |\sigma_0\rangle_{\mathrm{C}}
\end{aligned} \tag{3.179}$$

where we have introduced a "connected" expectation value via

$$\langle A\, B\, C\rangle_{\mathrm{C}} \equiv \langle A\, B\, C\rangle - \langle A\rangle \langle B\, C\rangle - \langle B\rangle \langle A\, C\rangle - \langle C\rangle \langle A\, B\rangle + 2 \langle A\rangle \langle B\rangle \langle C\rangle \tag{3.180}$$

The connected expectation value measures the "correlated" part of an expectation value in the following sense: Whenever one of the three operators, say A is uncorrelated with the others such that it can be factored out of any expectation value, then the quantity defined in (3.180) vanishes. One can use this to argue that indeed (3.179) is a continuous function of its momenta. More precisely, consider sets of local operators

$$\mathcal{O}_j^r = T \mathcal{O}_{j+1}^r T^\dagger \tag{3.181}$$

related via the lattice translation operator T as shown above, and their Fourier trans-

forms

$$\mathcal{O}^r_q = \sum_j e^{iqj} \mathcal{O}^r_j \tag{3.182}$$

Then one can argue that

$$\left\langle \mathcal{O}^a_{q_1} \, \mathcal{O}^b_{q_2} \, \mathcal{O}^c_{q_3} \right\rangle_{\mathrm{C}} \quad , \tag{3.183}$$

where $\sum_i q_i = 0$, is a continuous function of the momenta, while the unconnected expectation value is in general *not* continuous at $q_i = 0$ for any q_i. To see this, consider the unconnected version of (3.183):

$$\left\langle \mathcal{O}^a_{q_1} \, \mathcal{O}^b_{q_2} \, \mathcal{O}^c_{q_3} \right\rangle = \sum_{j_1, j_2, j_3} e^{iq_1 j_1 + iq_2 j_2 + iq_3 j_3} \left\langle \mathcal{O}^a_{j_1} \, \mathcal{O}^b_{j_2} \, \mathcal{O}^c_{j_3} \right\rangle \tag{3.184}$$

We regard the operators $\mathcal{O}^r_j$ as "local" in the sense that they are uncorrelated at large distances:

$$\left\langle \mathcal{O}^a_{j_1} \, \mathcal{O}^b_{j_2} \, \mathcal{O}^c_{j_3} \right\rangle \approx \left\langle \mathcal{O}^a_{j_1} \, \mathcal{O}^b_{j_2} \right\rangle \left\langle \mathcal{O}^c_{j_3} \right\rangle \qquad \text{for} \quad |j_3 - j_1|, \, |j_3 - j_2| \gg 1 \tag{3.185}$$

and similarly for $\mathcal{O}^a_{j_1}$, $\mathcal{O}^b_{j_2}$. If the state in which the expectation value is taken has translational invariance, then $\left\langle \mathcal{O}^r_j \right\rangle$ is a constant independent of j which is nonzero in general. However, it is then clear due to the oscillatory nature of the exponential in (3.184), that the uncorrelated pieces such as (3.185) corresponding to regions where the operators are well separated in (3.184) do not contribute as long as the momenta q_i are non-zero. This no longer true in general when any of the q_i vanishes. Then, contributions from spatially well separated regions such as (3.185) will suddenly give large contributions, which are completely absent as long as all q_i are finite. This discontinuous behavior is indeed regularized in the connected expectation value (3.184). The subtraction of uncorrelated pieces does not alter the result for non-zero q_i's. However, when any q_i equals zero, contributions from terms such as (3.185) will be subtracted, which do not occur at finite q_i. Hence the "connected" version (3.183) will be continuous.

We see that in the approximation (3.179), $\tilde{f}_b$ will be continuous, in particular at zero momentum transfer, although this is not true for any of the two terms defining $\tilde{f}_b$ in (3.176). This may easily be verified directly at the Majumdar-Gosh point $\alpha = .5$.

To obtain the same result without this crude approximation, we rewrite $\tilde{f}_b$ as

$$\tilde{f}_b(k_1, k_2, k_3) = \int d\omega_1 \, d\omega_2 \, \frac{\tilde{A}(k_1, k_2, k_3, \omega_1, \omega_2)}{\big(\epsilon(k_2) - \epsilon(k_3) + \omega_2\big)\big(\epsilon(k_2) - \epsilon(k_1) + \omega_1\big)} \tag{3.186}$$

where a spectral function

$$\tilde{A}(k_1, k_2, k_3, \omega_1, \omega_2) \tag{3.187}$$

$$= \frac{J^3}{N_e} \sum_{\sigma_1,\sigma_2}{}' \langle\sigma_0|\, \gamma_{k_2-k_3}\, |\sigma_2\rangle \langle\sigma_2|\, \gamma_{k_3-k_1}\, |\sigma_1\rangle \langle\sigma_1|\, \gamma_{k_1-k_2}\, |\sigma_0\rangle\ \delta(\omega_1 + E_{\sigma_0} - E_{\sigma_1})\, \delta(\omega_2 + E_{\sigma_0} - E_{\sigma_2})$$

$$- \frac{J^3}{N_e}\ \langle\sigma_0|\, \gamma_{k_3-k_1}\, |\sigma_0\rangle \sum_{\sigma}{}' \langle\sigma_0|\, \gamma_{k_2-k_1}\, |\sigma\rangle \langle\sigma|\, \gamma_{k_1-k_2}\, |\sigma_0\rangle\ \delta(\omega_1 + E_{\sigma_0} - E_{\sigma})\, \delta(\omega_2 + E_{\sigma_0} - E_{\sigma}) \tag{3.188}$$

was introduced. One can now argue that since the denominator in (3.186) is bounded from below by the spin gap Δ_s, it is sufficient to show the continuity of $\tilde{A}$ as function of momenta. For this it is enough to consider the Fourier transform

$$\tilde{A}(k_1, k_2, k_3, t_1, t_2) = \frac{J^3}{N_e} \langle\sigma_0|\ \gamma_{k_2-k_3}(t_1 + t_2)\ \gamma_{k_3-k_1}(t_1)\ \gamma_{k_1-k_2}(0)\ |\sigma_0\rangle_{\mathrm{C}} \tag{3.189}$$

where Heisenberg operators

$$\gamma_q(t) = \exp(itH_s)\, \gamma_q \exp(-itH_s) \tag{3.190}$$

have been introduced. Indeed, by inserting complete sets of states in (3.189) it is easily shown that

$$\tilde{A}(k_1, k_2, k_3, \omega_1, \omega_2) = \frac{1}{(2\pi)^2} \int dt_1 dt_2\ e^{i\omega_1 t_1 + i\omega_2 t_2} \tilde{A}(k_1, k_2, k_3, t_1, t_2) \tag{3.191}$$

is satisfied. Note that in the gapped case $\alpha > \alpha_c$ spin correlations decay exponentially in time, and hence the connected expectation value in (3.189) will be exponentially suppressed for times $|t_1|, |t_2| >> 1/J$. At finite t, however, we can still regard the operator $\gamma_j(t)$ as local in the sense displayed in (3.185). (3.189) is then precisely of the form (3.183), and the arguments given above will apply such that (3.189) is a continuous function of momenta. The Fourier transform (3.191) will then have the same property. This implies the continuity of $\tilde{f}_b$ in (3.178), which leads to

$$B_3^b = 0 \tag{3.192}$$

Note that the above arguments for the continuity of f_b could also have been used at second order, providing an alternative route to the arguments applied in appendix B. At second order, this may serve as an independent check. However, while the line of thoughts given in appendix B may appeal somewhat more to physical intuition, only the reasoning used in the present appendix generalizes to higher orders.
Finally, we examine the contribution from E_3^a. From the definition (3.174a) we have:

$$
\begin{aligned}
E_3^a = &- N_e \int_{-k_f}^{k_f} \frac{dk_1}{2\pi} \int_{k_f}^{2\pi-k_f} \frac{dk_2}{2\pi} \int_{k_f}^{2\pi-k_f} \frac{dk_3}{2\pi}\; f_a(k_1,k_2,k_3) \\
&- N_e \frac{k_f}{\pi} \int_{-k_f}^{k_f} \frac{dk_1}{2\pi} \int_{k_f}^{2\pi-k_f} \frac{dk_2}{2\pi}\; \big(f_a(k_1,k_1,k_2) + f_a(k_1,k_2,k_1) \big)
\end{aligned}
\tag{3.193}
$$

When calculating B_3^a from (3.175), one still finds that derivatives of the integrand do not enter. This is because k_f enters the integrand only symmetrically after the first derivative is taken, hence further derivation gives rise to vanishing terms as $k_f \to 0$. The result is:

$$
\begin{aligned}
B_3^a = \frac{1}{4\pi} \int_0^{2\pi} dk \Big(& f_a(\eta,-\eta,k) + f_a(-\eta,\eta,k) - 2f_a(0,0,k) \\
& + f_a(\eta,k,-\eta) + f_a(-\eta,k,\eta) - 2f_a(0,k,0) \Big)
\end{aligned}
\tag{3.194}
$$

Once again, an infinitesimal η enters contributions from the first term in (3.193), which is E_3^{1a} and does not include processes with zero momentum transfer. Note that unlike in the case of E_3^{1b}, there are no extra terms involved here that regularize processes with zero momentum transfer in the middle vertex of (3.164). Hence, $f_a(k_1,k_2,k_3)$ will in general not be continuous at $k_2 = k_3$. However, such processes have no weight in both (3.193) and (3.194). It is hence convenient, although not necessary, to define the regularized function

$$
\begin{aligned}
\tilde{f}_a(k_1,k_2,k_3) = &\frac{J^3}{N_e} \sum_{\sigma_1,\sigma_2} \frac{\langle\sigma_0|\,\gamma_{k_3-k_1}\,|\sigma_2\rangle\,\langle\sigma_2|\,\gamma_{k_2-k_3}\,|\sigma_1\rangle\,\langle\sigma_1|\,\gamma_{k_1-k_2}\,|\sigma_0\rangle}{\big(\epsilon(k_3)-\epsilon(k_1)+E_{\sigma_2}-E_{\sigma_0}\big)\big(\epsilon(k_2)-\epsilon(k_1)+E_{\sigma_1}-E_{\sigma_0}\big)} \\
&- \frac{J^3}{N_e} \sum_{\sigma} \frac{\langle\sigma_0|\,\gamma_{k_2-k_1}\,|\sigma\rangle\,\langle\sigma|\,\gamma_{k_1-k_2}\,|\sigma_0\rangle}{\big(\epsilon(k_2)-\epsilon(k_1)+E_{\sigma_1}-E_{\sigma_0}\big)^2}\,\langle\sigma_0|\,\gamma_{k_2-k_3}\,|\sigma_0\rangle
\end{aligned}
\tag{3.195}
$$

The continuity of $\tilde{f}_a$ as function of momenta follows in analogy with the continuity of $\tilde{f}_b$. In the integration domain of (3.194), f_a and $\tilde{f}_a$ are identical almost everywhere. Hence f_a can be replaced by $\tilde{f}_a$, and $B_3^a = 0$ follows by continuity. It has thus been shown that

$$
B_3 = 0 \tag{3.196}
$$

is indeed satisfied.

We now proceed by showing $6C_3 = \pi^2 A_{3,\phi\phi}$. To see this, we assume that the functions $\tilde{f}_a(k_1,k_2,k_3)$ and $\tilde{f}_b(k_1,k_2,k_3)$, which have been argued to be continuous, are also "smooth" in the sense that second derivatives exist. We then rewrite (3.177) as

$$E_3^b = +\,N_e \int_{-k_f}^{k_f} \frac{dk_1}{2\pi} \int_{k_f}^{2\pi-k_f} \frac{dk_2}{2\pi} \int_{-k_f}^{k_f} \frac{dk_3}{2\pi} \ \Big(\tilde{f}_b(k_1,k_2,k_3) - \tilde{f}_b(k_1,k_2,k_1)\Big) \tag{3.197}$$

the integrand is then proportional to $(k_1 - k_3)$, which implies that $E_3^b \sim k_f^4$, and hence E_3^b, neither contributes to C_3 nor $A_{3,\phi\phi}$. Hence we have

$$C_3 = C_3^a + C_3^c \tag{3.198}$$

$$\text{where :} \qquad C_3^\tau = \frac{\pi^3}{6N_e} \frac{\partial^3}{\partial k_f^3} E_3^\tau \bigg|_{k_f=0} \tag{3.199}$$

When differentiating the first term of E_3^a in (3.193), one derivative has to act on the k_1 integral, in order to remove an overall factor of k_f. The remaining two derivatives may either act on the other two integrals, or both on the integrand, since a single derivative on the integrand leads to a vanishing terms, as explained above. Similarly, in the second term of (3.193) all derivatives have to act on the two integrals and the overall factor of k_f. The result is:

$$C_3^a = -\frac{1}{6\cdot 4} \int_0^{2\pi} dk_2 \int_0^{2\pi} dk_3 \ \frac{\partial^2}{\partial k_f^2} \tilde{f}_a(k_f,k_2,k_3)\bigg|_{k_f=0} \\ - \tilde{f}_a(0,0,0) + \tilde{f}_a(0,0,0) + \tilde{f}_a(0,0,0) \tag{3.200}$$

where f_a has now been replaced by $\tilde{f}_a$, as explained below (3.195). Since

$$\begin{aligned} E_3^c \equiv E_3^5 + E_3^7 &= -N_e \left(\frac{k_f}{\pi}\right)^3 \tilde{f}_a(0,0,0) \\ \Longrightarrow C_3^c &= -\tilde{f}_a(0,0,0) \end{aligned} \tag{3.201}$$

we have

$$C_3 = -\frac{1}{6\cdot 4} \int_0^{2\pi} dk_2 \int_0^{2\pi} dk_3 \ \frac{\partial^2}{\partial k_f^2} \tilde{f}_a(k_f,k_2,k_3)\bigg|_{k_f=0} \tag{3.202}$$

The only contribution to A_3 comes from E_3^a. One easily finds from (3.193)

$$A_3 = \frac{\pi}{N_e} \frac{\partial}{\partial k_f} E_3^a = -\frac{1}{4\pi^2} \int_{k_f}^{2\pi-k_f} dk_2 \int_{k_f}^{2\pi-k_f} dk_3 \ \tilde{f}_a(0,k_2,k_3) \tag{3.203}$$

As in (3.115), we find that in the presence of a flux $L\phi$, we need to make the replace-

ment

$$\tilde{f}_a(0, k_2, k_3) \longrightarrow \tilde{f}_a(\phi, k_2 + \phi, k_3 + \phi) \tag{3.204}$$

This gives

$$A_{3,\phi\phi} = -\frac{1}{4\pi^2} \int_{k_f}^{2\pi - k_f} dk_2 \int_{k_f}^{2\pi - k_f} dk_3 \ \frac{\partial^2}{\partial \phi^2} \tilde{f}_a(\phi, k_2 + \phi, k_3 + \phi) \Big|_{\phi=0} \tag{3.205}$$

As in the second order case, one finds upon a shift of the integration variables that a comparison with (3.202) yields indeed:

$$\underline{\underline{6C_3 = \pi^2 A_{3,\phi\phi}}} \tag{3.206}$$

Bibliography

[1] J. G. Bednorz and K. A. Müller. Possible High-Tc Superconductivity in the Ba-La-Cu-O System. *Z. Phys. B 64, 189*, 1986.

[2] C. H. Maule, J. N. Tothill, P. Strange, and J. A. Wilson. An optical investigation into the $3d^1$ and $3d^2$ transition-metal halides and oxyhalides, compounds near to delocalisation. *J. Phys. C: Sol. St. 21, 2153*, 1988.

[3] R. J. Beynon and J. A. Wilson. TiOCl-TiOBr – are these RVB d^1, $S = 1/2$ materials? *J. Phys. Cond. Mat. 5, 1983*, 1993.

[4] P. W. Anderson. *The Theory of Superconductivity in the High-T_c Cuprate Superconductors*. Princeton University Press, Princeton, 1997.

[5] E. Carlson, V. J. Emery, S. A. Kivelson, and D. Orgad. Concepts in High Temperature Superconductivity. cond-mat/0206217, to appear in *'The Physics of Conventional and Unconventional Superconductors'* ed. by K. H. Bennemann and J. B. Ketterson (Springer-Verlag), 2002.

[6] M. R. Norman and C. Pepin. The Electronic Nature of High Temperature Cuprate Superconductors. cond-mat/0302347, 2003.

[7] J. Nagamatsu, N. Nakagawa, T. Muranaka, Y. Zenitani, and J. Akimitsu. Superconductivity at 39 K in magnesium diboride. *Nature*, 2001.

[8] M. K. Wu, J. R. Ashburn, C. J. Torng, P. H. Hor, R. L. Meng, L. Gao, Z. J. Huang, Y. Q. Wang, and C. W. Chu. Superconductivity at 93 K in a new mixed-phase Yb-Ba-Cu-O compound system at ambient pressure. *Phys. Rev. Lett. 58, 908*, 1987.

[9] S. Martin, A. T. Fiory, R. M. Fleming, L. F. Schneemeyer, and J. V. Waszczak. Normal-state transport properties of $Bi_{2+x}Sr_{2-y}CuO_{6+\delta}$ crystals. *Phys. Rev. B 41, 846*, 1990.

[10] A. Kaminski, J. Mesot, H. Fretwell, M. R. Campuzano, J. C.and Norman, M. Randeria, H. Ding, T. Sato, T. Takahashi, T. Mochiku, K. Kadowaki, and H. Hoechst. Quasiparticles in the superconducting state of $Bi_2Sr_2CaCu_2O_8$. *Phys. Rev. Lett. 84, 1788*, 2000.

[11] W. W. Jr. Warren, R. E. Walstedt, G. F. Brennert, R. J. Cava, R. Tycko, R. F. Bell, and G. Dabbagh. Cu spin dynamics and superconducting precursor effects in planes above Tc in $YBa_2Cu_3O_6.7$. *Phys. Rev. Lett. 62, 1193*, 1989.

[12] H. Alloul, T. Ohno, and P. Mendels. ^{89}Y NMR evidence for a fermi-liquid behavior in $YBa_2Cu_3O_{6+x}$. *Phys. Rev. Lett. 63, 1700*, 1989.

[13] A. G. Loeser, Z.-X. Shen, D. S. Dessau, D. S. Marshall, C. H. Park, P. Fournier, and A. Kapitulnik. Excitation Gap in the Normal State of Underdoped $Bi_2Sr_2CaCu_2O_{8+\delta}$. *Science 273, 325*, 1996.

[14] H. Ding et al. Spectroscopic evidence for a pseudogap in the normal state of underdoped high-T_c superconductors. *Nature 382, 51*, 1996.

[15] P. W. Anderson. The Resonating Valence Bond State in La_2CuO_4 and Superconductivity. *Science 235, 1196*, 1987.

[16] G. Baskaran, Z. Zou, and P. W. Anderson. The resonating valence bond state and high-Tc superconductivity – A mean field theory. *Solid State Commun. 63, 973*, 1987.

[17] I. Affleck and J. B. Marston. Large-n limit of the Heisenberg-Hubbard model: Implications for high-T_c superconductors. *Phys. Rev. B 37, 3774*, 1988.

[18] G. Kotliar and J. Liu. Superexchange mechanism and d-wave superconductivity. *Phys. Rev. B 38, 5142*, 1988.

[19] N. Nagaosa and P. A. Lee. Ginzburg-Landau theory of the spin-charge-separated system. *Phys. Rev. B 45, 966*, 1992.

[20] P. A. Lee, N. Nagaosa, T.-K. Ng, and X.-G. Wen. SU(2) formulation of the t-J model: Application to underdoped cuprates. *Phys. Rev. B 57, 6003*, 1998.

[21] A. H. MacDonald, Girvin S. M., and D. Yoshioka. t/U expansion for the Hubbard model. *Phys. Rev. B 37, 9753*, 1988.

[22] M. U. Ubbens and P. A. Lee. Superconductivity phase diagram in the gauge-field description of the $t - J$ model. *Phys. Rev. B 49, 6853*, 1994.

[23] D. H. Kim and P. A. Lee. Theory of Spin excitations in Undoped and Underdoped Cuprated. *Ann. Phys. 272, 130*, 1999.

[24] C. Mudry and E. Fradkin. Mechanism of spin and charge separation in one-dimensional quantum antiferromagnets. *Phys. Rev. B 50, 11409*, 1994.

[25] E. Manousakis. The spin-$\frac{1}{2}$ Heisenberg antiferromagnet on a square lattice and its application to the cuprous oxides. *Rev. Mod. Phys. 63, 1*, 1991.

[26] Wen, X.-G. and Wilczek, F. and Zee, A. Chiral Spin States and Superconductivity. *Phys. Rev. B 39, 11413*, 1989.

[27] G. Misguich, C. Lhuillier, and B. Bernu. Spin-liquid phase of the multiple-spin exchange Hamiltonian on the triangular lattice. *Phys. Rev. B 60, 1064*, 1999.

[28] J. B. Fouet, P. Sindzingre, and C. Lhuillier. An investigation of the quantum $J_1 - J_2 - J_3$ model on the honeycomb lattice. *Eur. Phys. J. B 20, 241*, 2001.

[29] A. Seidel, C. A. Marianetti, F. C. Chou, G. Ceder, and P. A. Lee. $S = \frac{1}{2}$ chains and spin-Peierls transition in TiOCl. *Phys. Rev. B 67, 020405(R)*, 2003.

[30] Y. Tokura and N. Nagaosa. Orbital Physics in Transition-Metal Oxides. *Science 288, 462*, 2000.

[31] G. Khaliullin and S. Maekawa. Orbital Liquid in Three-Dimensional Mott Insulator: $LaTiO_3$. *Phys. Rev. Lett. 85, 3950*, 2000.

[32] V.I. Anisimov, F. Aryasetiawan, and A.I. Lichtenstein. First-principles calculations of the electronic structure and spectra of strongly correlated systems: the LDA+U method. *J. Phys. Cond. Mat. 9, 767*, 1997.

[33] O.K. Andersen. Linear methods in band theory. *Phys. Rev. B, 12, 3060*, 1975.

[34] S.Y. Savrasov. Linear-response theory and lattice dynamics: A muffin-tin-orbital approach. *Phys. Rev. B, 54, 16470*, 1996.

[35] V.H. Schäfer, F. Wartenpfuhl, and E. Weise. Über Titanchloride V, Titan(III)-Oxychlorid. *Z. Anorg. Allg. Chem. 295, 268*, 1958.

[36] J. C. Bonner and M. E. Fisher. Linear magnetic chains with anisotropic coupling. *Phys. Rev. 135, A640*, 1964.

[37] W. E. Hatfield. New magnetic and structural results for uniformly spaced, alternatingly spaced, and ladder-like copper (II) linear chain compounds. *J. Appl. Phys. 52, 1985*, 1981.

[38] S. Eggert, I. Affleck, and M. Takahashi. Susceptibility of the spin 1/2 Heisenberg antiferromagnetic chain. *Phys. Rev. Lett. 73, 332*, 1994.

[39] K. Hirakawa and Y. Kurogi. One-Dimensional Antiferromagnetic Properties of $KCuF_3$. *Prog. Theor. Phys. Suppl. 46, 147*, 1970.

[40] T. Ami, M. K. Crawford, R. L. Harlow, Wang Z. R., D. C. Johnston, Q. Huang, and R. W. Erwin. Magnetic susceptibility and low-temperature structure of the linear chain cuprate Sr_2CuO_3. *Phys. Rev. B 51, 5994*, 1995.

[41] R. E. Peierls. *Quantum theory of solids.* Claredon, Oxford, 1955.

[42] E. B. Kolomeisky and J. P. Straley. Peierls instability of a one-dimensional quantum liquid. *Phys. Rev. B 53, 12553*, 1996.

[43] J. Sólyom. The Fermi gas model of one-dimensional conductors. *Adv. Phys. 28, 201*, 1979.

[44] R. Shankar. Renormalization Group Approach to Interacting Fermions. *Rev. Mod. Phys. 66, 129*, 1994.

[45] F. D. M. Haldane. General relation of correlation exponents and spectral properties of one-dimensional fermi systems: Application to the anisotropic $s = \frac{1}{2}$ heisenberg chain. *Phys. Rev. Lett. 45, 1358*, 1980.

[46] E. Pytte. Peierls instability in Heisenberg chains. *Phys. Rev. B 10, 4637*, 1974.

[47] M. C. Cross and D. S. Fisher. A new theory of the spin-Peierls transition with special relevance to the experiments on TTFCuBDT. *Phys. Rev. B 19, 402*, 1979.

[48] S. Sachdev. *Quantum Phase Transitions*. Cambridge Univ. Pr., Cambridge, 2001.

[49] I. Affleck. In *'Dynamical Properties of Unconventional Magnetic Systems'* A. T. Skjeltorp et al. Eds., chapter *Soliton Confinement and the Excitation Spectrum of Spin-Peierls Antiferromagnets*, cond-mat/9705127. Kluwer Academic Publishers, 1998.

[50] D. E. Moncton, R. J. Birgeneau, L. V. Interrante, and F. Wudl. X-Ray Scattering Study of Spin-Lattice Dimerization in a Quasi One-Dimensional Heisenberg Antiferromagnet. *Phys. Rev. Lett. 39, 507*, 1977.

[51] M. Hase, I. Terasaki, and K. Uchinokura. Observation of the spin-Peierls transition in linear Cu^{2+} (spin-1/2) chains in an inorganic compound $CuGeO_3$. *Phys. Rev. Lett. 70, 3651*, 1993.

[52] J. Riera and A. Dobry. Magnetic susceptibility in the spin-Peierls system $CuGeO_3$. *Phys. Rev. B 51, 16098*, 1995.

[53] L. P. Regnault, M. Aïn, B. Hennion, G. Dhalenne, and A. Revcolevschi. Inelastic-neutron-scattering investigation of the spin-Peierls system $CuGeO_3$. *Phys. Rev. B 53, 5579*, 1996.

[54] E. Abel and Y. S. Lee. . to be published.

[55] T. Imai and F. C. Chou. Novel Spin-Gap Behavior in Layered S=1/2 Quantum Spin System TiOCl. to be published, cond-mat/0301425, 2003.

[56] V. Kataev, J. Baier, A. Moeller, L. Jongen, G. Meyer, and A. Freimuth. Orbital order in the low-dimensional quantum spin system TiOCl probed by ESR. to be published, cond-mat/0305317, 2003.

[57] P. Lemmens, K. Y. Choi, G. Caimi, L. Degiorgi, N. N. Kovaleva, A. Seidel, and F. C. Chou. Giant phonon anomalies in the pseudo-gap phase of TiOCl. to be published, cond-mat/0305317.

[58] Lemmens, P. and Guntherodt, G. and Gros, C. Magnetic light scattering in low-dimensional quantum spin systems. *Physics Reports, 376, 1*, 2003.

[59] J. W. Bray et al. In *'Extended Linear Chain Compounds'*, chapter 7, pages 353,415. Plenum Press, New York, 1983.

[60] M. Imada. Spin Peierls Fluctuation and Nonlinear Excitations in One-Dimensional Systems. *Prog. Theor. Phys. Supp. 113, 203*, 1993.

[61] M. Imada. Spin-gap state and superconducting correlations in a one-dimensional dimerized t-J model. *Phys. Rev. B 48, 550*, 1993.

[62] E. Dagotto and T. M. Rice. Surprises on the Way from One- to Two-Dimensional Quantum Magnets: The Ladder Materials. *Science 271, 618*, 1996.

[63] A. Tanaka and X. Hu. Quantal Phases, Disorder Effects, and Superconductivity in Spin-Peierls Systems. *Phys. Rev. Lett. 88, 127004*, 2002.

[64] Schönhammer, K. Interacting fermions in one dimension: The Tomonaga-Luttinger model. *cond-mat/9710330*, 1997.

[65] F. D. M. Haldane. Demonstration of the "Luttinger liquid" character of Bethe-ansatz-soluble models of 1-D quantum fluids. *Phys. Lett. 81A, 153*, 1981.

[66] F. D. M. Haldane. 'Luttinger liquid theory' of one-dimensional quantum fluids. I. Properties of the Luttinger model and their extension to the general 1D interacting spinless Fermi gas. *J. Phys. C. 14, 2585*, 1981.

[67] J. Voit. One-dimensional Fermi liquids. *Rep. Prog. Phys. 58, 977*, 1995.

[68] H. J. Schulz, G. Cuniberti, and P. Pieri. In *'Field Theories for Low-Dimensional Condensed Matter Systems',* G. Morandi et al. Eds., chapter *Fermi liquids and Luttinger liquids*, cond-mat/9807366. Springer, 2000.

[69] Heidenreich, R. and Seiler, R. and Uhlenbrock, D. A. The Luttinger Model. *J. Stat. Phys. 22, 27*, 1980.

[70] de L. Kronig, R. Zur Neutrinotheorie des Lichtes III. *Physica 2, 968*, 1935.

[71] K. Huang. *Quantum Field Theory.* Wiley-Interscience, 1998.

[72] F. D. M. Haldane. Effective Harmonic-Fluid Approach to Low-Energy Properties of One-Dimensional Quantum Fluids. *Phys. Rev. Lett. 47, 1840*, 1981.

[73] J. von Delft and H. Schoeller. Bosonization for Beginners — Refermionization for Experts. *Annalen Phys. 7, 225*, 1998.

[74] Schönhammer, K. to be published in *'Interacting Electrons in Low Dimensions'*,, chapter *'Luttinger Liquids: The Basic Concepts'*, cond-mat/0305035. Kluwer Academic Publishers, 2003.

[75] S. Rao and Sen D. An introduction to bosonization and some of its applications. cond-mat/0005492, 2000.

[76] R. Shankar. Bosonization: how to make it work for you in Condensed Matter. *Acta Phys. Pol. B 26, 1835*, 1995.

[77] Sénéchal, D. An introduction to bosonization. cond-mat/9908262, 1999.

[78] A. O. Gogolin, A. A. Nersesyan, and A. M. Tsvelik. *Bosonization Approach to Strongly Correlated Systems*. Cambridge University, 1999.

[79] W. Kohn. Theory of the insulating state. *Phys. Rev. 133, A171*, 1964.

[80] Shastry, B. S. and Sutherland, B. Excitation Spectrum of a Dimerized Next-Neighbor Antiferromagnetic Chain. *Phys. Rev. Lett. 47, 964*, 1981.

[81] Zotos, X. and Prelovek, P. and Sega, I. Single-hole effective masses in the t-J model. *Phys. Rev. B 42, 8445*, 1990.

[82] Raas, C. and Löw, U. and Uhrig, G. S. Spin-Phonon Chains with Bond Coupling. *Phys. Rev. B 65, 144438*, 2002.

[83] M. Nakamura. Spin-Gap Phase in the One-Dimensional t-J-J'-model. *J. Phys. Soc. Jpn. 67, 717*, 1998.

[84] M. Ogata, M. U. Luchini, S. Sorella, and F. F. Assaad. Phase diagram of the one-dimensional t-J model. *Phys. Rev. Lett. 66, 2388*, 1991.

[85] M. Ogata, M. U. Luchini, and T. M. Rice. Spin gap in a generalized one-dimensional t-J model. *Phys. Rev. B 44, 12083*, 1991.

[86] R. Jullien and F. D. M. Haldane. Finite-Size Scaling Study of Dimerisation in the Frustrated 1D $S = \frac{1}{2}$ Antiferromagnet. *Bull. Am. Phys. Soc. 28, 344*, 1983.

[87] K. Okamoto and K. Nomura. Fluid-dimer critical point in $S = \frac{1}{2}$ antiferromagnetic Heisenberg chain with next nearest neighbor interactions. *Phys. Lett. 169A, 433*, 1992.

[88] F. D. M. Haldane. Spontaneous dimerization in the $S = 1/2$ Heisenberg antiferromagnetic chain with competing interactions. *Phys. Rev. B 25, 4925*, 1982.

[89] K. Nomura and K. Okamoto. Critical properties of $S = \frac{1}{2}$ antiferromagnetic XXZ chain with next-nearest-neighbour interactions. *J. Phys. A 27, 5773*, 1994.

[90] H. J. Schulz. Correlation exponents and the metal-insulator transition in the one-dimensional Hubbard model. *Phys. Rev. Lett. 64, 2831*, 1990.

[91] T. Xiang and N. d'Ambrumenil. Charge-spin separation and the ground-state wave function of the one-dimensional t-J model. *Phys. Rev. B 45, 8150*, 1992.

[92] C. K. Majumdar and D. K. Gosh. On Next-Nearest-Neighbor Interaction in Linear Chain II. *J. Math. Phys. 10, 1399*, 1969.

[93] W. J. Caspers and W. Magnus. Some exact excited states in a linaer antiferromagnetic spin system. *Phys. Lett. 88A, 103*, 1982.

[94] I. Affleck, T. Kennedy, E. H. Lieb, and H. Tasaki. Valece Bond Ground States in Isotropic Quantum Antiferromagnets. *Comm. Math. Phys. 115, 477*, 1988.

[95] G. Baym. *Lectures on Quantum Mechanics*. Addison-Wesley, 1973.